ACCELERATED IMPLEMENTATION OF INTELLIGENT COMPACTION TECHNOLOGY FOR EMBANKMENT SUBGRADE SOILS, AGGREGATE BASE, AND ASPHALT PAVEMENT MATERIALS

Final Report
Kansas US69 Field Project
August 17 to 25, 2008

Prepared By

David J. White, Ph.D.
Pavana KR. Vennapusa, Ph.D.
Heath Gieselman
Rachel Goldsmith
Luke Johanson
Bradley Fleming
S. Caleb Douglas, P.E.

Earthworks Engineering Research Center (EERC)
Department of Civil Construction and Environmental Engineering
Iowa State University
2711 South Loop Drive, Suite 4600
Ames, IA 50010-8664
Phone: 515-294-1463
www.eerc.iastate.edu

May 08, 2009

TABLE OF CONTENTS

LIST OF FIGURES

LIST OF TABLES

ACKNOWLEDGMENTS

This study was funded by US FHWA research project DTFH61-07-C-R0032 "Accelerated Implementation of Intelligent Compaction Technology for Embankment Subgrade Soils, Aggregate Base, and Asphalt Pavement Materials". George Chang from the Transtec Group, Inc. is the Principal Investigator for this research project. Robert D. Horan is the project facilitator and assisted with scheduling rollers for the project. Stan Rakowski with Sakai Heavy Industries Ltd., Nick Oetken with Caterpillar, Inc. provided IC rollers and field support during the project. Kei Uchiyama with Sakai Heavy Industries, Ltd. provided assistance with Sakai software. KSDOT personnel, contractor personnel, and many others assisted with the coordination and participated in the field demonstrations and their assistance and interest is greatly appreciated.

SYMBOLS

a	Vibration amplitude
A_{Ω}	Acceleration at fundamental frequency
$A_{X\Omega}$	Acceleration at X-order harmonic
A'	Machine acceleration
b	machine internal loss coefficient used in MDP calculation
b_0	Intercept in a linear regression equation
b_1, b_2, b_3	Regression coefficients
CBR	California bearing ratio
CCV	Sakai Compaction control value
CCV_{PD}	Sakai CCV measurements from padfoot roller
CCV_{SD}	Sakai CCV measurements from smooth drum roller
DPI	Dynamic cone penetration index
d_0	measured settlement under plate
E	Elastic modulus
E_{LWD}	Elastic modulus determined from light weight deflectometer
E_{LWD-Z2}	Elastic modulus determined from 200-mm plate Zorn light weight deflectometer
$E_{FWD-D4.5}$	Elastic modulus determined from 450-mm plate Dynatest falling weight deflectometer
E_{V1}	Initial modulus from 300-mm diameter static plate load test
E_{V2}	Reload modulus from 300-mm diameter static plate load test
f	Vibration frequency
F	Shape factor
g	Acceleration of gravity
G_s	Specific gravity
LL	Liquid limit
m	machine internal loss coefficient used in MDP calculation
MDP	Caterpillar Machine drive power
MDP_{80}	See description in text
MDP_{40}	See description in text

P_g	Gross power needed to move the machine
PL	Plastic limit
PI	Plasticity index
r	Radius of the plate
v	Roller velocity
w	Moisture content
w_{opt}	Optimum moisture content
W	Roller weight
α	Slope angle (roller pitch from a sensor)
σ_0	Applied stress
η	Poisson's ratio
γ_d	Dry unit weight
γ_{dmax}	Maximum dry unit weight
$\gamma(h)$	Semivariogram

EXECUTIVE SUMMARY

This report presents results from a field investigation conducted on the US69 highway project in Kansas. Caterpillar and Sakai intelligent compaction (IC) rollers measuring *Compaction Control Value* (CCV) and *Machine Drive Power* (MDP) measurement values, respectively, were investigated by conducting field testing on cohesive subgrade materials. This field project aimed to: (a) evaluate the effectiveness of the padfoot roller IC measurements in assessing the compaction quality of cohesive subgrade materials; (b) develop correlations between padfoot roller IC measurements and various conventionally used in-situ point measurements; and (c) evaluate the advantages of using IC technology for production compaction.

Results indicate that the CCV and MDP measurement values are repeatable. Linear regression analysis produced poor to good correlations between IC and point measurement values. Reasons for cases with poor correlations are attributed to influence of underlying support conditions, variations in moisture content, and narrow range of IC and point measurement values at the test locations. Multiple regression analysis indicated that IC measurements are influenced by amplitude and in some cases by moisture content and grade slope, in correlations with in-situ point measurements. For two cases in this project, compaction using high amplitude setting resulted in comparatively similar or higher relative compaction than using low amplitude or static settings.

Color-coded maps of IC data with 100% coverage information provided the opportunity to visualize compaction quality over a production area or at a given point location. This opportunity can be beneficial to make informed decisions on compaction process to promptly adjust process control measures. Geostatistical analysis methods (i.e., semivariogram analysis) in combination with univariate statistics were applied to production area IC measurements to quantify spatial non-uniformity of the compacted materials. The results from these anlaysis methods showed interesting trends in change in compaction quality (in terms of spatial continuity and non-uniformity) with increasing pass. Implementing such analysis methods in construction QC/QA procedures represent a paradigm shift in how compaction analysis and specifications could be implemented in the future.

CCV measurements obtained from padfoot roller were well correlated with measurements obtained from smooth drum roller at this site. Although there was scatter in the relationships, the trends were quite encouraging. The CCV padfoot roller measurements demonstrate similar advantages as the smooth drum roller measurements.

The results and anlaysis presented in this report should be of significant interest to the pavement, geotechnical, and construction engineering community and are anticipated to promote implementation of IC compaction monitoring technologies into earthwork construction practice in the United States.

INTRODUCTION

The Iowa State University research team conducted field investigation on the US69 project located near Pleasanton, Kansas from August 17–25, 2008 using Caterpillar and Sakai single drum intelligent compaction (IC) rollers. The project involved constructing calibration and production test areas with fine grained cohesive subgrade materials (identified as Type II materials in the project proposal). An open house was conducted near the end of the investigation to disseminate results from current and previous IC projects. Kansas DOT, contractor, and University of Kansas personnel and manufacturer representatives participated in the open house.

Caterpillar IC roller equipped with *machine drive power* (MDP) and Sakai IC roller equipped with *compaction control value* (CCV) measurement systems were evaluated on the project. The two machines were initially setup with padfoot drums. To the authors' knowledge this is first project to document Sakai CCV measurements for the padfoot roller configuration. Sakai padfoot drum was outfitted with a smooth drum shell kit near the end of the project for comparison to padfoot IC measurements. Both machines were equipped with real time kinematic (RTK) global positioning system (GPS) and proprietary on-board display and documentation systems. Goals of this field investigation were to:

- Evaluate the effectiveness of the padfoot roller IC measurement values – MDP and CCV, in assessing the compaction quality of Type II fine grained cohesive subgrade materials
- Develop project specific correlations between padfoot roller IC measurement values and various conventionally used in-situ point measurements in earthwork quality control (QC) and quality assurance (QA) practice, and
- Evaluate the advantages of using the technology for production compaction operations.

Calibration test strips involved obtaining IC measurement values on different materials encountered on the project in conjunction with in-situ point measurements at multiple roller passes for correlation analysis. IC measurements were obtained at different machine vibration amplitude settings (i.e., static, low, and high amplitudes) to evaluate the influence of amplitude on the correlations. Production work involved obtaining IC measurements during compaction of seven lifts of cohesive subgrade materials in an embankment with in-situ QC/QA point measurements at select random locations. Obtaining spatially referenced IC measurement values during production compaction provide the opportunity to: (a) evaluate the impact of pass coverage information; (b) perform real-time data analysis and visualization, (c) identify isolated soft spots, (d) link to calibration data and specifications, (e) quantify and characterize non-uniformity. Some of these advantages have been demonstrated using data obtained from production test areas. Geostatistical analysis methods (i.e., semivariogram) in combination with conventional statistics were used to characterize and quantify non-uniformity of compacted fill materials using data from production test areas.

This report presents brief background information for the two measurement systems evaluated in this study (CCV and MDP) and documents the results and analysis from the test beds and the field demonstration activities. Results presented in this report with padfoot roller IC measurements in comparison with conventionally used point measurements (i.e., nuclear moisture-density gauge, light weight deflectometer, falling weight deflectometer, static plate load test, and dynamic cone penetrometer) are of high priority among many state DOTs and contractor personnel. These results should be of significant interest to the pavement, geotechnical, and construction engineering community and are anticipated to promote implementation of IC compaction monitoring technologies into earthwork construction practice in the United States.

BACKGROUND

Roller-Integrated Compaction Control Value (CCV)

Sakai *Compaction Control Value* (CCV) is a vibratory-based technology which makes use of an accelerometer mounted to the roller drum to create a record of machine-ground interaction with the aid of GPS. The concept behind determination of CCV is that as the ground stiffness increases, the roller drum starts to enter into a "jumping" motion which results in vibration accelerations at various frequency components. This is illustrated in Figure 1.

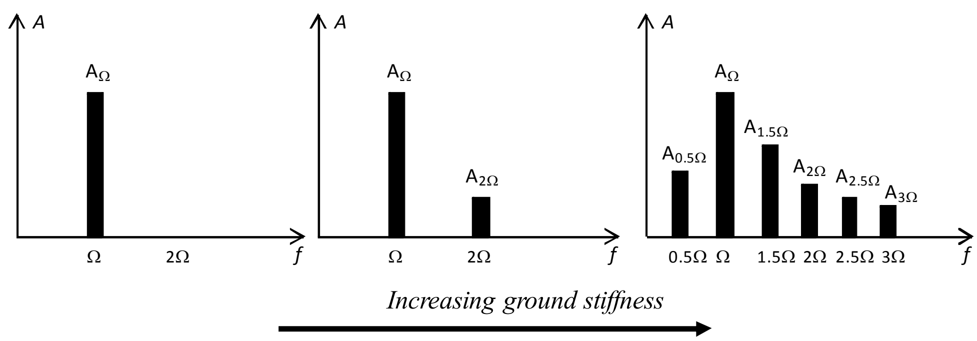

Figure 1. Changes in amplitude spectrum with increasing ground stiffness (modified from Sakai Manual)

The CCV is calculated using the acceleration data from first subharmonic (0.5Ω), fundamental (Ω), and higher-order harmonics (1.5Ω, 2Ω, 2.5Ω, 3Ω) as presented in Eq. 1.

$$CCV = \left[\frac{A_{0.5\Omega} + A_{1.5\Omega} + A_{2\Omega} + A_{2.5\Omega} + A_{3\Omega}}{A_{0.5\Omega} + A_{\Omega}} \right] \times 100 \qquad (1)$$

The vibration acceleration signal from the accelerometer is transformed through the Fast Fourier Transform (FFT) method and then filtered through band pass filters to detect the acceleration amplitude spectrum (Nohse and Kitano 2002, Scherocman et al. 2007). The Sakai SV610 padfoot roller used on the project is shown in Figure 2. A smooth drum shell kit was installed on the padfoot roller near the end of the project (Figure 2). The features of the two roller setups are summarized in Table 1. A computer display unit is mounted in front of the operator seat (see Figure 2) for on-board visualization of roller position, CCV, pass coverage and temperature (for asphalt only) information using Aithon MT software. Hereafter in this report, the CCV data obtained from padfoot and smooth drum roller setups are referenced as CCV_{PD} and CCV_{SD}, respectively.

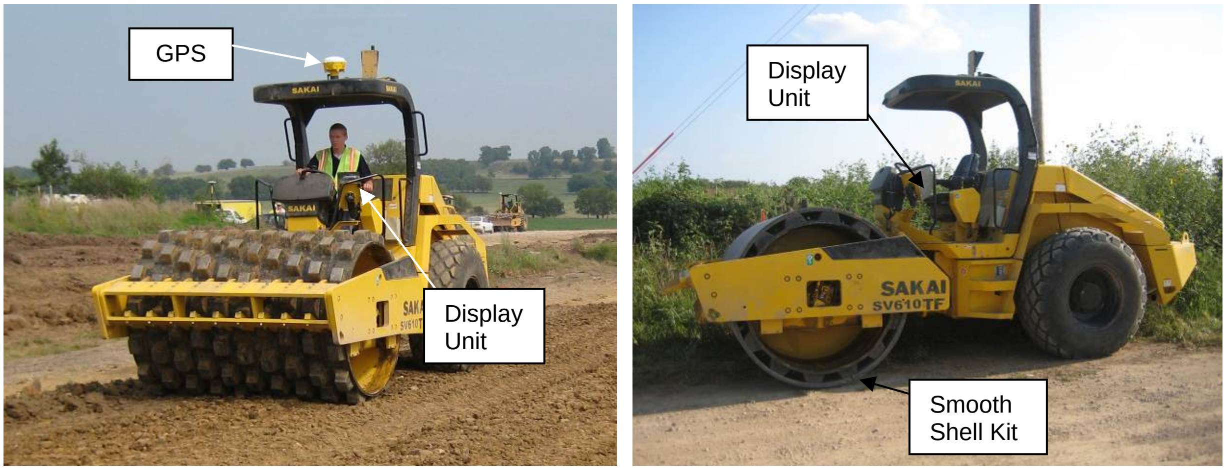

Figure 2. Sakai SV610 roller with padfoot and smooth drum setup used on the project

Table 1. Features of the Sakai roller used on the project

Feature	Description
Model	Sakai SV610 padfoot and smooth drum shell kit
Drum Weight	Padfoot: 69 kN (gross) Smooth: 91 kN (gross)
Drum Width	2.13 m
Frequency	33 Hz (low amplitude setting) and 26 Hz (high amplitude setting
Theoretical Amplitude	Padfoot: 0.93 mm (low amplitude) and 2.19 mm (high amplitude) Smooth: 0.63 mm (low amplitude) and 1.48 mm (high amplitude)
Centrifugal Force	Low Amplitude: 181 kN High Amplitude: 260 kN
Measurement	Sakai CCV (Compaction Control Value) CCV_{PD}: CCV obtained from padfoot drum setup CCV_{SD}: CCV obtained from smooth drum shell kit setup
Display Software	Aithon MT 1.0.0.4
GPS coordinates	UTM Zone 15N (NAD83)
Documentation	Location (Northing/Easting and Latitude/Longitude), Elevation, CCV, Temperature, Frequency, Date/Time, Direction (forward/backward), Vibration (On/Off), Vibration Control (amplitude setting), GPS Quality

Roller-Integrated Machine Drive Power (MDP) Value

A CP56 padfoot roller equipped with *machine drive power* (MDP) system (Figure 3) was used in this study. Controlled field studies documented by White and Thompson (2008), Thompson and White (2008), and Vennapusa et al. (2009) verified that MDP values can reliably indicate soil compaction for granular and cohesive soils. Detailed background information on the MDP system is provided by White et al. (2005).

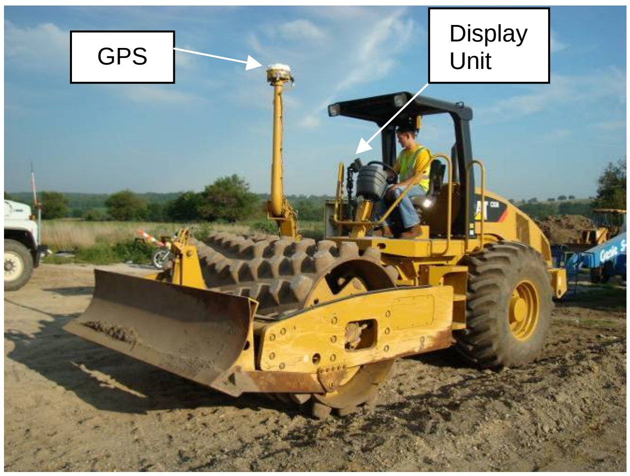

Figure 3. Caterpillar CS56 padfoot roller used on the project

The basic premise of determining soil compaction from changes in equipment response is that the efficiency of mechanical motion pertains not only to the mechanical system but also to the physical properties of the material being compacted. MDP is calculated using Eq. 2.

$$MDP = P_g - Wv\left(Sin\alpha + \frac{A'}{g}\right) - (mv + b) \quad (2)$$

where P_g = gross power needed to move the machine (kJ/s), W = roller weight (kN), A' = machine acceleration (m/s^2), g = acceleration of gravity (m/s^2), α = slope angle (roller pitch from a sensor), v = roller velocity (m/s), and m (kJ/m) and b (kJ/s) = machine internal loss coefficients specific to a particular machine (White et al. 2005). MDP is a relative value referencing the material properties of the calibration surface, which is generally a hard compacted surface (MDP = 0 kJ/s). Positive MDP values therefore indicate material that is less compact than the calibration surface, while negative MDP values would indicate material that is more compacted than the calibration surface (i.e. less roller drum sinkage). The MDP values (hereafter referred to as MDP_{80} or MDP_{40} depending on the setting) obtained from the machine used in this research study were recalculated to range between 1 and 150 using Eqs. 3 and 4.

$$MDP_{80} = 108.47 - 0.717(MDP) \quad (3)$$

$$MDP_{40} = 54.23 - 0.355(MDP) \quad (4)$$

Eq. 3 was used for testing from 08/18/2008 to 08/19/2008 where the calibration surface with MDP = 0 kJ/s was scaled to MDP_{80} = 150, and a soft surface with MDP = 108.47 kJ/s (80000 lb-ft/s) was scaled to MDP_{80} = 1. To increase resolution, Eq. 4 was used from 08/20/2008 to 08/22/2008, where the calibration surface with MDP = 0 kJ/s was scaled to MDP_{40} = 150 and a soft surface with MDP = 54.23 kJ/s (40000 lb-ft/s) was scaled to MDP_{40} = 1. A computer display unit is mounted in front of the operator seat (see Figure 3) for on-board visualization of roller position, MDP, vibration amplitude, frequency, and pass coverage information using AccuGrade software. The MDP values are displayed as Caterpillar Compaction Value (CCV) on the on-board AccuGrade display unit. The roller features are summarized in Table 2.

Table 2. Features of the Caterpillar padfoot roller used on the project

Feature	Description
Model	Caterpillar CS56
Drum Weight	60 kN
Drum Geometry	2.13 m width and 1.55 m diameter (over pads)
Frequency	30 Hz
Theoretical Amplitude	0.90 mm (low amplitude) 1.80 mm (high amplitude)
Centrifugal Force	Low Amplitude: 133 kN High Amplitude: 266 kN
Measurement	MDP_{80} or MDP_{40} (shown as CCV in the output)
Display Software	AccuGrade
GPS coordinates	UTM Zone 15N (NAD83)
Output Documentation	Date/Time, Location (Northing/Easting/Elevation of left and right ends of the roller drum), Speed, CCV, Frequency, Amplitude, Direction (forward/backward), Vibration (On/Off)

EXPERIMENTAL TESTING

Description of Test Beds

A total of seven test beds (TBs) consisting of cohesive subgrade clay materials were constructed and tested in this field study. A summary of each test bed with material conditions, machine amplitude settings used for compaction, number of passes, and in-situ point measurements obtained is provided in Table 3 and Table 4 for calibration test areas and production test areas, respectively. A summary of soil index properties for each test bed material is provided in Table 5. A summary sheet for each test bed showing construction photos and a brief description of the construction process is provided in the Appendix.

TBs 1, 2, 3 (lift 4 calibration), 4, and 5 involved construction of calibration test strips by obtaining in-situ point measurements at multiple roller passes. TB3 involved obtaining IC measurements during production construction with seven lifts of weathered shale and lean clay fill materials placed over wet/soft foundation subgrade layer. In-situ point measurements were obtained at select locations on the foundation subgrade and on each lift after final pass. TBs 6 and 7 involved mapping a production area consisting of stiff weathered shale and relatively soft lean clay subgrade materials, respectively.

Table 3. Summary of test beds and in-situ testing (calibration test strips)

TB	Date	Machine	Drum	Amplitude Setting	Notes/In-situ Test Measurements
1 Lane 1	08/18	C	Padfoot	Static	*w*, γ_d, CBR, and $E_{LWD\text{-}Z2}$ after 9 passes
1 Lane 2				0.90 mm	
1 Lane 1	08/18	S	Padfoot	0.93 mm	$E_{FWD\text{-}D4.5}$ after mapping passes
1 Lane 2				2.19 mm	
2 Lane 1	08/18	C	Padfoot	0.90 mm	*w*, γ_d, and $E_{LWD\text{-}Z2}$ after 12 passes
2 Lane 2				Static	*w*, γ_d, CBR, and $E_{LWD\text{-}Z2}$ after 0, 1, 2, 4, 8, and 12 passes
2 Lane 3				1.80 mm	*w*, γ_d, and $E_{LWD\text{-}Z2}$ after 12 passes
4 Lane 1	08/19	S	Padfoot	2.19 mm	None
4 Lane 2				0.93 mm	*w*, γ_d, CBR, and $E_{LWD\text{-}Z2}$ after 0, 1, 4, and 13 passes, and $E_{FWD\text{-}D4.5}$ after 13 passes
4 Lane 3				2.19 mm	
3 Lift 4 Calibration	08/20	S	Padfoot	2.19 mm	*w*, γ_d, and $E_{LWD\text{-}Z2}$ after 0, 1, 2, 4, 8, and 12 passes
5*	08/20	C	Padfoot	Static	*w*, γ_d, CBR, and $E_{LWD\text{-}Z2}$ after 4 pass

Notes: C – Caterpillar, S – Sakai, *w* – moisture content, γ_d – dry unit weight, CBR – California bearing ratio determined from dynamic cone penetrometer (DCP) test, $E_{LWD\text{-}Z2}$ – elastic modulus determined using Zorn 200 mm plate diameter light weight deflectometer (LWD), $E_{FWD\text{-}D4.5}$ – elastic modulus determined using Dynatest 450 mm plate diameter falling weight deflectometer (FWD) test, *Soft/wet organic soils.

Table 4. Summary of test beds and in-situ testing (production areas)

TB	Date	Machine(s)	Drum	Amplitude Setting	Notes/In-situ Test Measurements
3 Lift 0	08/19/2008	C	Padfoot	0.90	w, γ_d, CBR, and $E_{LWD\text{-}Z2}$ after 3 passes
3 Lift 1	08/19/2008	C	Padfoot	0.90	w, γ_d, and $E_{LWD\text{-}Z2}$ after 3 to 8 passes
3 Lift 2	08/19/2008	C	Padfoot	0.90	
3 Lift 3	08/20/2008	C	Padfoot	0.90	
3 Lift 4	08/20/2008	C	Padfoot	0.90	
3 Lift 5	08/20/2008	C	Padfoot	0.90	w, γ_d, CBR, and $E_{LWD\text{-}Z2}$ after 4 passes
3 Lift 6	08/21/2008	S	Padfoot	0.93	w, γ_d, and $E_{LWD\text{-}Z2}$ after 4 passes
3 Lift 6	08/21/2008	C	Padfoot	0.90	Mapping pass after Caterpillar padfoot roller passes
3 Lift 7	08/21/2008	C	Padfoot	0.90	w, γ_d, CBR, and $E_{LWD\text{-}Z2}$ after 4 passes
3 Lifts 1-5	08/19/2008 to 08/21/2008	S	Padfoot	2.19 mm	Mapping pass after Caterpillar padfoot roller passes
6	08/20/2008	S	Padfoot	0.93 mm	$E_{LWD\text{-}Z2}$, E_{V1}, E_{V2}, and $E_{FWD\text{-}D4.5}$ after padfoot mapping passes
7	08/20/2008	S	Padfoot	2.19 mm	
6	08/22/2008	S	Smooth	0.63 mm	
7	08/22/2008	S	Smooth	1.48 mm	

Notes: C – Caterpillar, S – Sakai, w – moisture content, γ_d – dry unit weight, CBR – California bearing ratio determined from dynamic cone penetrometer (DCP) test, $E_{LWD\text{-}Z2}$ – elastic modulus determined using Zorn 200 mm plate diameter light weight deflectometer (LWD), E_{V1} and E_{V2} – initial and reload moduli determined from static plate load test (PLT), $E_{FWD\text{-}D4.5}$ – elastic modulus determined using Dynatest 450 mm plate diameter falling weight deflectometer (FWD) test.

Table 5. Summary of soil index properties

Parameter	Lean Clay Subgrade – TBs 1, 2, and 4	Foundation Layer Fat Clay Subgrade – TB3	Weathered Shale Subgrade – TB3	Lean Clay Subgrade – TB3
Soil ID	Soil # 1	Soil # 2	Soil # 3	Soil # 4
Standard Proctor Test				
γ_{dmax} (kN/m^3)	17.63	15.30	19.40	17.48
w_{opt}	14.2	22.5	12.0	16.7
Modified Proctor Test				
γ_{dmax}	19.12	17.60	20.61	18.77
w_{opt}	12.1	15.9	9.6	14.7
Gravel Content (%) (> 4.75mm)	13	0	11	7
Sand Content (%) (4.75mm – 75μm)	30	4	18	21
Silt Content (%) (75μm – 2μm)	36	47	46	39
Clay Content (%) (< 2μm)	21	49	25	33
Liquid Limit, LL (%)	28	54	35	36
Plastic Limit, LL (%)	16	20	18	16
Plasticity Index, PI	12	34	17	20
AASHTO	A-6(4)	A-7-6(36)	A-6(10)	A-6(12)
USCS	CL	CH	CL	CL
Specific Gravity, G_s	2.66	2.63	2.75	2.66

In-situ Testing Methods

Five different in-situ testing methods were employed in this study to evaluate the in-situ soil engineering properties (Figure 4): (a) 200-mm plate diameter Zorn LWD setup with 50 mm drop height to determine elastic modulus (E_{LWD-Z2}), (b) Dynamic Cone Penetrometer (DCP) to determine California bearing Ratio (CBR), (c) calibrated nuclear moisture-density gauge (NG), (d) 450-mm plate diameter Dynatest FWD to determine elastic modulus ($E_{FWD-D4.5}$), and (e) 300-mm diameter static PLT to determine initial (E_{V1}) and re-load modulus (E_{V2}). LWD, DCP, NG, and PLT tests were conducted by the ISU research team with aid of the geotechnical mobile lab, and FWD tests were conducted by Kansas Department of Transportation (KSDOT) personnel.

LWD tests were performed following manufacturer recommendations (Zorn 2003) and the E_{LWD-Z2} value was determined using Eq. 4, where E = elastic modulus (MPa), d_0 = measured settlement (mm), η = Poisson's ratio, σ_0 = applied stress (MPa), r = radius of the plate (mm), F = shape factor depending on stress distribution (assumed as $\pi/2$) (see Vennapusa and White 2009a). When padfoot roller was used for compaction, the material was carefully excavated down to the bottom of the pad to create a level surface for LWD testing.

$$E = \frac{(1-\eta^2)\sigma_0 r}{d_0} \times F \tag{4}$$

DCP test was performed in accordance with ASTM D6951-03 to determine dynamic cone penetration index (DPI) and calculate CBR using Eq. 5. The DCP test results are presented in this report as CBR point values or CBR profiles. When the data is presented as point values, the data represents an average CBR of the compaction layer depth.

$$CBR = \frac{292}{DPI^{1.12}} \tag{5}$$

$E_{FWD\text{-}D4.5}$ values were determined from the stiffness values using Eq. 4. Stiffness values were provided by Transtec. Static PLT's were conducted by applying a static load on 300 mm diameter plate against a 6.2kN capacity reaction force. The applied load was measured using a 90-kN load cell and deformations were measured using three 50-mm linear voltage displacement transducers (LVDTs). The load and deformation readings were continuously recorded during the test using a data logger. The E_{V1} and E_{V2} values were determined from Eq. 4 using deflection values at 0.1 and 0.2 MPa applied contact stresses as illustrated in Figure 5.

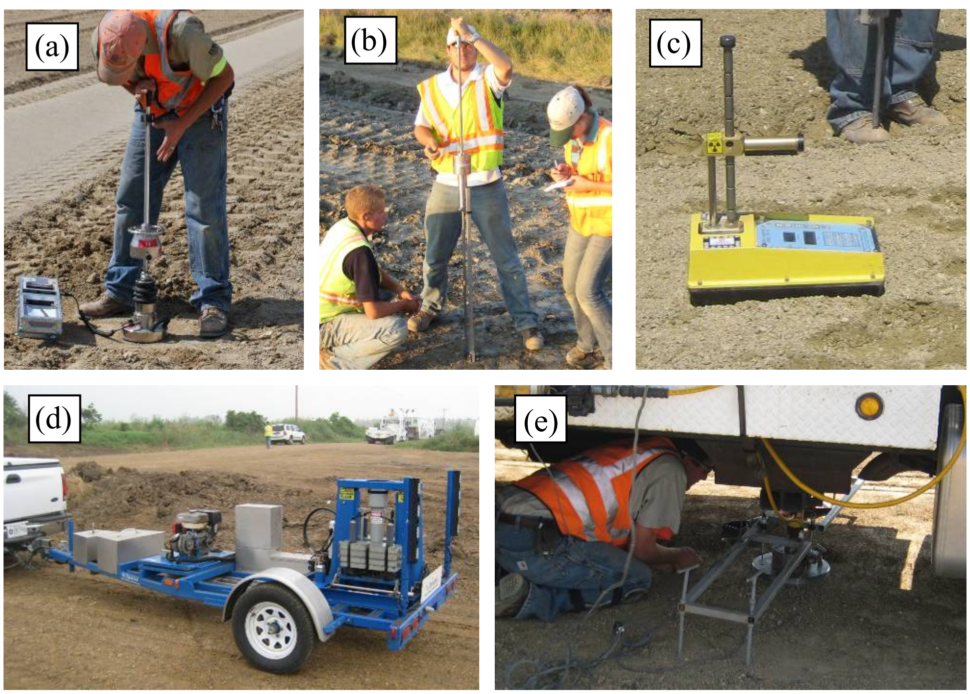

Figure 4. In-situ testing methods used on the project: (a) 200-mm plate diameter Zorn LWD, (b) dynamic cone penetrometer, (c) nuclear moisture-density gauge, (d) KSDOT 450-mm plate diameter Dynatest FWD, and (e) 300-mm plate diameter static PLT

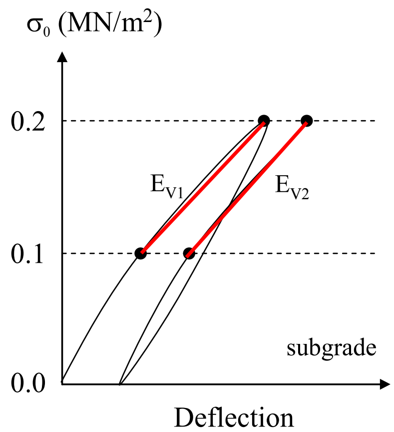

Figure 5. E_{V1} and E_{V2} determination procedure from static PLT for subgrade materials

EXPERIMENTAL TEST RESULTS

Caterpillar and Sakai Test Strips – TB1

Construction of TB and Test Results

TB 1 consisted of a relatively stiff compacted lean clay subgrade material (USCS classification: CL). The test bed area was generally sloping down from south towards north (see elevation map in Figure 7). Testing involved obtaining IC measurement values from multiple roller passes in two roller lanes (see Figure 6) and conducting in-situ point measurements (w, γ_d, CBR, $E_{LWD\text{-}Z2}$, and $E_{FWD\text{-}D4.5}$) for comparison. The two lanes were mapped using the Caterpillar padfoot roller for nine passes, followed by the Sakai padfoot roller for two passes. Static and low amplitude settings were used with the Caterpillar roller on lanes 1 and 2, respectively. Low and high amplitude settings were used with the Sakai roller on lanes 1 and 2, respectively. The Caterpillar roller was operated in two different directions (driving uphill and downhill) to evaluate the influence of driving grade slope on the MDP_{80} values. MDP_{80} and elevation outputs from AccuGrade software and CCV_{PD} output from Aithon MT software are shown in Figure 7.

Figure 8 and Figure 9 show MDP_{80} values obtained from lanes 1 and 2, respectively for multiple roller passes along with change in elevation along the test bed. The MDP_{80} values appear repeatable when operated in one direction but not reproducible with change in direction of travel. The MDP_{80} values were affected by the grade slope in the direction of travel. Linear regression relationship between slope angle (α) and MDP_{80} values indicates a decrease in MDP_{80} values with increasing slope angle (see Figure 8 and Figure 9). The regression relationships produced an R^2 value = 0.6. Comparison between in-situ point measurements and MDP_{80} values is presented in Figure 10, Figure 11, and Figure 12. Changes in MDP_{80} along the lanes generally tracked well with changes in in-situ point measurements. Regression analysis results between in-situ point measurements and spatially paired nearest point MDP_{80} are presented later in this report.

CCV$_{PD}$ measurements from two consecutive mapping passes on lanes 1 and 2 in comparison with in-situ point measurements are presented in Figure 13, Figure 14, and Figure 15. Results indicate that CCV$_{PD}$ measurements are repeatable for the two passes and that changes observed in CCV$_{PD}$ across the lanes track well with changes in in-situ point measurements. Regression analysis results between in-situ point measurements and spatially paired nearest point CCV$_{PD}$ are presented later in this report.

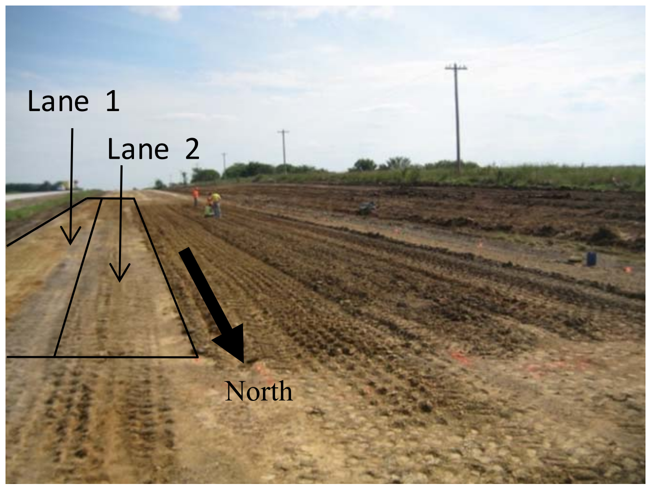

Figure 6. Picture showing lanes 1 and 2 on TB1

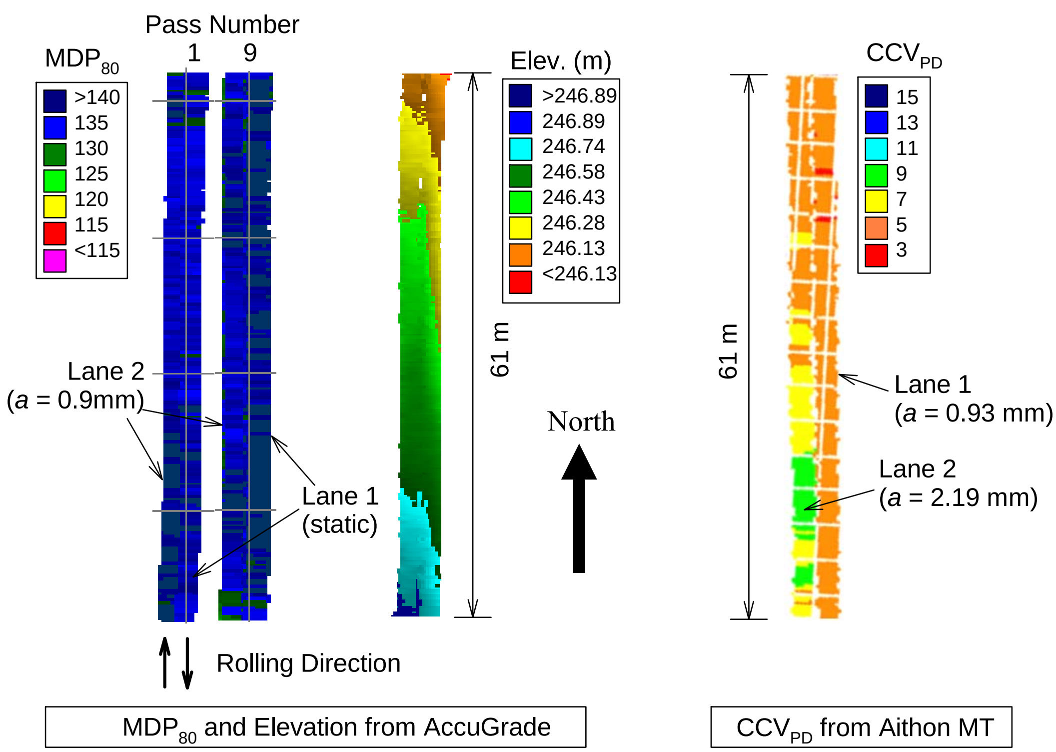

Figure 7. MDP$_{80}$ and elevation maps from Caterpillar AccuGrade software and CCV$_{PD}$ map from Sakai Aithon MT software – TB1 subgrade clay material lanes 1 and 2

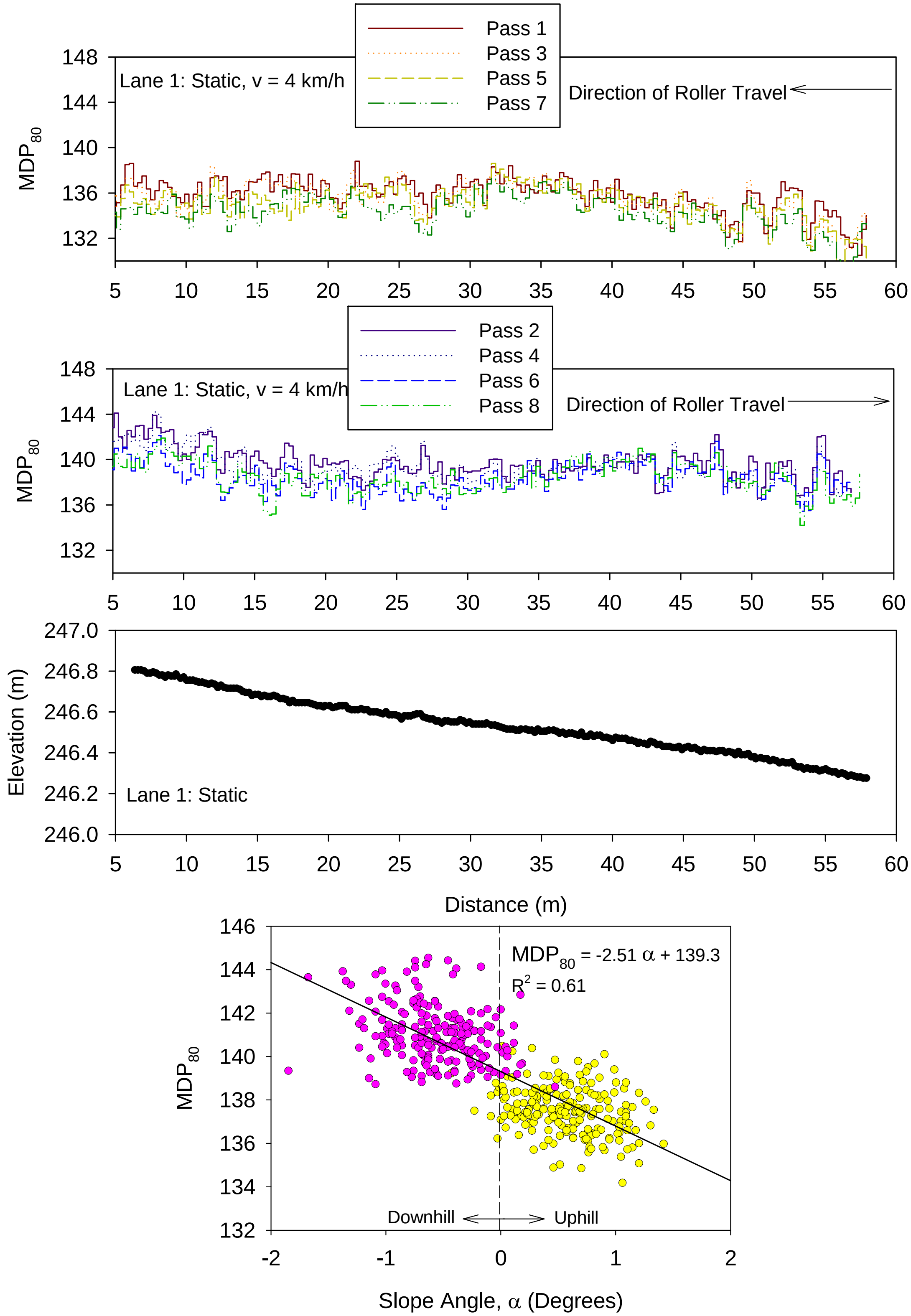

Figure 8. MDP_{80} for multiple roller passes on TB1 subgrade clay material lane 1 and linear regression relationship between slope angle and MDP_{80}

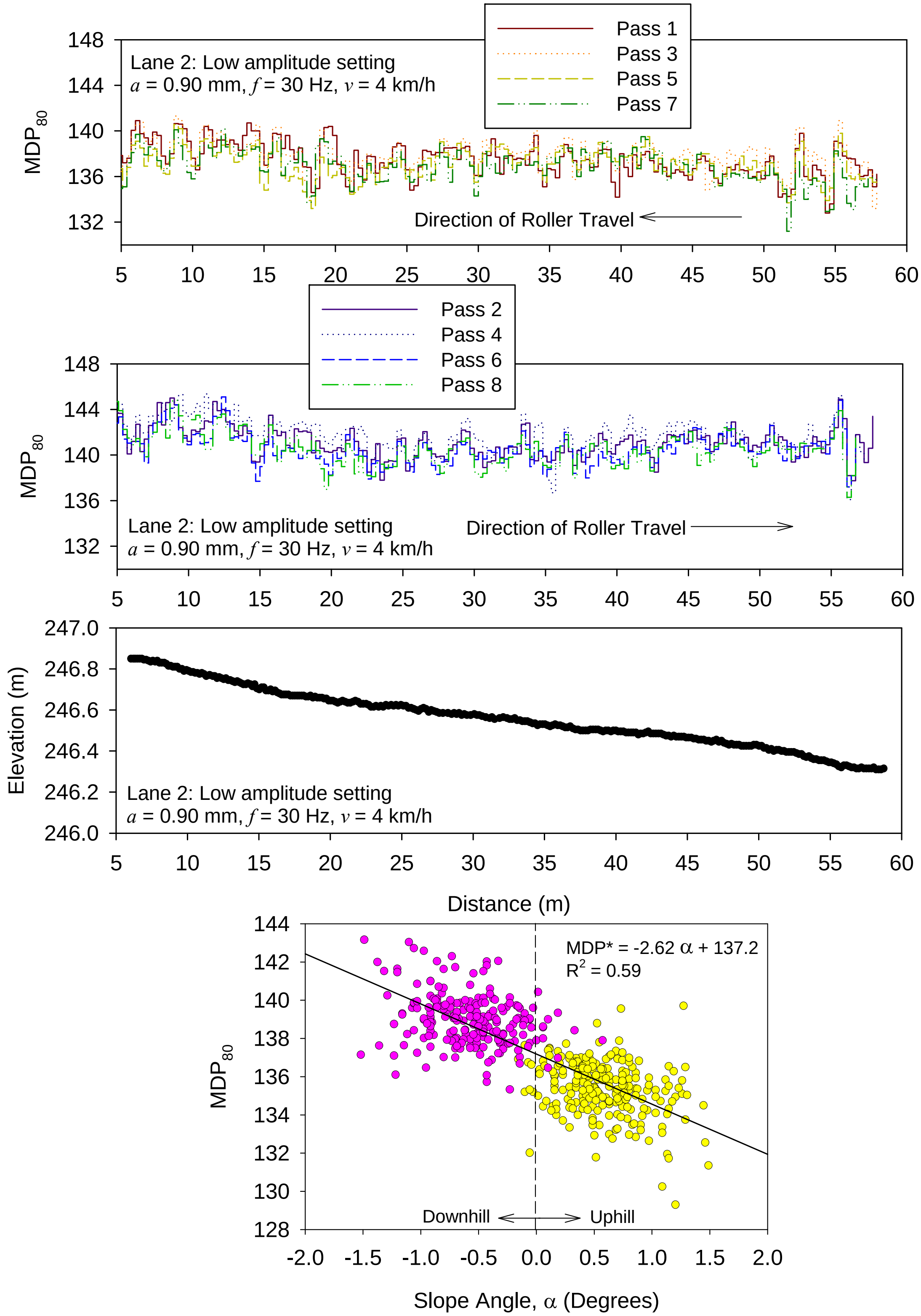

Figure 9. MDP_{80} for multiple roller passes on TB1 subgrade clay material lane 2 and linear regression relationship between slope angle and MDP_{80}

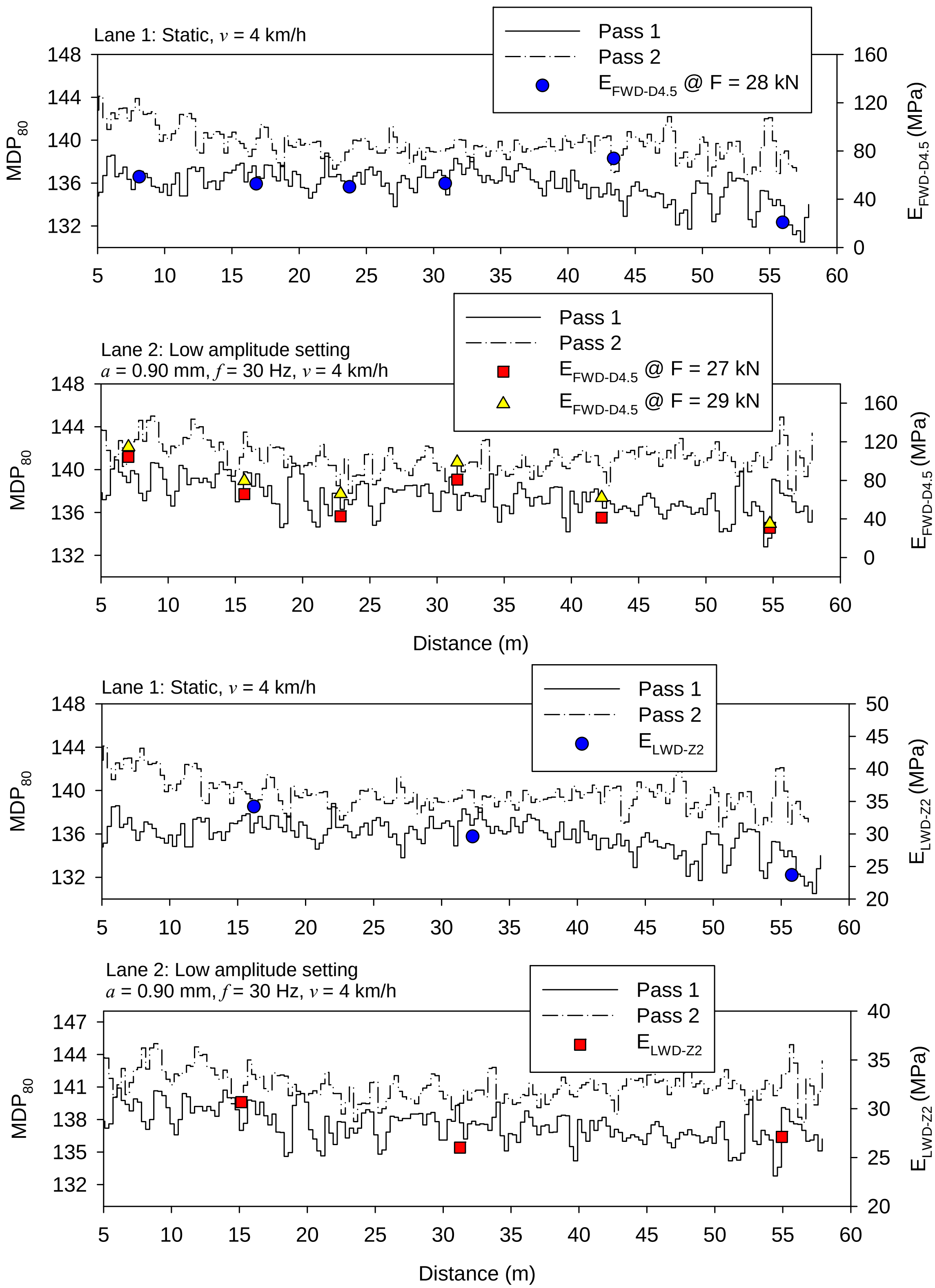

Figure 10. Comparison between MDP_{80} and E_{LWD-Z2} (top) and $E_{FWD-D4.5}$ (bottom) point measurements – TB1 subgrade clay material (note: passes 1 and 2 with opposite machine direction of travel)

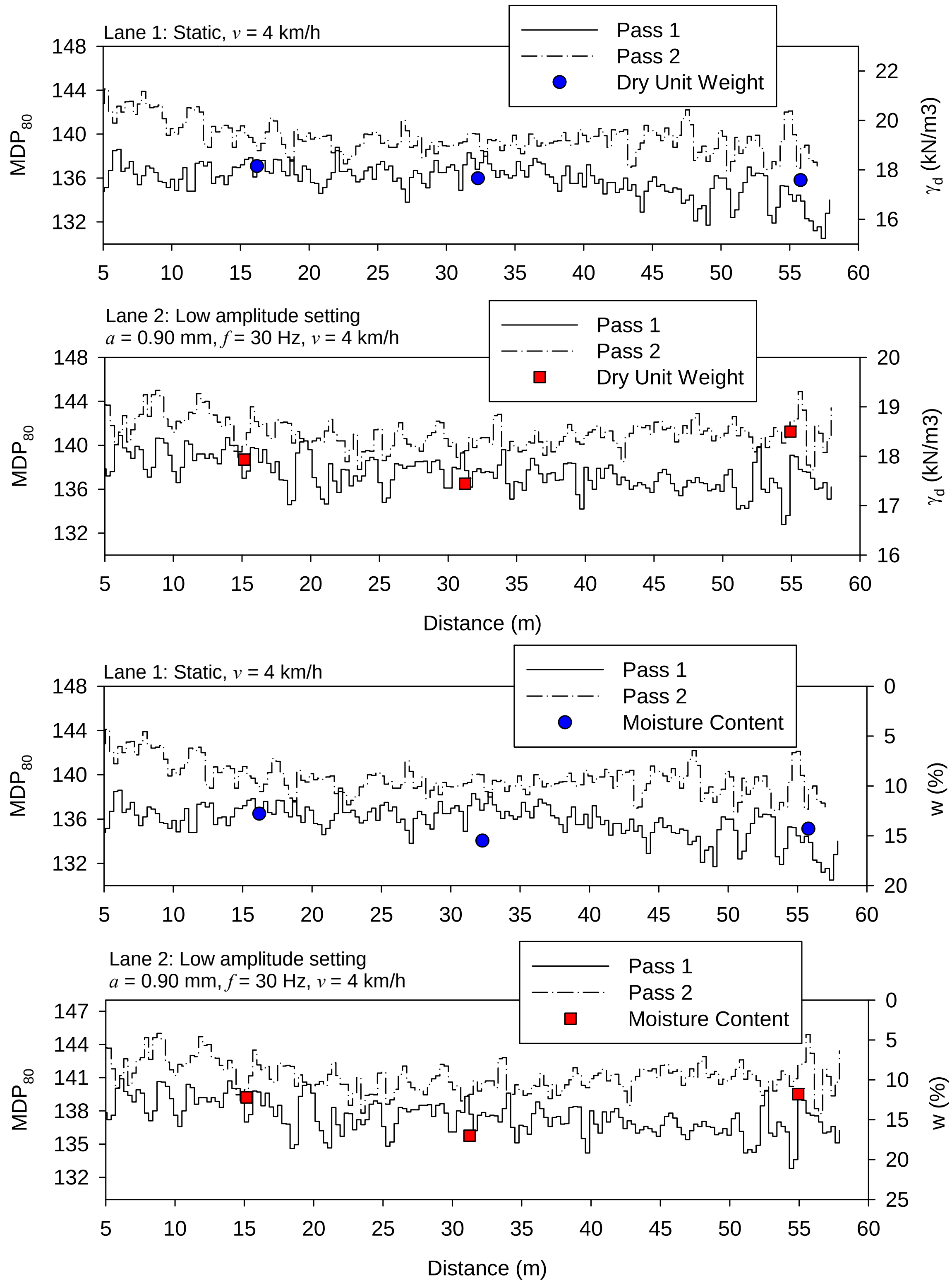

Figure 11. Comparison between MDP_{80} and nuclear moisture-density gauge point measurements – TB1 subgrade clay material (note: passes 1 and 2 with opposite machine direction of travel)

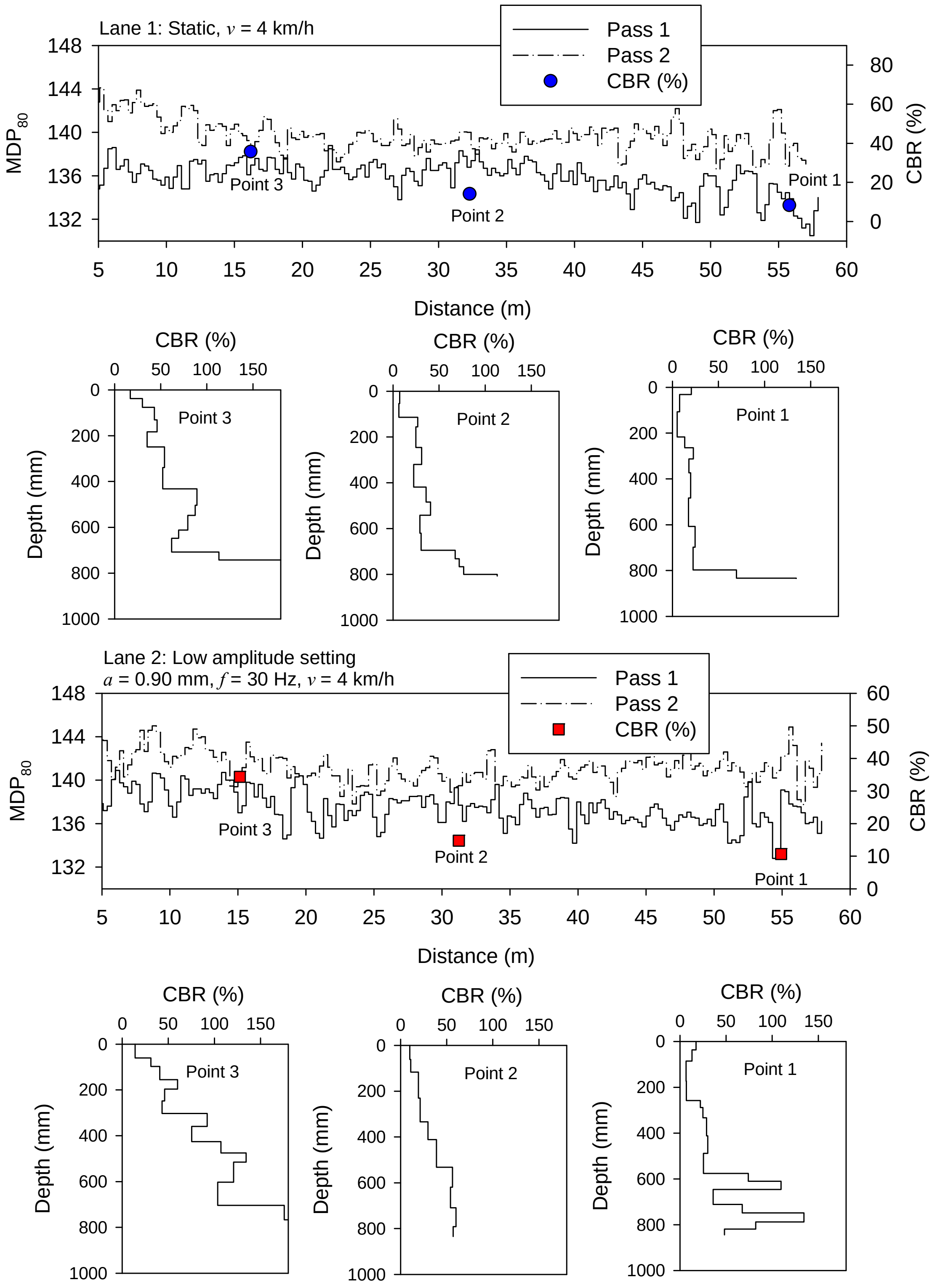

Figure 12. Comparison between MDP_{80} and DCP-CBR point measurements –TB1 subgrade clay material (note: passes 1 and 2 with opposite machine direction of travel)

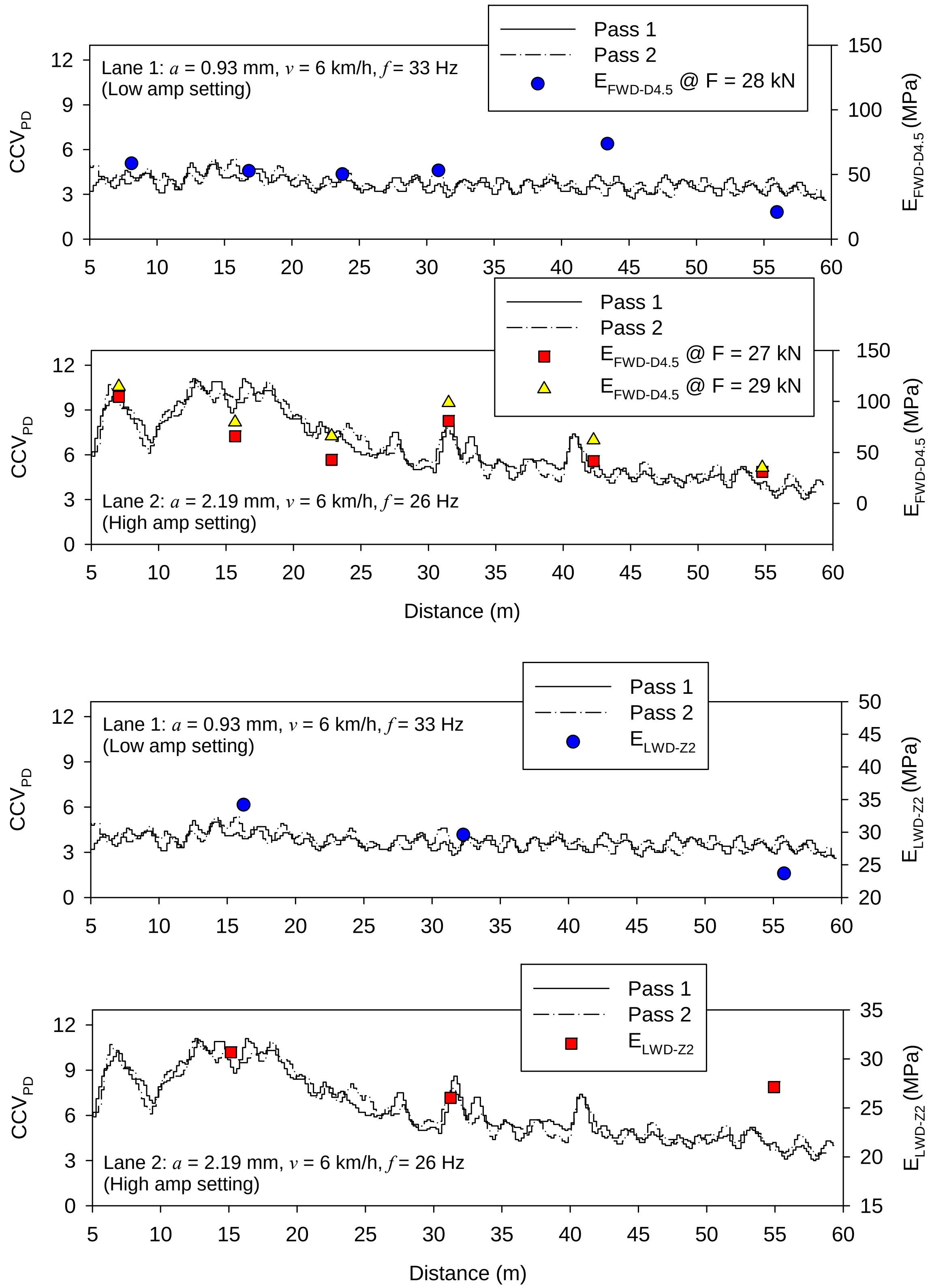

Figure 13. Comparison between CCV_{PD} and in-situ $E_{FWD-D4.5}$ and E_{LWD-Z2} point measurements – TB1 subgrade clay material

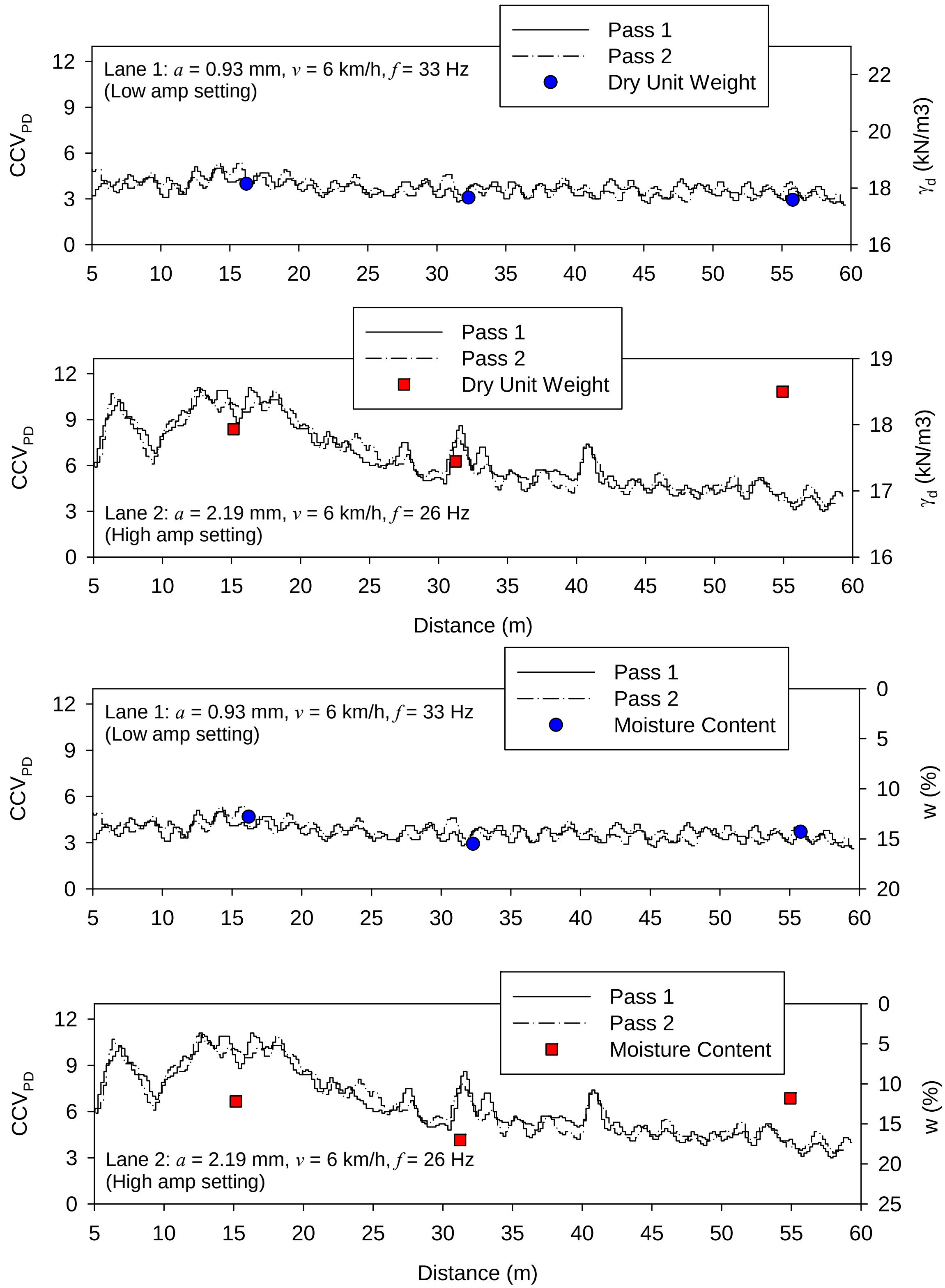

Figure 14. Comparison between CCV_{PD} and nuclear moisture-density gauge point measurements – TB1 subgrade clay material

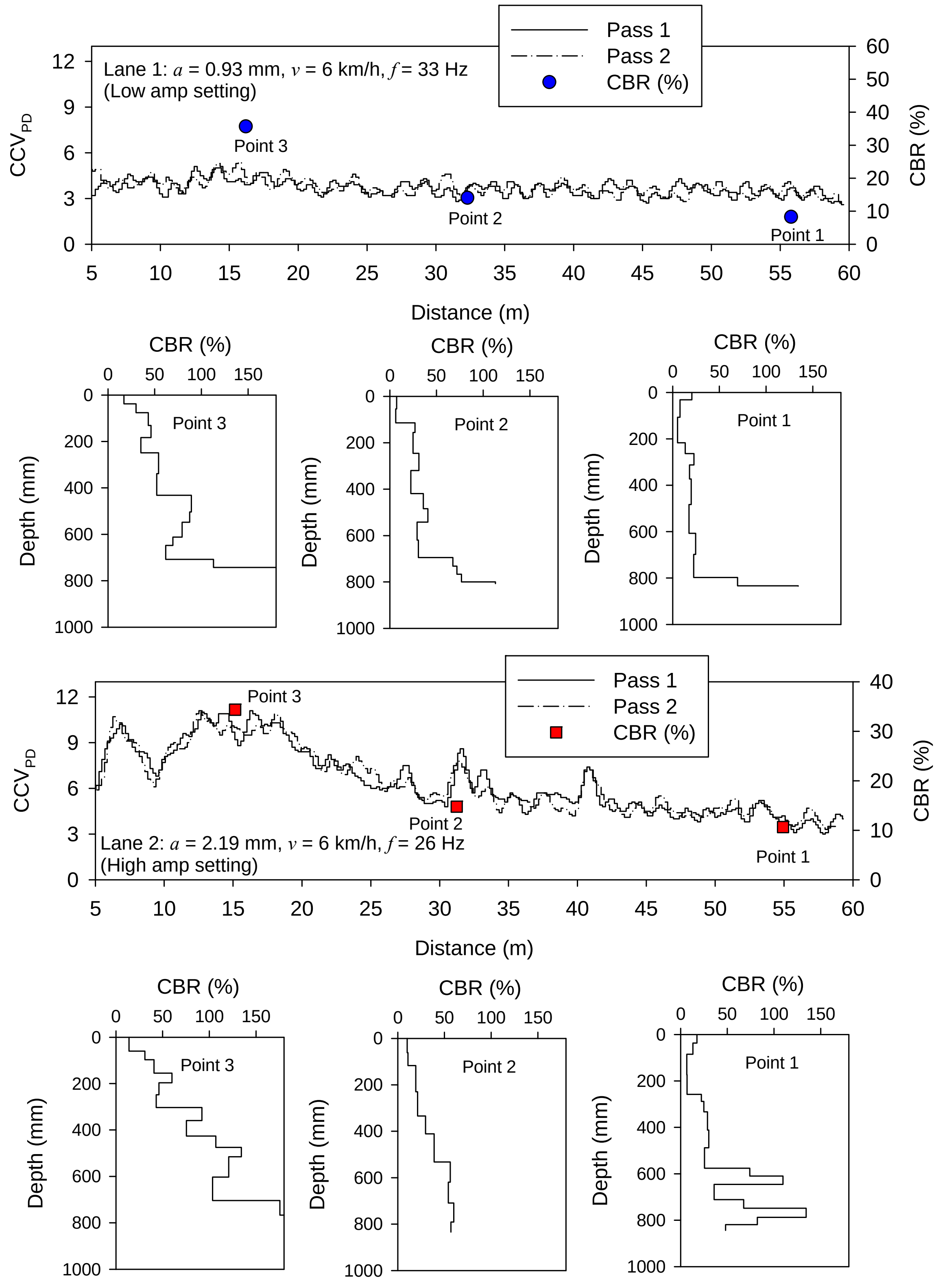

Figure 15. Comparison between CCV_{PD} and DCP-CBR point measurements –TB1 subgrade clay material (note: passes 1 and 2 with opposite machine direction of travel)

Summary of Key Findings

- MDP_{80} values are repeatable provided the direction of travel along the test bed is constant. The values are not reproducible with change in direction of travel along the test bed.
- MDP_{80} values were influenced by the sloping grade in the direction of travel. Regression relationship between slope angle (α) and MDP_{80} values produced an R^2 value = 0.6. The relationship indicates a decrease in MDP_{80} values with increasing slope angle.
- The CCV_{PD} values are repeatable.
- The MDP_{80} and CCV_{PD} values along the test bed generally track well with changes in in-situ point measurements.

Caterpillar MDP$_{80}$ Calibration Test Strips – TB2 Subgrade Clay

Construction of Test Bed and Test Results

TB2 was located adjacent to TB1 (see Figure 16 and Figure 17) and consisted of lean clay subgrade material (USCS classification: CL). The area was generally sloping down from south towards north. The test bed was prepared by scarifying the existing subgrade material with the ripper on a motor grader to a depth of about 200 to 250 mm and was compacted using the Caterpillar padfoot roller in three lanes (lanes 1 to 3) (see Figure 16 and Figure 17). Photographs showing preparation and construction of the test bed are presented in Figure 17. To help avoid the influence of sloping grade on MDP_{80} values (as indicated earlier in the results from TB1); the driving direction was kept constant for all three lanes (see Figure 16). Lanes 1, 2, and 3 were compacted in low, static, and high amplitude settings, respectively as illustrated in Figure 16. The area was compacted with 12 roller passes. In-situ w, γ_d, CBR, and $E_{LWD\text{-}Z2}$ point measurements were obtained after 1, 2, 4, and 8 roller passes on lane 2. In-situ w, γ_d, and $E_{LWD\text{-}Z2}$ point measurements were obtained after 12 roller passes on lanes 1 and 3.

MDP_{80} and elevation data for multiple passes on lanes 1, 2, and 3 are presented in Figure 18. The MDP_{80} data indicates that the values are repeatable and generally increase with roller passes. Comparison between MDP_{80} and different in-situ point measurements for lanes 1 and 3 are presented in Figure 19 and for lane 2 are presented in Figure 20 and Figure 21. Results indicate that all point measurements generally track well with variations observed in MDP_{80} measurements along the lanes. Results from linear regression analysis between MDP_{80} and in-situ point measurements are presented later in this report. Figure 22 shows average MDP_{80} compaction curves for lanes 1, 2, and 3. The average MDP_{80} (per pass) values for lanes 1 and 3 generally increased with roller passes. The average MDP_{80} values for lane 2 did not show a consistent increase. On average, MDP_{80} measurements with low and high amplitude settings showed similar compaction curves.

Average in-situ point measurement (per pass) compaction curves are shown in Figure 22. For lane 2, average $E_{LWD\text{-}Z2}$ increased from pass 1 to 8 and then no considerable increase was observed from pass 8 to 12. Similarly, average γ_d values on lane 2 increased from pass 1 to 4 and then no considerable increase was observed from pass 4 to 12. Figure 23 shows in-situ w-γ_d results after pass 12 in comparison with laboratory w-γ_d relationships determined from standard and modified Proctor tests. After pass 12, average γ_d on lanes 1, 2, and 3 were at about 89%, 91%, and 96% of the standard Proctor γ_{dmax}, respectively. The average w on lanes 1, 2, and 3 after pass 12 were at about -2%, 0.4%, and 0.4% of the standard Proctor w_{opt}, respectively.

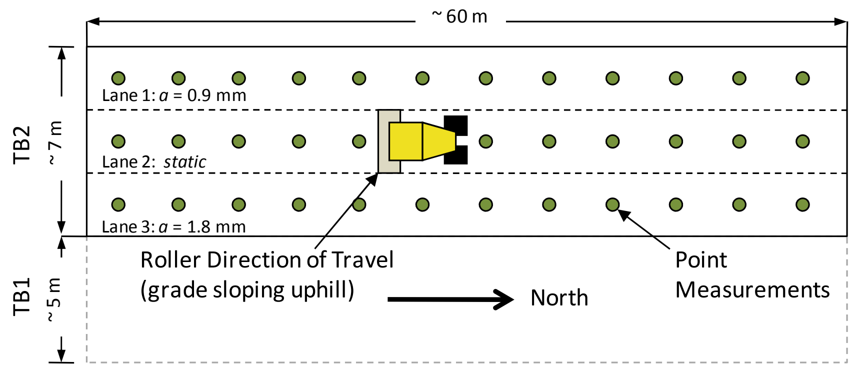

Figure 16. Experimental testing setup on TB2 (TB1 shown for reference)

Figure 17. Photographs showing construction process and test bed layout – TB 2 lanes 1, 2, and 3 subgrade clay material (TB1 shown for reference)

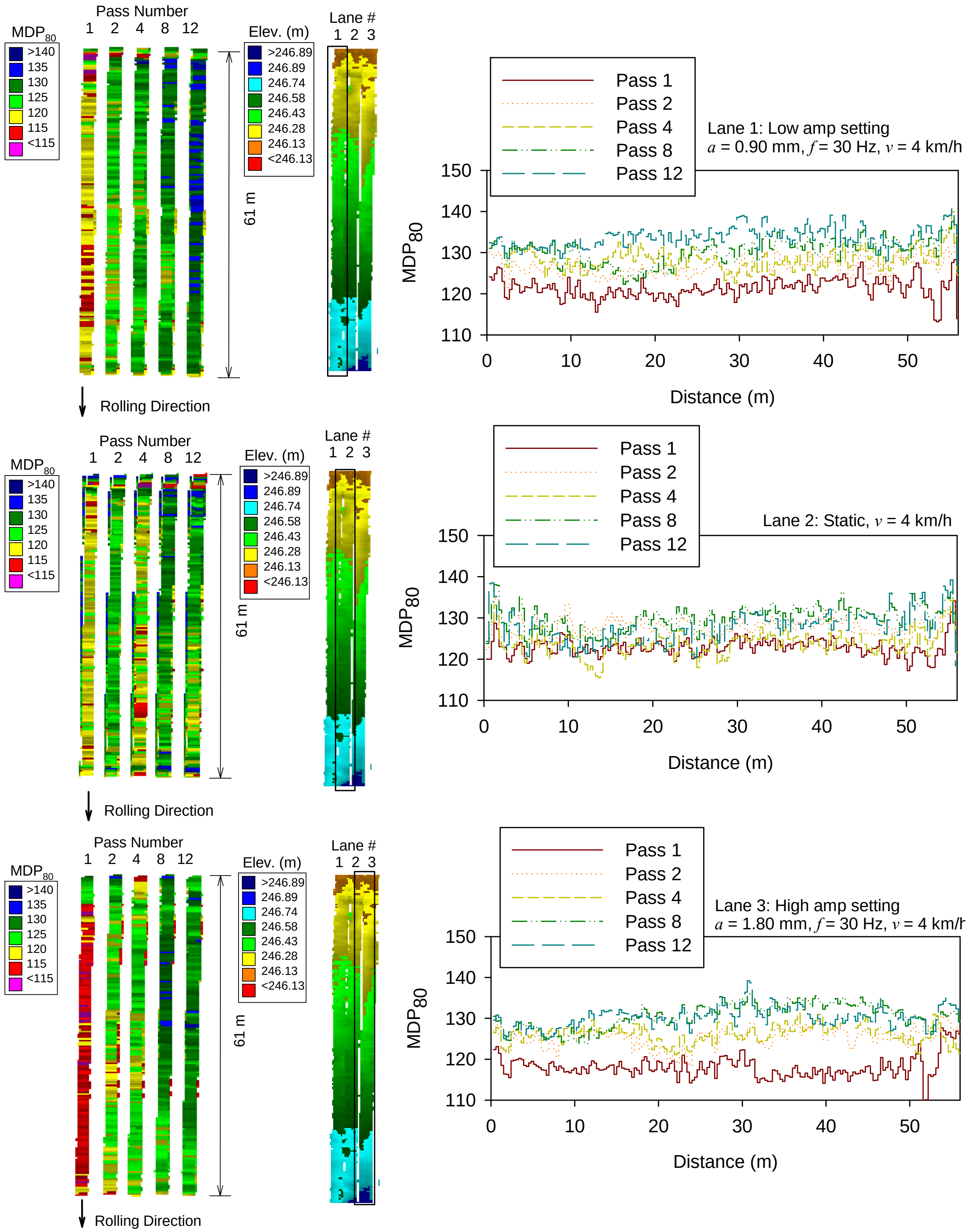

Figure 18. MDP$_{80}$ measurements for multiple passes on TB2 subgrade clay material lanes 1, 2, and 3

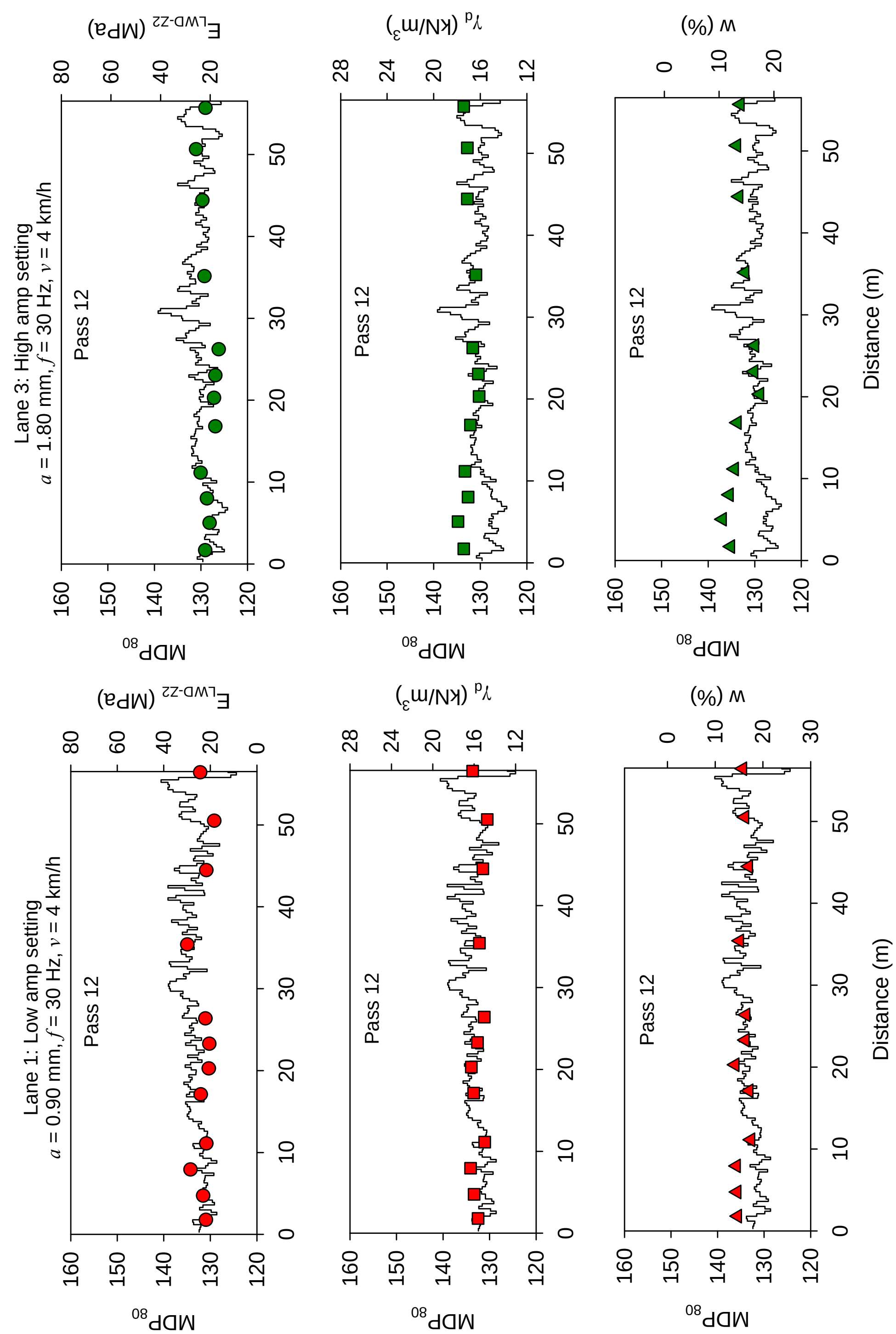

Figure 19. Comparison between pass 12 MDP_{80} measurements and in-situ point measurements on TB2 lanes 1 and 3 subgrade clay material

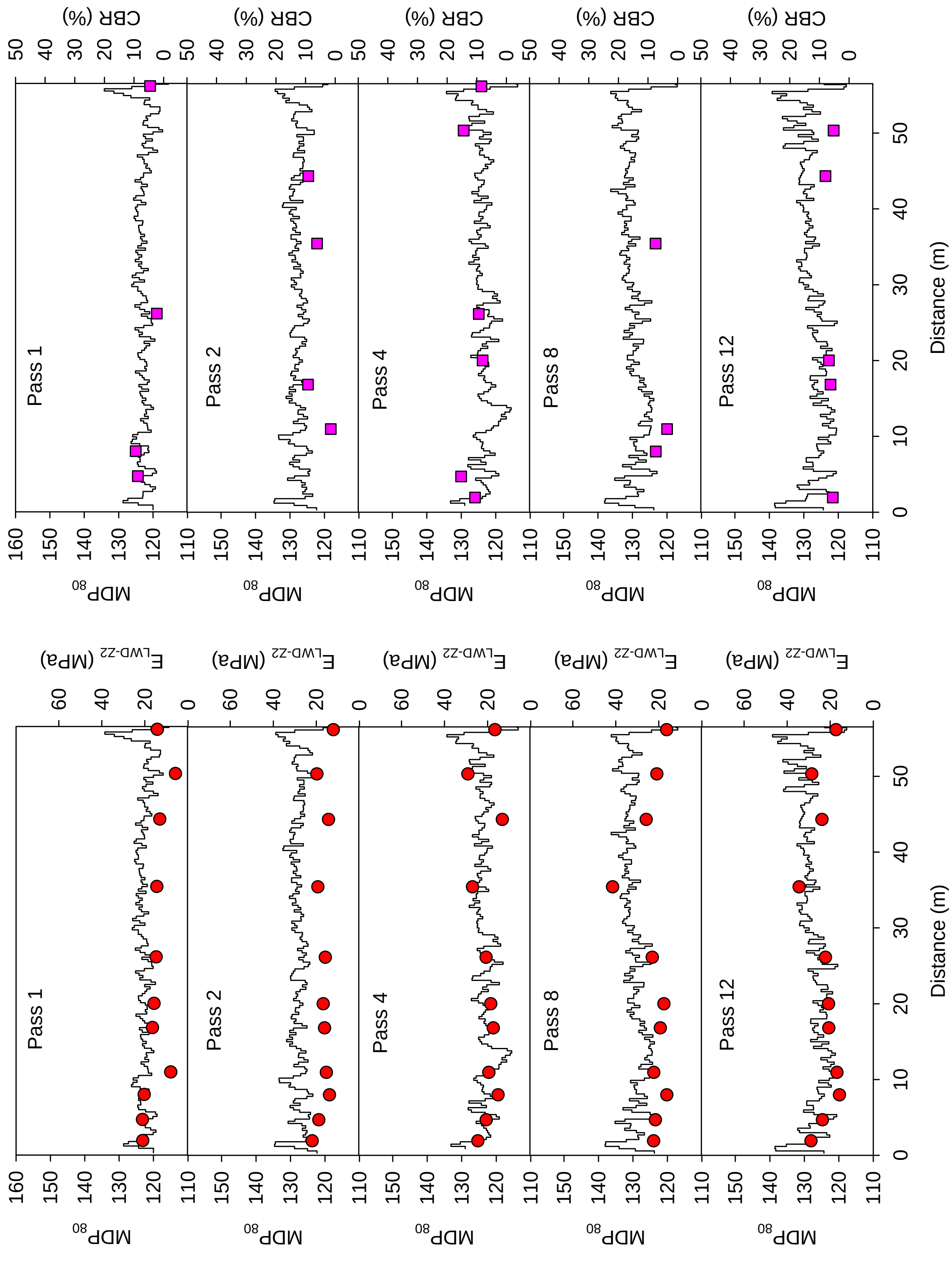

Figure 20. Comparison between MDP_{80} measurements (static) and in-situ $E_{LWD\text{-}Z2}$ and CBR point measurements from multiple passes on TB2 lane 2 subgrade clay material

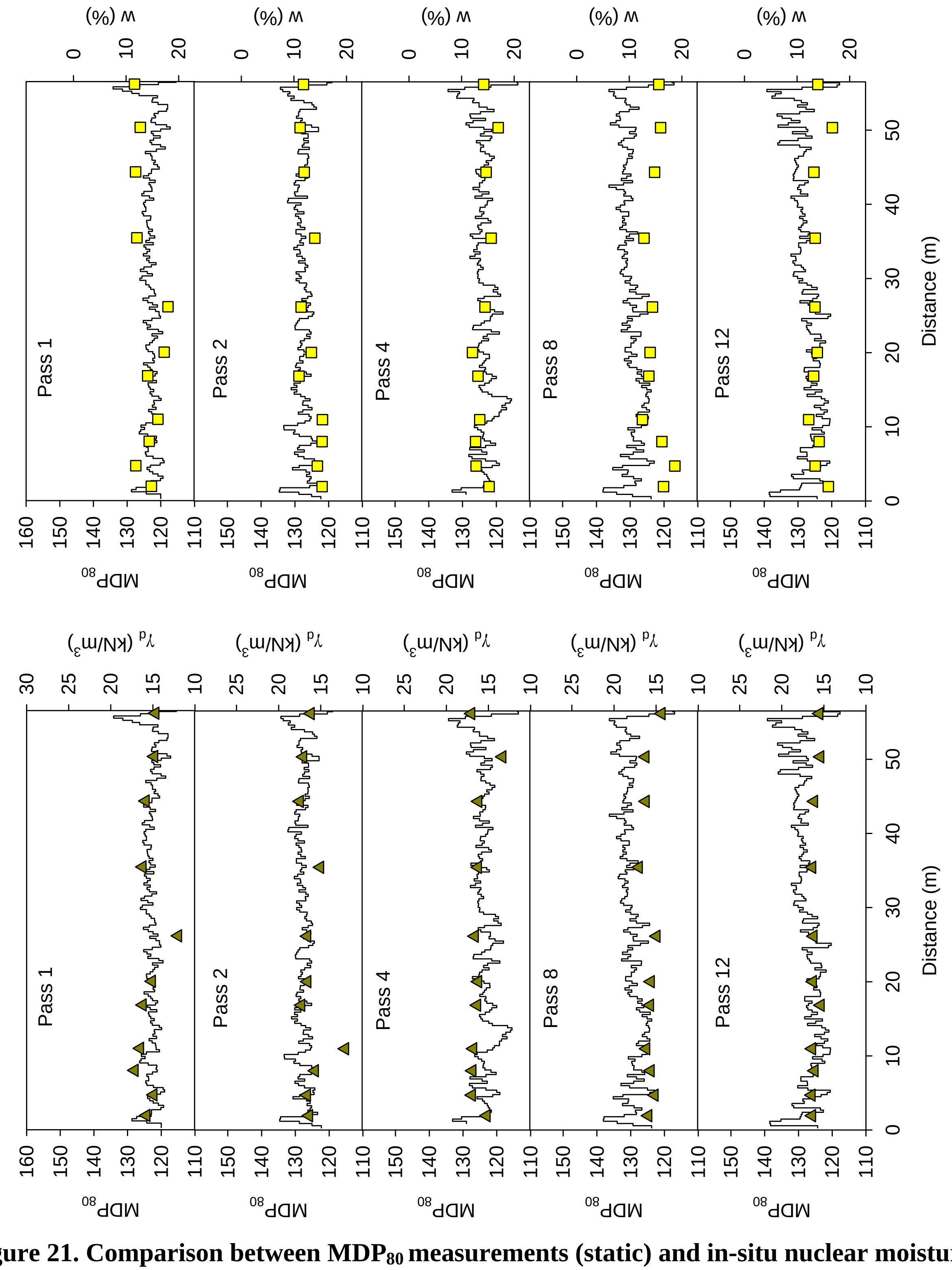

Figure 21. Comparison between MDP_{80} measurements (static) and in-situ nuclear moisture-dry unit weight point measurements from multiple passes on TB2 lane 2 subgrade clay material

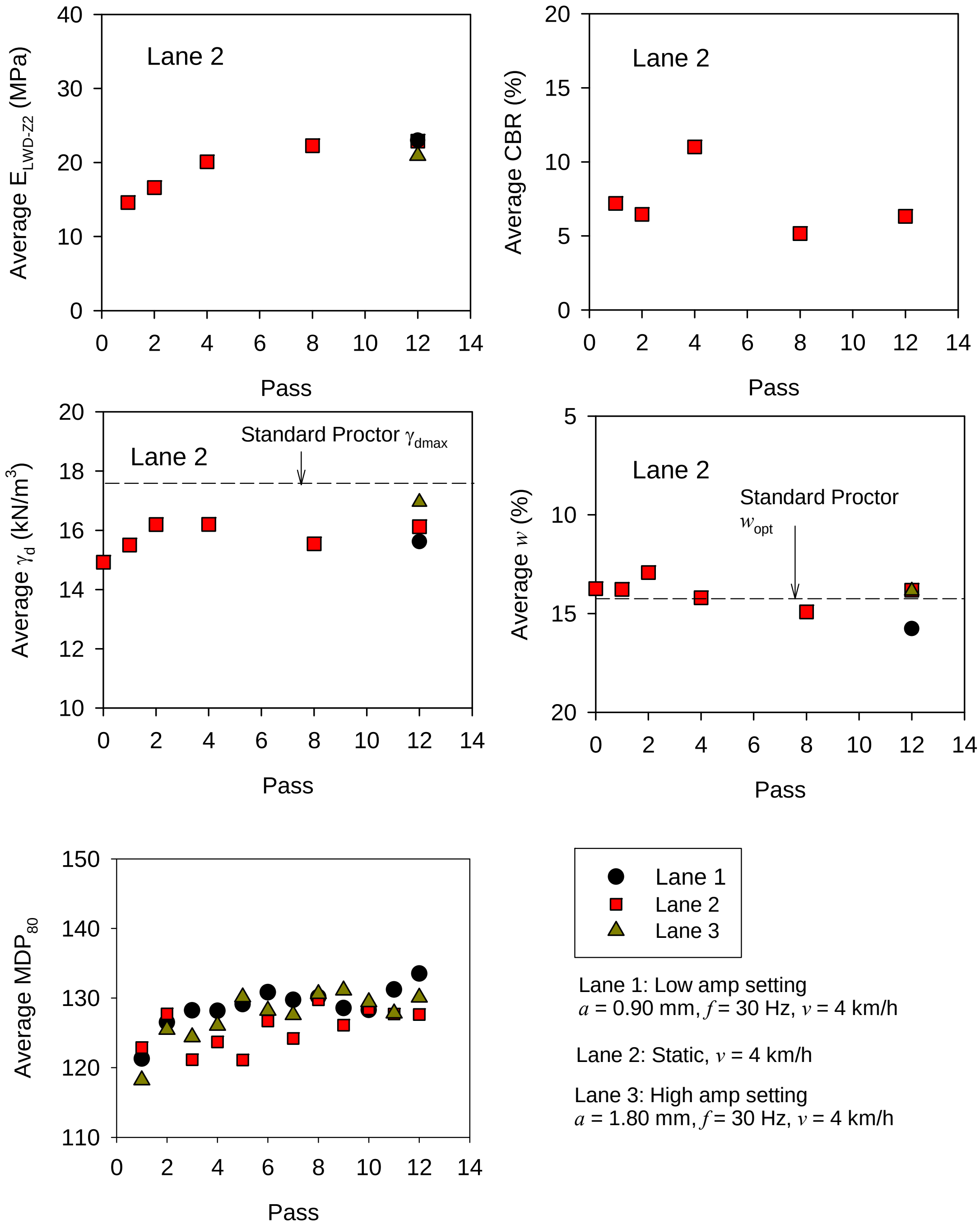

Figure 22. Comparison between average in-situ point measurement and average MDP_{80} per pass compaction growth on TB2 subgrade clay material

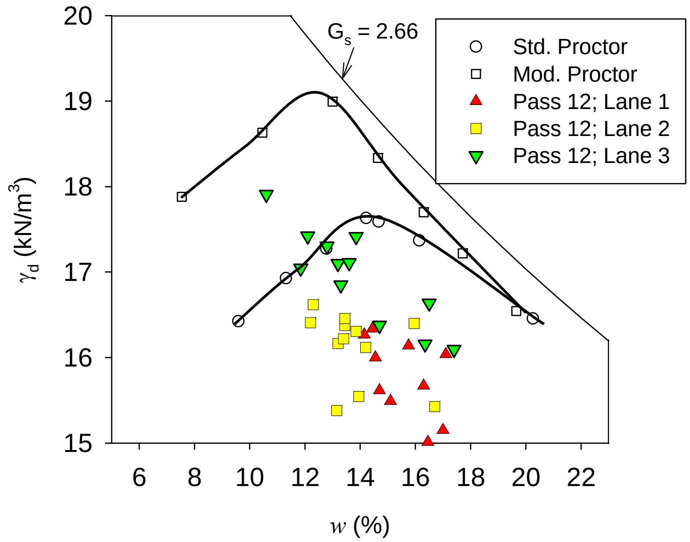

Figure 23. Comparison between laboratory Proctor curves and in-situ moisture-dry unit weight point measurements after pass 12 on TB2 subgrade clay material

Summary of Key Findings

- MDP_{80} values are repeatable and the values generally increased with roller passes similar to in-situ point measurements.
- Lane 3 compacted using high amplitude setting resulted in higher dry unit weights (96% of standard Proctor γ_{dmax}) compared to lane 2 compacted in static mode (91% of standard Proctor γ_{dmax}) (note that the two lanes had average moisture content of about + 0.4% of w_{opt}).
- The variations in MDP_{80} measurements along the test bed lanes 2 and 3 generally tracked well with changes observed in in-situ point measurements.

Sakai CCV_{PD} Calibration Test Strips – TB4 Subgrade Clay

Construction of Test Bed and Test Results

TB4 was located in the same area as TB2 and consisted of lean clay subgrade material (USCS classification: CL). The test bed was prepared by scarifying the compacted TB2 subgrade material to a depth of about 200 to 250 mm and was compacted using the Sakai padfoot roller in three lanes (lanes 1 to 3) as shown in Figure 24 and Figure 25. Photographs showing preparation and construction of the test bed are presented in Figure 25. Lanes 1, 2, and 3 were compacted using high, low, and high amplitude settings, respectively as illustrated in Figure 24, for 12 roller passes. In-situ w, γ_d, CBR, and E_{LWD-Z2} point measurements were obtained after 1, 2, 4, and 8 roller passes on lanes 2 and 3. $E_{FWD-D4.5}$ point measurements were obtained on lanes 2 and 3 after 12 roller passes.

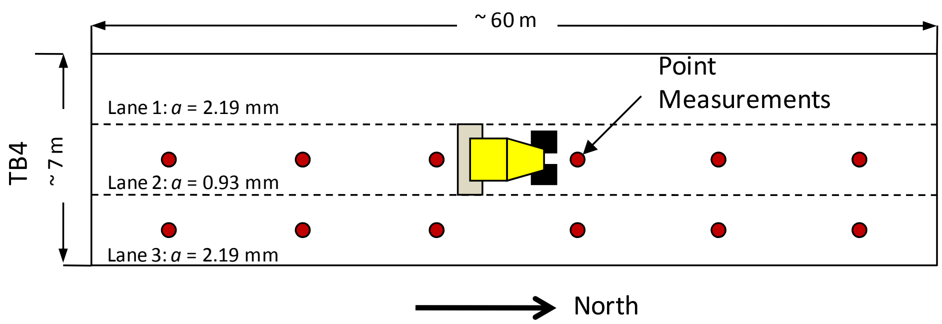

Figure 24. Experimental testing setup on TB4

Figure 25. Photographs showing construction and setup of lanes for compaction and testing on TB4 subgrade clay material

CCV_{PD} data for multiple passes and average CCV_{PD} (per pass) compaction curves on lanes 1, 2, and 3 are presented in Figure 26. CCV_{PD} data shown in Figure 26 indicate that the values are repeatable and generally increase with roller passes. Lanes 1 and 3 compacted using high amplitude setting showed similar CCV_{PD} values. On average, CCV_{PD} values obtained on lanes 1 and 3 were higher than CCV_{PD} values obtained on lane 2 compacted using low amplitude setting. The influence of vibration amplitude on CCV_{PD} values is further assessed using multiple regression analysis presented later in this report. Comparison between CCV_{PD} and different in-situ point measurements for lanes 2 and 3 are presented in Figure 27 and Figure 28, respectively. Results indicate that all point measurements track well with variations observed in CCV_{PD} measurements along the lanes. Results from regression analysis between CCV_{PD} and in-situ point measurements are presented later in this report.

Average in-situ point measurement and CCV_{PD} (per pass) compaction curves are shown in Figure 29 for lanes 2 and 3. The average γ_d measurements on lane 3 compacted with high amplitude setting showed slightly higher average relative compaction (101% of standard Proctor γ_{dmax}) than on lane 2 compacted with low amplitude setting (97% of standard Proctor γ_{dmax}). On average, E_{LWD-Z2}, γ_d, and CBR measurements increased from pass 1 to 12. On average, in-situ point measurements did not show considerably different results between lanes 2 and 3. Figure 30 shows in-situ w-γ_d results after pass 12 on lanes 2 and 3 in comparison with laboratory w-γ_d

relationships determined from standard and modified Proctor tests. After pass 12, average γ_d on lanes 2 and 3 were at about 97% and 101% of the standard Proctor γ_{dmax}, respectively. The average w on lanes 2 and 3 after pass 12 were at about -1.6%, and -0.7% of the standard Proctor w_{opt}, respectively.

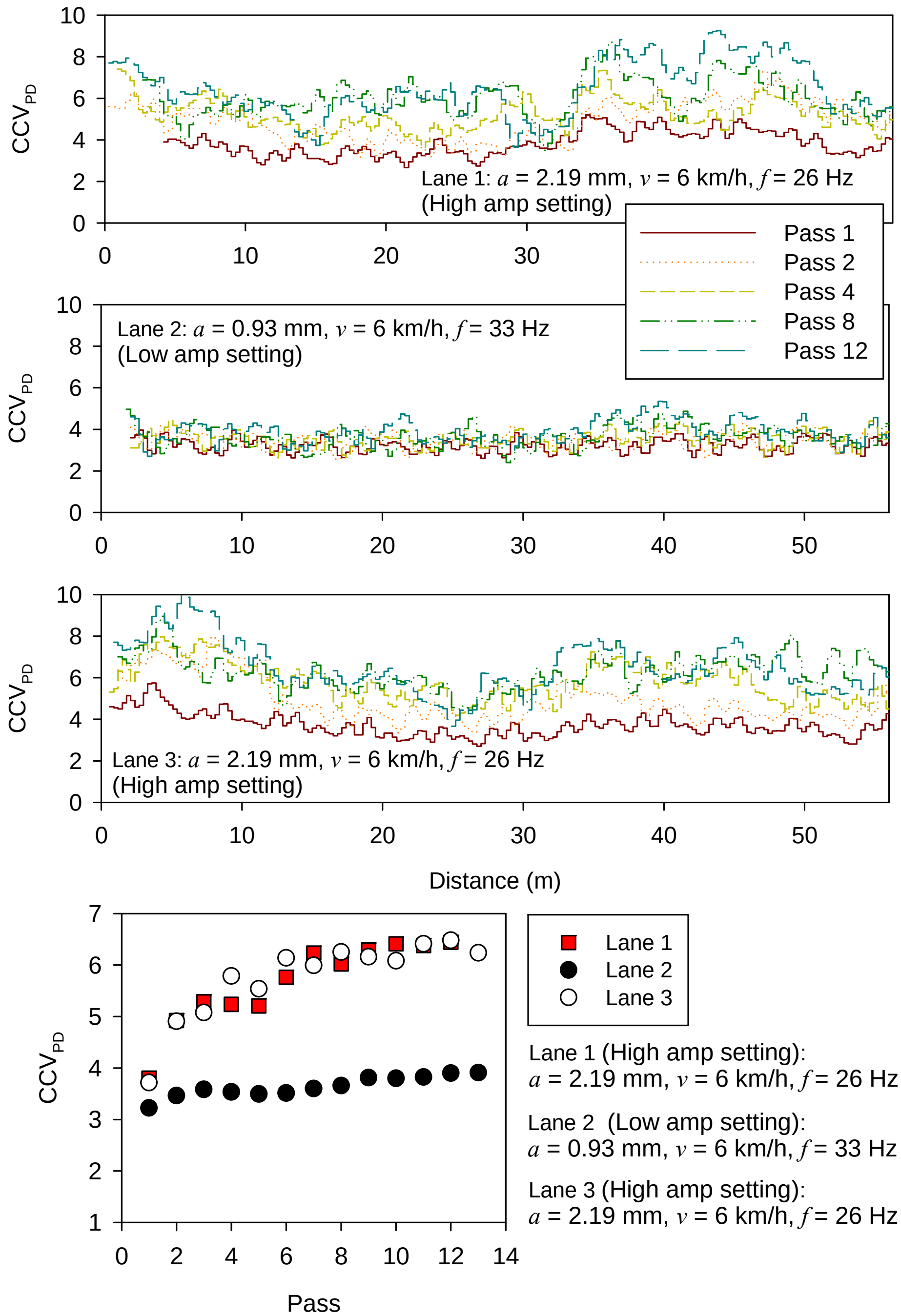

Figure 26. CCV_{PD} measurements for multiple passes and compaction growth curves on TB4 subgrade clay material lanes 1, 2, and 3

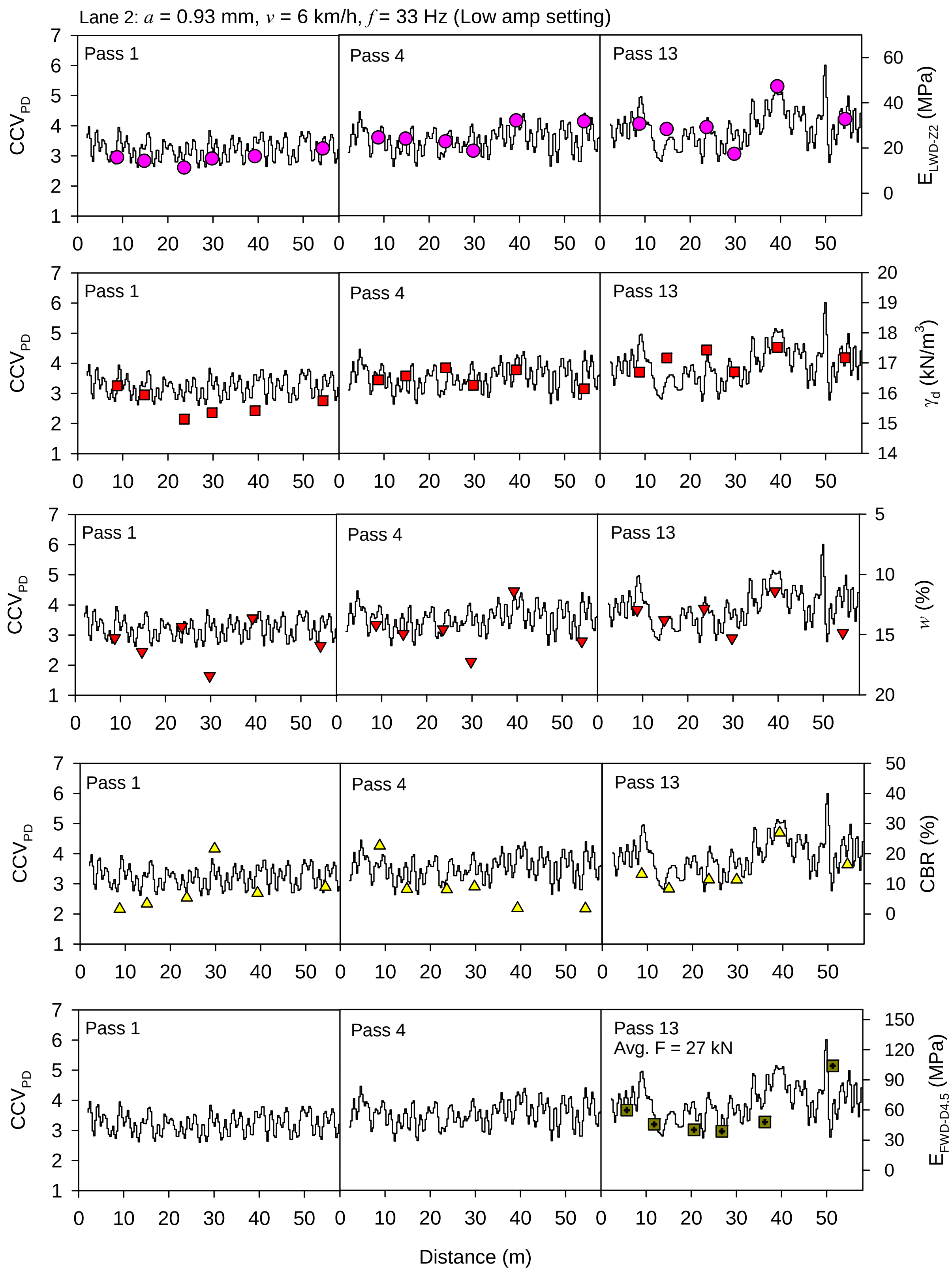

Figure 27. Comparison between CCV and in-situ point measurements – TB4 lane 2 subgrade clay material (USCS: CL)

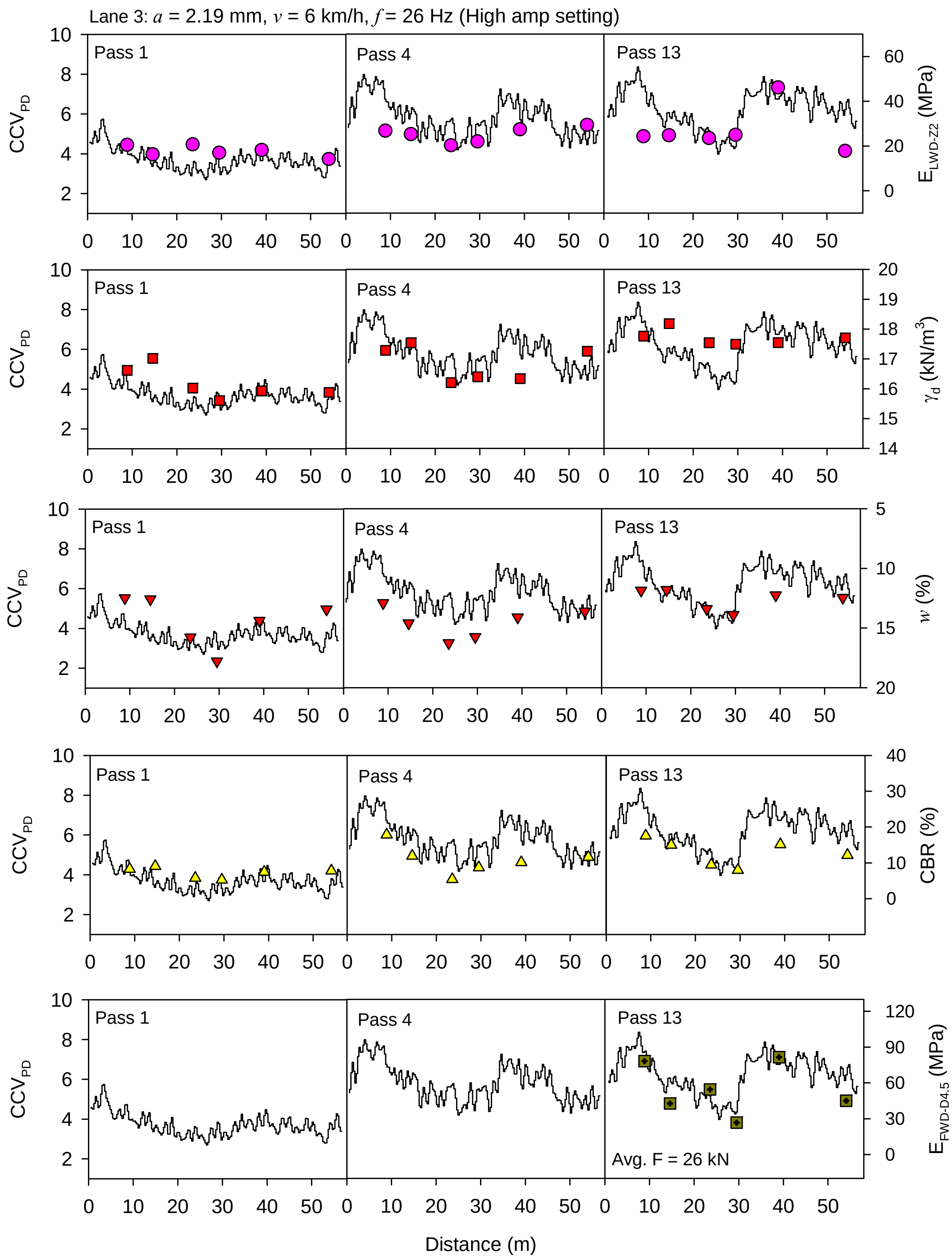

Figure 28. Comparison between CCV and in-situ point measurements – TB4 lane 3 subgrade clay material (USCS: CL)

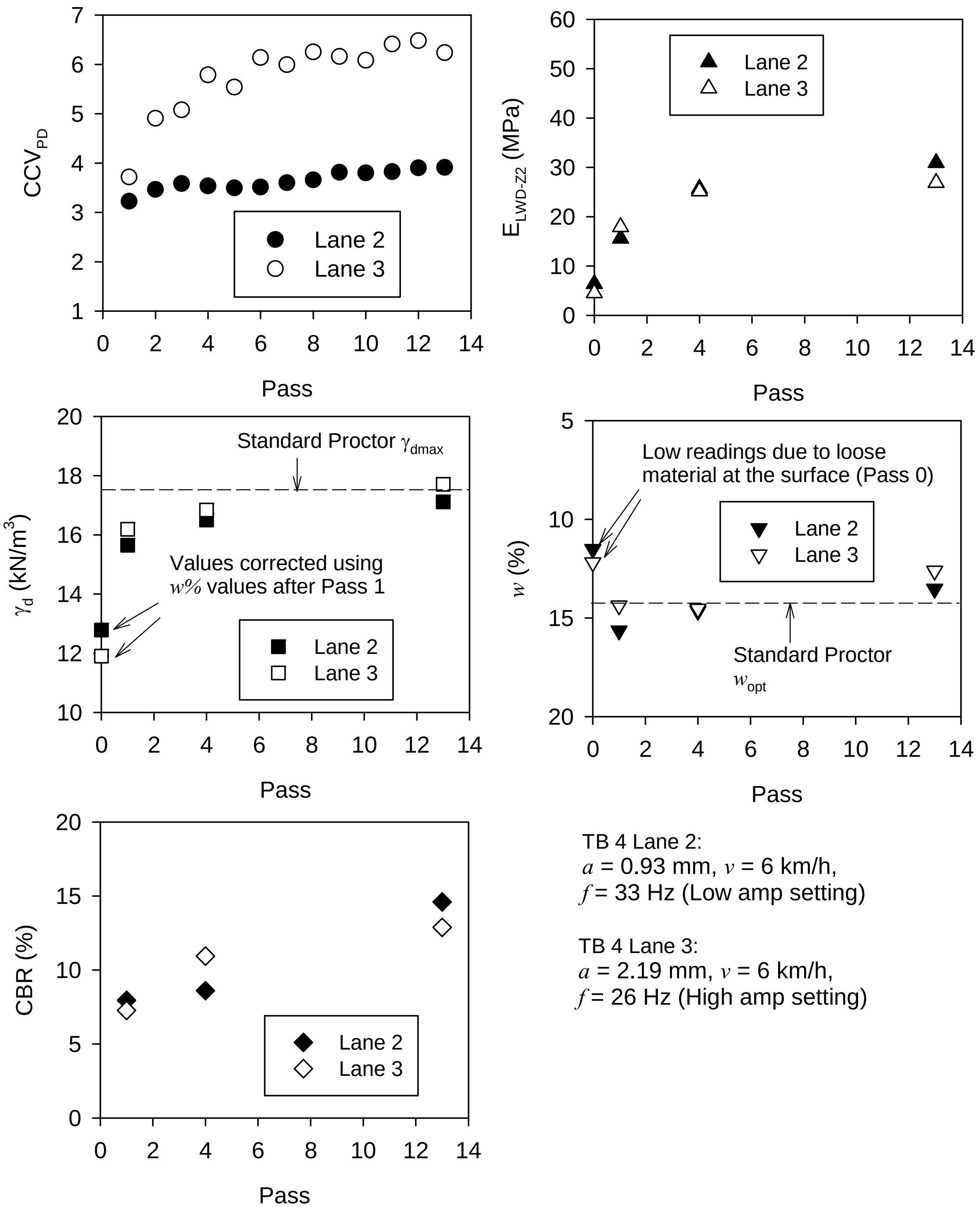

Figure 29. Comparison between CCV and in-situ point measurement compaction growth (average values per pass) with increasing roller passes – TB 4 lanes 2 and 3 subgrade clay (USCS: CL)

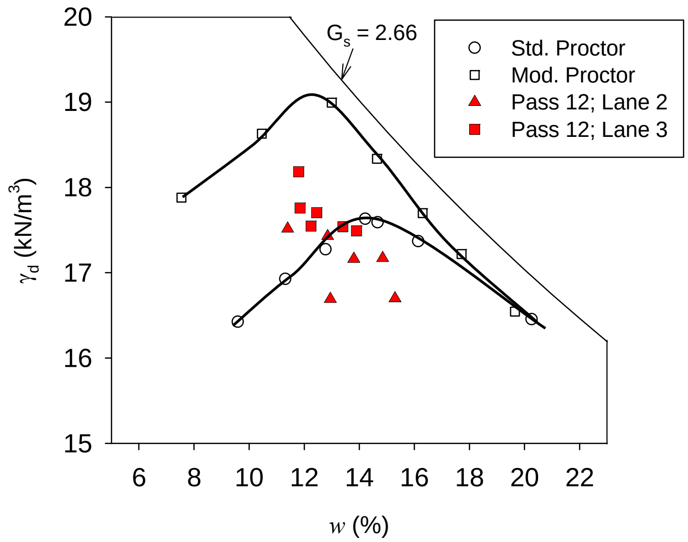

Figure 30. Comparison between laboratory w-γ_d relationship and in-situ w-γ_d point measurements after final pass on lanes 2 and 3 – TB 4 subgrade clay (USCS: CL)

Summary of Key Findings

- On average, CCV_{PD} measurements obtained from lanes 1 and 3 compacted using high amplitude setting showing similar CCV_{PD} compaction growth curves.
- CCV_{PD} values obtained from lane 2 compacted using low amplitude setting were lower than CCV_{PD} on lanes 1 and 3 compacted using high amplitude setting. For pass 13, average CCV_{PD} on lane 3 was about 1.6 times greater than CCV_{PD} on lane 2.
- CCV_{PD} values are repeatable and the values generally increased with increasing pass similar to in-situ point measurements.
- Lanes 2 and 3 compacted using low and high amplitude settings, respectively resulted in similar average γ_d, E_{LWD-Z2}, and CBR values after pass 13.
- The variations in CCV_{PD} measurements along lanes 2 and 3 tracked well with changes observed in in-situ point measurements.

Sakai CCV_{PD} Calibration Test Strip - TB 3 (Lift 4) Weathered Shale Fill

Construction of Test Bed and Test Results

The calibration test strip was located in TB3 production embankment lift 4 containing weathered shale fill material (USCS classification: CL). The area was prepared by placing approximately 200 to 250 mm thick fill material on a compacted weathered shale fill lift 3 subgrade layer. The test strip was compacted using the Sakai padfoot roller in one roller lane using high amplitude setting for 12 roller passes. In-situ w, γ_d, and E_{LWD-Z2} point measurements were obtained after 1, 2, 4, and 8 roller passes.

Figure 31 shows CCV_{PD} data for 1, 2, 4, 8, and 12 roller passes and indicate that CCV_{PD} data generally increase with roller passes. Comparison between CCV_{PD} and different in-situ point measurements are presented in Figure 32. Results show that all the point measurements track well with variations observed in CCV_{PD} measurements along the lane. Results from linear regression analysis between CCV_{PD} and in-situ point measurements are presented later in this report.

Average in-situ point measurement and CCV_{PD} measurement (per pass) compaction curves are presented in Figure 33. On average, CCV_{PD} showed increasing measurement values from 1 to 12 passes. Average E_{LWD-Z2} measurements showed a slight increase from pass 1 to 8 (about 1.03 times) and considerable increase from passes 8 to 12 (about 1.3 times). Average γ_d measurements showed increase in relative compaction from about 91% to 96% of standard Proctor γ_{dmax} from pass 1 to 8, and then no considerable difference was noted from passes 8 to 12 (<1% increase in relative compaction). Figure 34 shows in-situ w-γ_d results after pass 12 in comparison with laboratory w-γ_d relationships determined from standard and modified Proctor tests. After pass 12, average γ_d was about 97% of the standard Proctor γ_{dmax} and the average w was at about -0.6% of the standard Proctor w_{opt}.

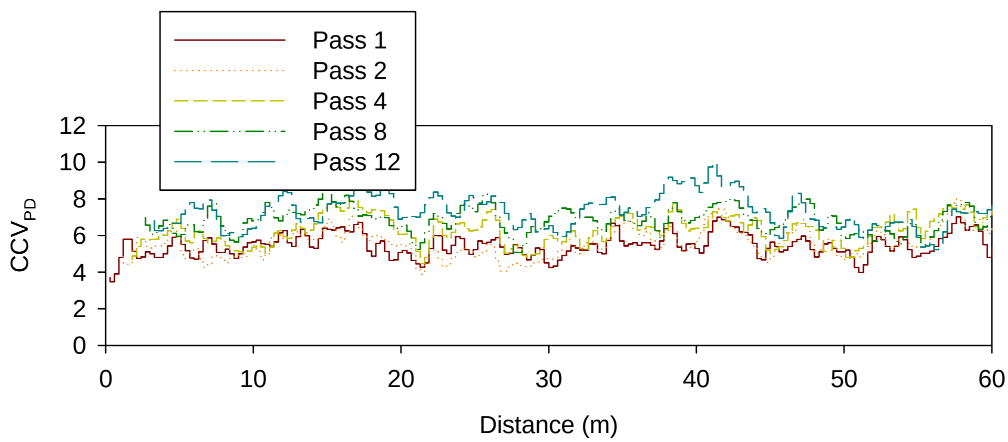

Figure 31. CCV_{PD} measurements from multiple passes on TB3 lift 4 weathered shale fill material (a = 2.19 mm, f = 26 Hz, v = 6 km/h)

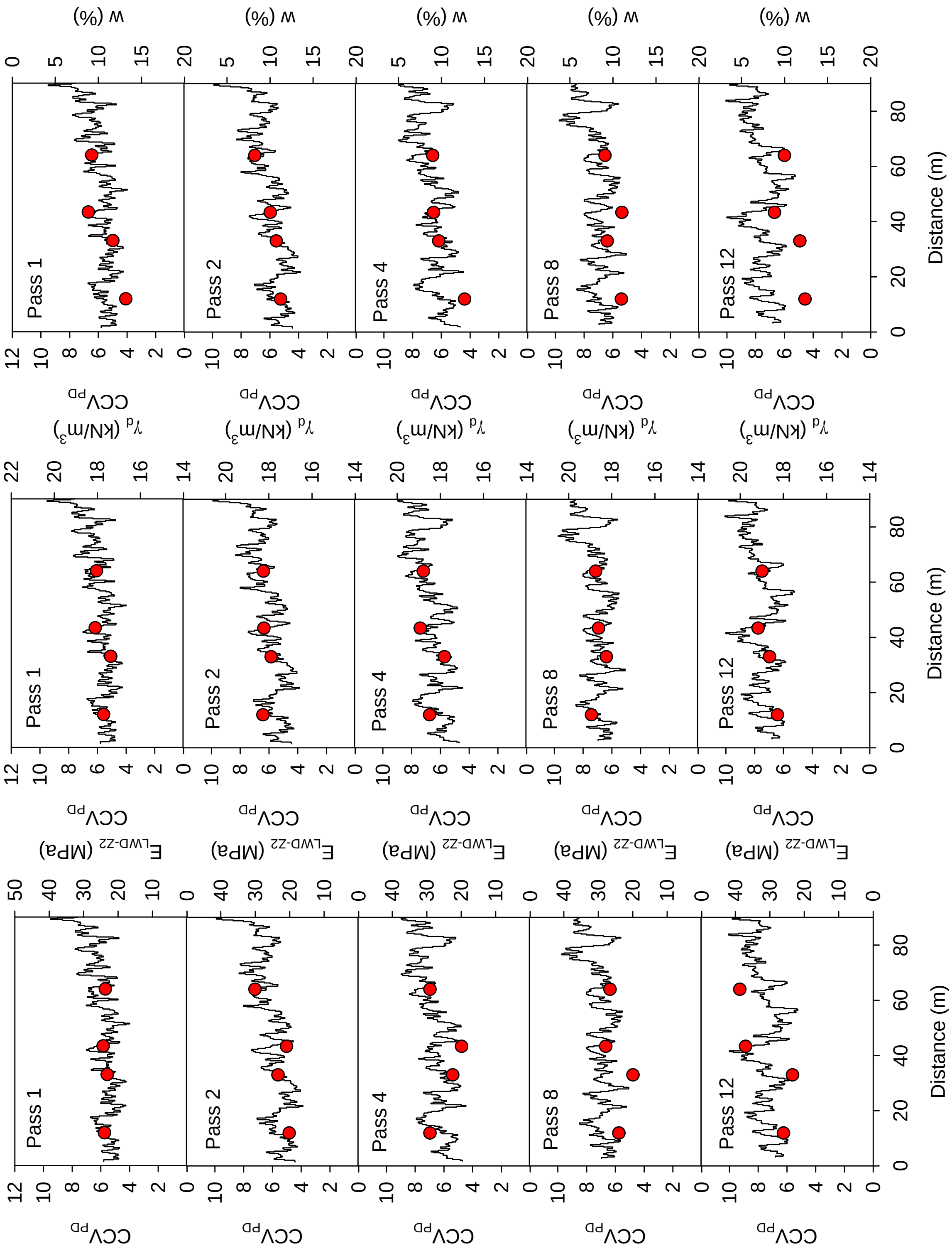

Figure 32. Comparison between CCV$_{PD}$ and in-situ point measurements from multiple passes on TB3 lift 4 weathered shale fill material (*a* = 2.19 mm, *f* = 26 Hz, *v* = 6 km/h)

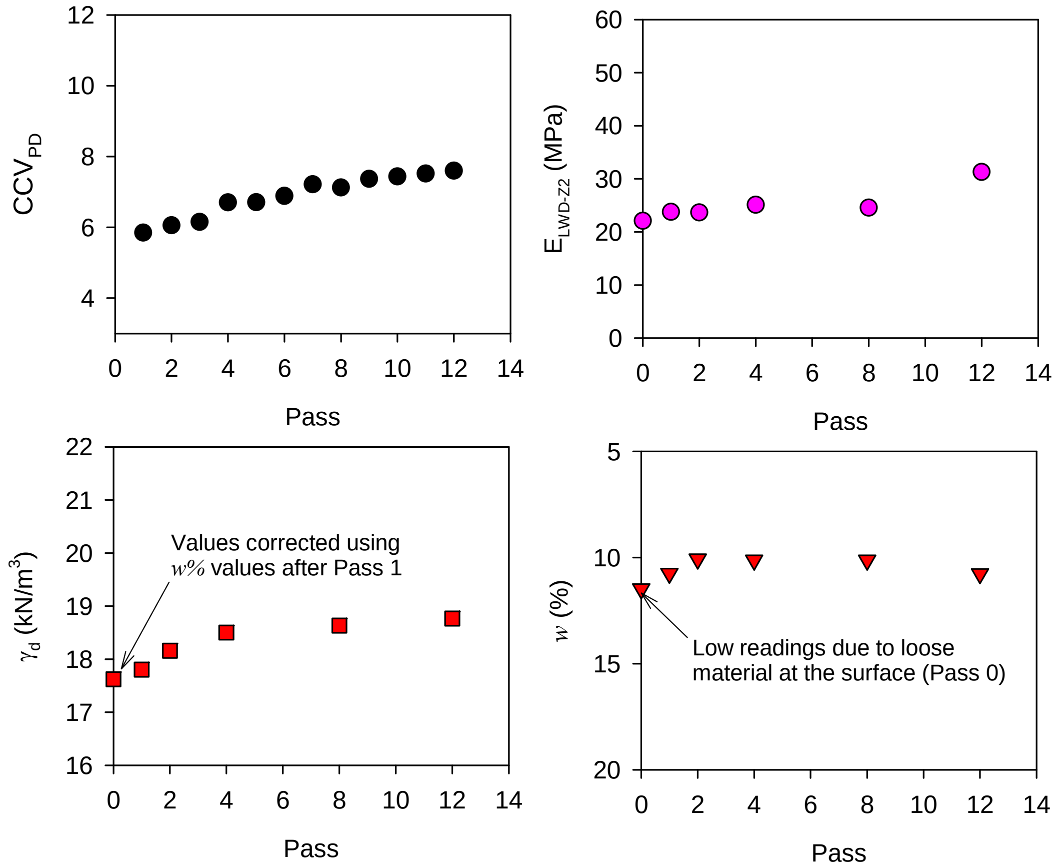

Figure 33. Comparison between average CCV_{PD} (a = 2.19 mm, f = 26 Hz, v = 6 km/h) and in-situ point measurement compaction growth per pass on TB3 lift 4 weathered shale fill material

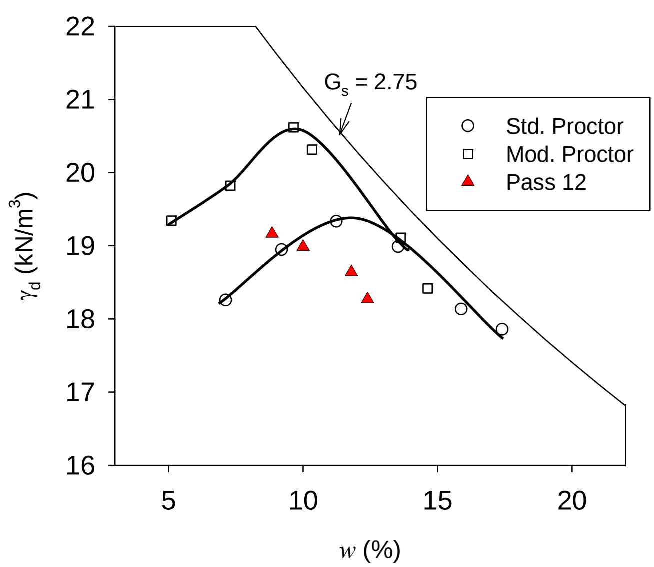

Figure 34. Comparison between laboratory Proctor curves and in-situ moisture-dry unit weight point measurements after pass 12 on TB3 lift 4 weathered shale fill material

Summary of Key Findings

- CCV_{PD} values are repeatable and the values generally increased with increasing pass similar to in-situ point measurements.
- The variations in CCV_{PD} measurements along the test bed tracked well with changes observed in in-situ point measurements.

Caterpillar and Sakai Production Compaction – TB 3

Construction of test bed

TB3 involved constructing a production area with seven lifts of weathered shale (USCS classification: CL) and lean clay (USCS classification: CL) subgrade fill materials placed over a wet foundation clay (USCS classification: CH) subgrade layer. Photographs taken during construction process on the test bed are presented in Figure 35. Compaction was performed using Caterpillar and Sakai padfoot IC rollers. Results obtained from the Caterpillar roller are presented in Figure 36 to Figure 39, and results obtained from the Sakai roller are presented Figure 40 and Figure 41.

The foundation layer was compacted with three roller passes using the Caterpillar padfoot roller at the low amplitude setting. Following compaction passes, the area was mapped using the Sakai padfoot roller at the high amplitude setting. After compaction and testing on the foundation layer, weathered shale and lean clay subgrade fill materials were placed in seven lifts with nominal loose lift thicknesses of about 200 to 300 mm over the foundation layer. Weathered shale fill was placed on the west side and lean clay fill was placed on the east side of the test bed as shown on Figure 35. The Caterpillar padfoot roller was used for compacting lifts 1 to 4 for 3 to 8 roller passes, and lifts 5 and 7 for 4 roller passes. The Sakai padfoot roller was used in compacting lift 6 with 4 roller passes. Following compaction passes on lifts 1 to 5, a mapping pass was performed using the Sakai padfoot roller and in-situ point measurements were obtained at select point locations for correlation analysis.

For compaction up to lift 2, MDP_{80} measurement values were obtained from the Caterpillar roller. It was determined that MDP_{80} measurement range and resolution was low and to better capture the variations in soil compaction properties, the machine settings were modified to obtain MDP_{40} measurement values and used for the rest of the project. Calculations for MDP_{40} and MDP_{80} are described in the background section of this report.

Results and Discussion

Figure 36 shows MDP_{80} maps for three roller passes, elevation map, and pass coverage maps for the foundation layer. Also shown in Figure 36 is a compaction curve of average MDP_{80} with observed variability (standard deviation σ) at each pass. The elevation data indicates that the area generally slopes down from north to south. Similar to the findings on TB1, the MDP_{80} data on the foundation layer appears sensitive to driving grade slope with relatively high MDP_{80} values driving downhill (north to south) and relatively low MDP_{80} values driving uphill (south to north). After pass 3, average MDP_{80} driving downhill was about 124 while average MDP_{80} driving uphill was about 114. CCV_{PD} map and histogram of CCV_{PD} values for the foundation layer are presented in Figure 40. The average CCV_{PD} on the foundation layer was about 2.2. In-situ point measurements were conducted at seven randomly selected locations as shown in Figure 40. The measurements resulted in average $E_{LWD\text{-}Z2}$ = 11.7 MPa, γ_d = 14.24 kN/m^3 (93% of standard Proctor γ_{dmax}), w = 22.8% (+0.3% of standard Proctor w_{opt}), and CBR = 5.8.

MDP_{80} maps, elevation map, and pass coverage maps for lift 1 are presented in Figure 37. A color change in the elevation maps visually demonstrates the lift placement and its thickness across the test bed. An isolated soft/wet spot was identified with low MDP_{80} values on the map. A photograph of the soft/wet spot location is shown in Figure 37. About 3 to 4 passes were made across the test bed. Compaction curves shown on Figure 37 indicate that on average the MDP_{80} values increased with roller passes. By visual inspection of the materials, the weathered shale fill material was relatively stiffer compared to the lean clay fill material. Despite the effect of sloping grade, MDP_{80} values on lean clay fill were comparatively lower than on weathered shale fill, as expected (average MDP_{80} on weathered shale = 135 and average MDP_{80} on lean clay = 132). The CCV_{PD} map and histogram plots presented in Figure 40 for lift 1 also showed comparatively low CCV_{PD} values on the lean clay fill than compared to the weathered shale fill (average CCV_{PD} on lean clay = 2.6 and average CCV_{PD} on weathered shale = 4.2). In-situ point measurements obtained after final compaction pass at select random locations across the test bed (see Figure 40) resulted in average $E_{LWD\text{-}Z2}$ = 17.2 MPa and 20.7 MPa, γ_d = 17.73 and 16.18 kN/m^3, and w = 8.7 and 19.6% on weatherd shale and lean clay fill materials, respectively.

Similar results obtained on lift 2 are presented in Figure 38. About 4 passes were made across the test bed area with lean clay fill and 8 passes were made across the test bed area with weatherd shale fill. The compaction curves on weathered shale fill showed considerable increase in the average MDP_{80} from roller passes 1 to 4 and then no significant change was observed between pass 4 to 8. For the lean clay fill section, some increase in average MDP_{80} was observed from pass 1 and 2 and then no significant increase was observed from passes 2 to 4. Similar to lift 1, MDP_{80} values on lean clay fill were comparatively lower than the weathered shale fill section. CCV_{PD} map and histogram plots presented in Figure 40 for lift 2 also showed comparatively lower CCV_{PD} values on lean clay fill than on weathered shale fill. In-situ point measurements obtained after final compaction pass at select random locations across the test bed (see Figure 40) resulted in average $E_{LWD\text{-}Z2}$ = 18.5 MPa and 31.0 MPa, γ_d = 18.03 and 16.88 kN/m^3, and w = 9.6 and 18.1% on weatherd shale and lean clay fill materials, respectively.

Figure 39 shows results obtained from the Caterpillar roller on lift 3 after changing the measurement settings to obtain MDP_{40}. Elevation map, pass coverage maps, average MDP_{40} compaction curves on weathered shale and lean clay fill materials, and compaction curves at select point locations are included in Figure 39. Again, similar to lifts 1 and 2, MDP_{40} values on lean clay fill were comparatively lower than on weathered shale fill. The compaction curves on weathered shale and lean clay fill materials showed considerable increase in the average MDP_{40} from pass 1 to 2 and then no significant change was observed between passes 2 to 4. Similar compaction curves are noted at select point locations. In-situ point measurements obtained after the final compaction pass at select random locations across the test bed resulted in average $E_{LWD\text{-}}$

$_{Z2}$ = 22.8 MPa and 26.6 MPa, γ_d = 17.93 and 17.23 kN/m^3, and w = 8.9 and 17.7% on weatherd shale and lean clay fill materials, respectively.

CCV_{PD} results obtained from four compaction passes on lift 5 are presented in Figure 41. Histogram plots showing CCV_{PD} results separately for weathered shale and lean clay fill materials for 1 to 4 passes are presented in Figure 42. Similar to results on lifts 1 and 2, CCV_{PD} values showed comparatively low values on lean clay fill compared to weathered shale fill. The compaction curves showed at in-situ point measurement locations on Figure 41 and average CCV_{PD} values noted on histogram plots (Figure 42) indicate that CCV_{PD} generally from 1 to 4 passes. In-situ point measurements obtained after final compaction pass at select random locations across the test bed resulted in average $E_{LWD\text{-}Z2}$ = 26.2 MPa and 34.3 MPa, γ_d = 18.03 and 17.48 kN/m^3, w = 10.8 and 16.3%, and CBR = 16.4 and 8.3% on weatherd shale and lean clay fill materials, respectively.

Figure 35. Photographs showing construction process on TB3 production area

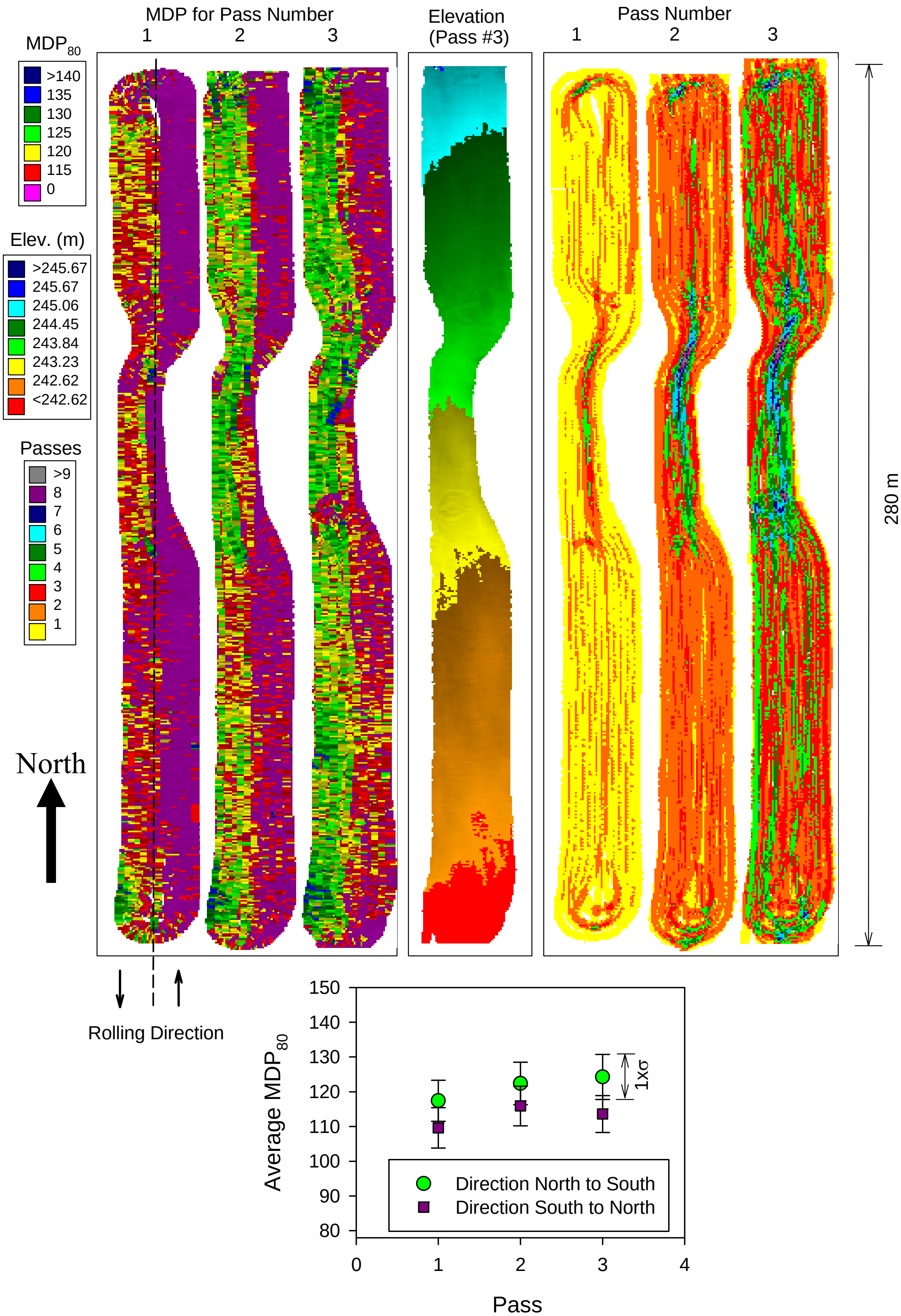

Figure 36. MDP$_{80}$, elevation, pass coverage, and average MDP$_{80}$ (a = 0.90 mm, f = 33 Hz, v = 4 km/h) per pass on TB3 foundation subgrade layer

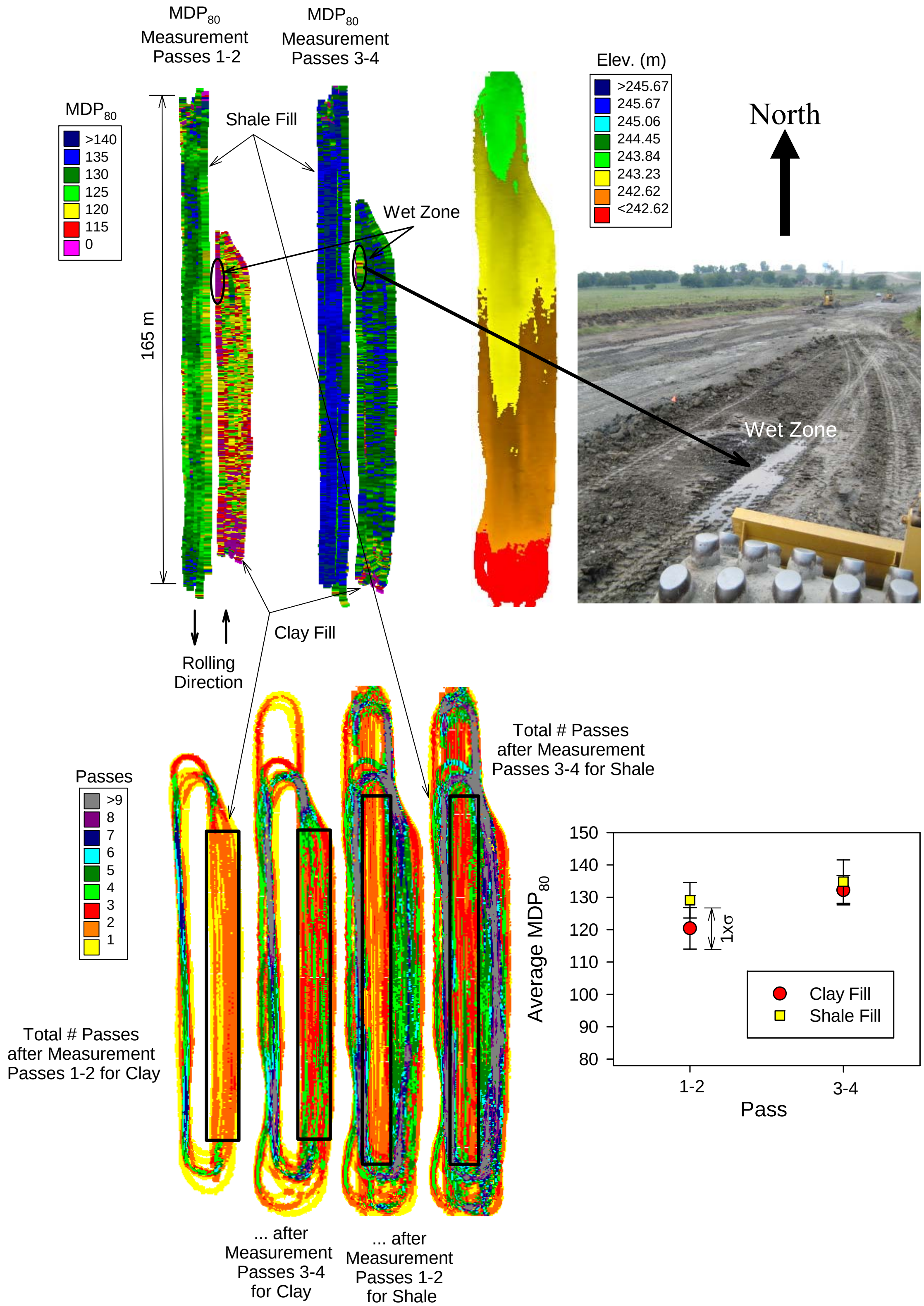

Figure 37. MDP$_{80}$, elevation, pass coverage, and average MDP$_{80}$ (a = 0.90 mm, f = 33 Hz, v = 4 km/h) per pass on TB3 lift 1 clay fill and shale fill material

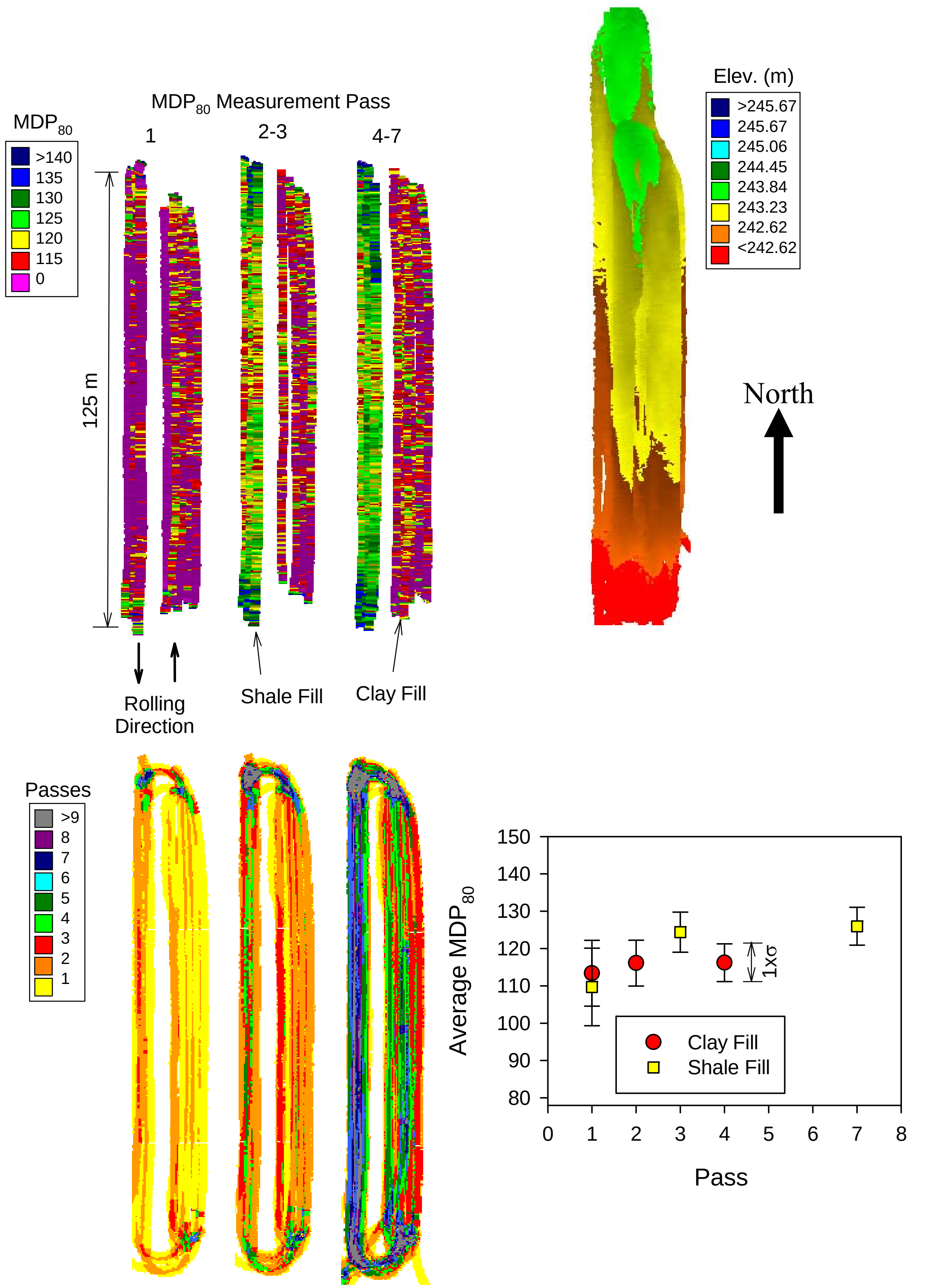

Figure 38. MDP$_{80}$, elevation, pass coverage, and average MDP$_{80}$ (a = 0.90 mm, f = 33 Hz, v = 4 km/h) per pass on TB3 lift 2 clay fill and shale fill material

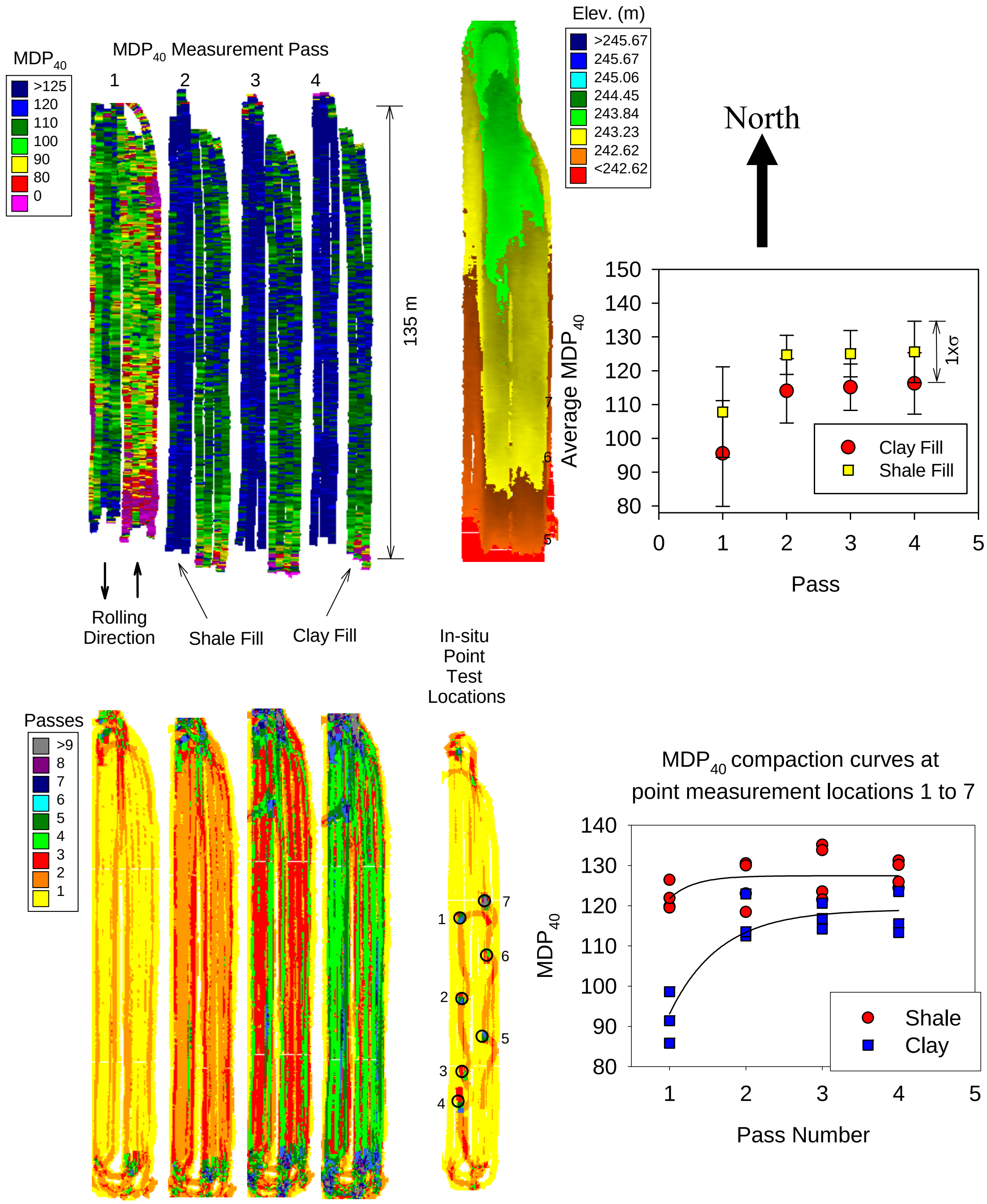

Figure 39. MDP$_{40}$, elevation, pass coverage, average MDP$_{40}$ (a = 0.90 mm, f = 33 Hz, v = 4 km/h) per pass, and MDP$_{40}$ at select point locations on TB3 lift 3 clay fill and shale fill material

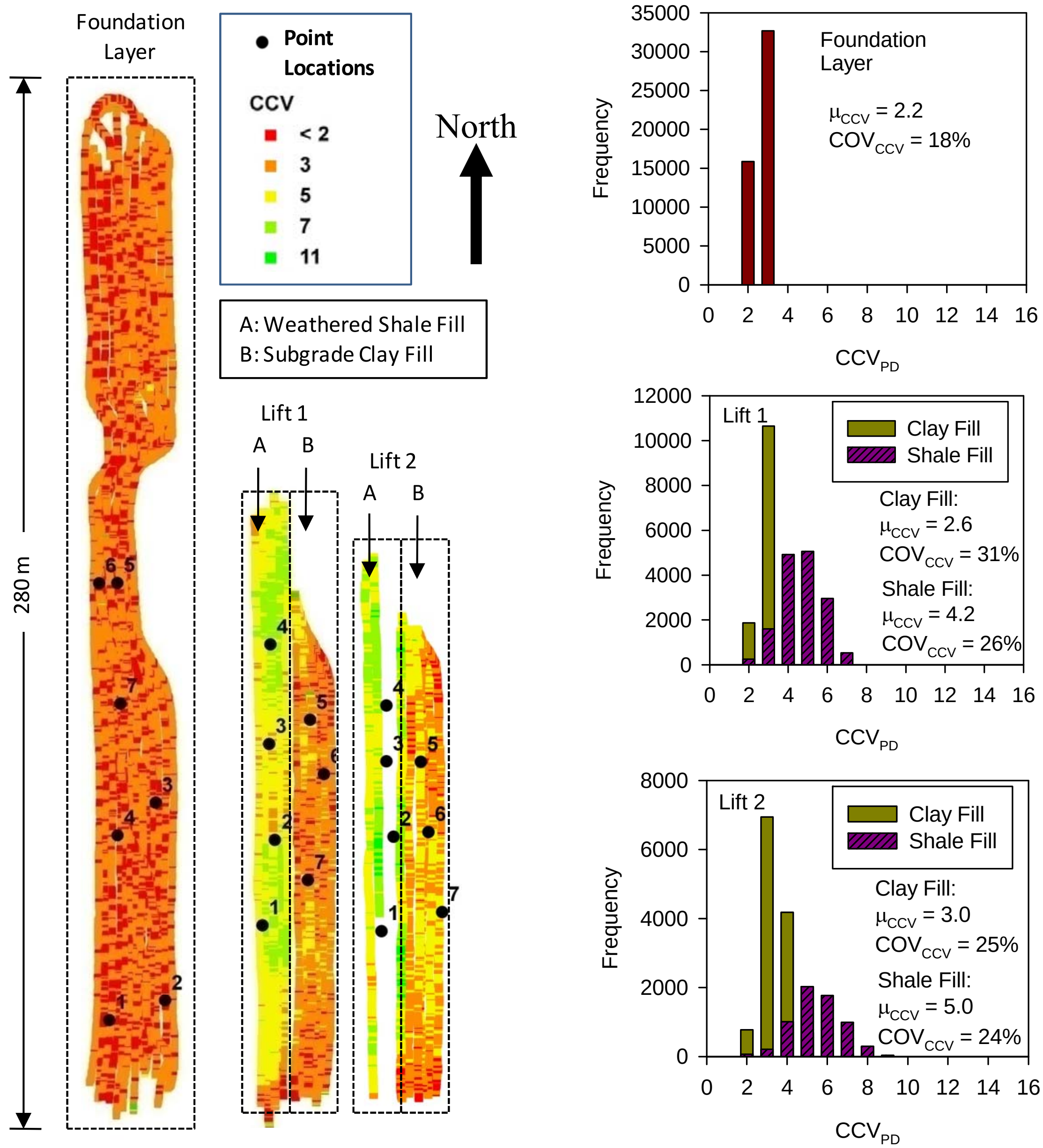

Figure 40. CCV$_{PD}$ maps on foundation layer and lifts 1 to 2 (a = 0.93 mm, f = 33 Hz, and v = 4 km/h)

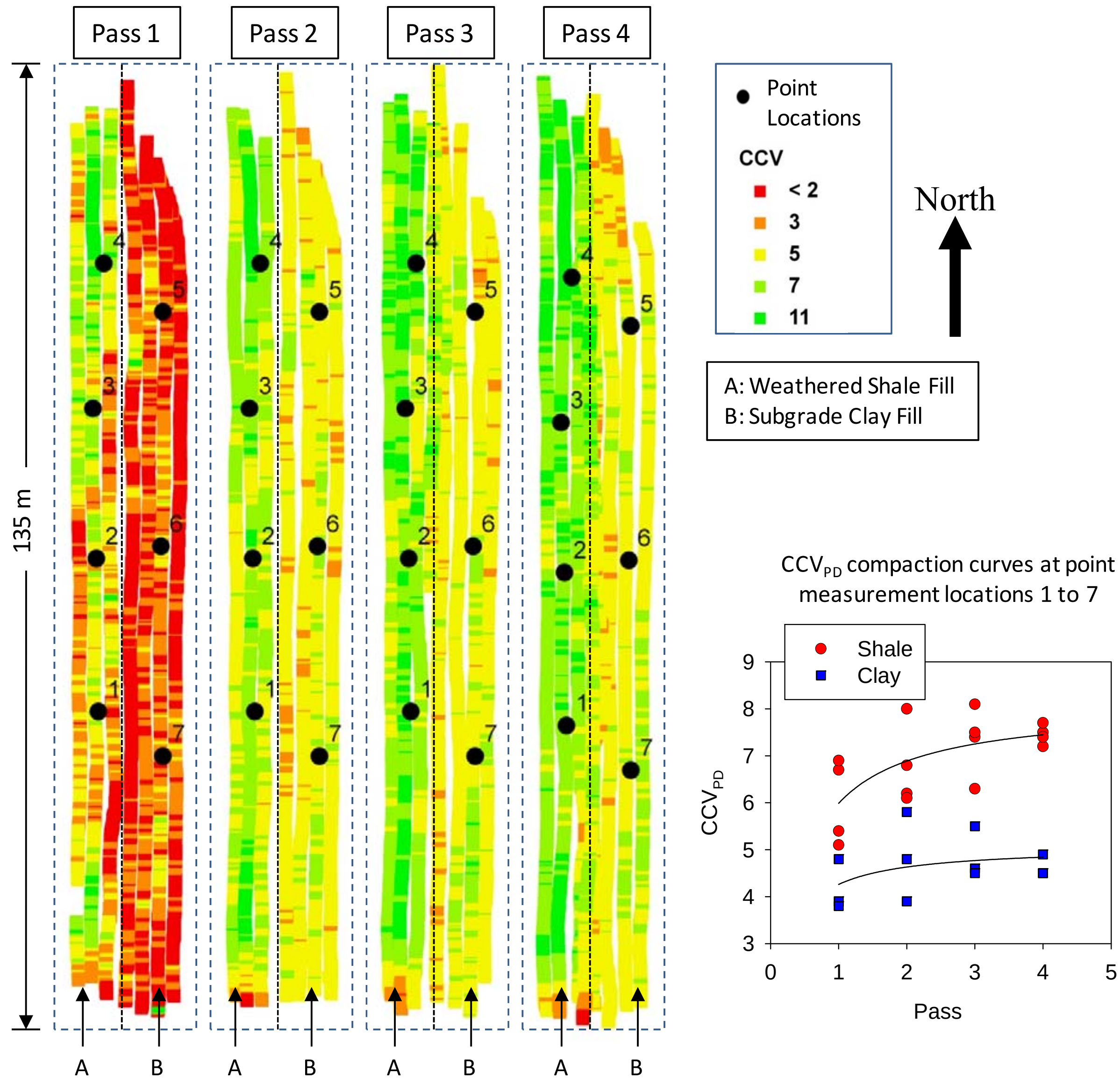

Figure 41. CCV_{PD} maps lift 4 for passes 1 to 4 and CCV_{PD} compaction curves at point measurement locations (a = 0.93 mm, f = 33 Hz, and v = 4 km/h)

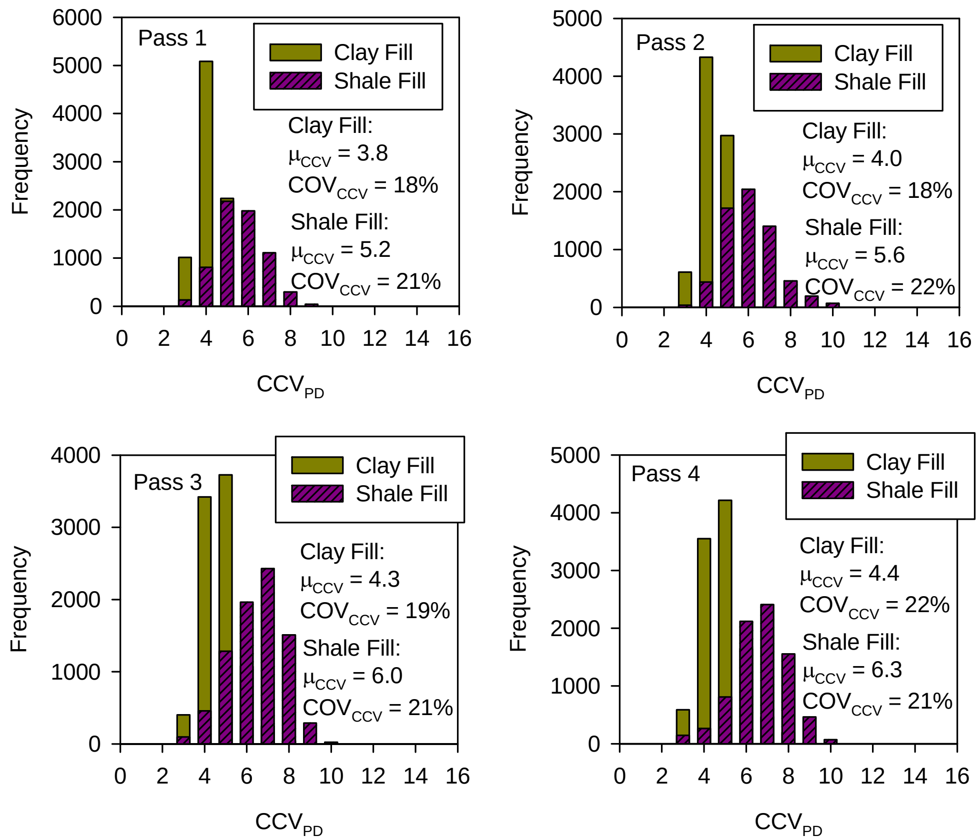

Figure 42. Histogram plots of CCV_{PD} measurement values on lift 6 clay and weathered shale fill materials for passes 1 to 4

Geostatistical Analysis of IC Measurements

Spatially referenced IC measurement values provide an opportunity to quantify "non-uniformity" of compacted fill materials. This topic is slowly gaining popularity among the pavement engineering community. Vennapusa and White (2009b) demonstrated the use of semivariogram analysis in combination with conventional statistical analysis to effectively address the issue of non-uniformity in quality assurance during earthwork construction. A semivariogram is a plot of the average squared differences between data values as a function of separation distance, and is a common tool used in geostatistical studies to describe spatial variation. A typical semivariogram plot is presented in Figure 43. The semivariogram $\gamma(h)$ is defined as one-half of the average squared differences between data values that are separated at a distance h (Isaaks and Srivastava 1989). If this calculation is repeated for many different values of h (as the sample data will support) the result can be graphically presented as experimental semivariogram shown as circles in Figure 43. More details on experimental semivariogram calculation procedure are available elsewhere in the literature (e.g., Clark and Harper 2002, Isaaks and Srivastava 1989).

To obtain an algebraic expression for the relationship between separation distance and experimental semivariogram, a theoretical model is fit to the data. Some commonly used models include linear, spherical, exponential, and Gaussian models. Previous work by White et al.

(2007a), White et al. (2007b), Vennapusa and White (2009b), and results from Texas field investigation conducted as part of this project showed that an exponential model generally fits well for IC measurement data. An exponential semivariogram is illustrated in Figure 43 as solid line. Three important features to construct a theoretical semivariogram include: sill ($C+C_0$), range (R), and nugget (C_0). These parameters are briefly described Figure 43. Arithmetic expressions and detailed descriptions of theoretical models can be found elsewhere in the literature (e.g., Clark and Harper 2002, Isaaks and Srivastava 1989). For the results presented in this section, the sill, range, and nugget values during theoretical model fitting were determined by checking the models for "goodness" using the modified Cressie goodness fit method (see Clark and Harper 2002) and cross-validation process (see Isaaks and Srivastava 1989). From a theoretical semivariogram model, a low "sill" and longer "range of influence" represent best conditions for uniformity, while the opposite represents an increasingly non-uniform condition.

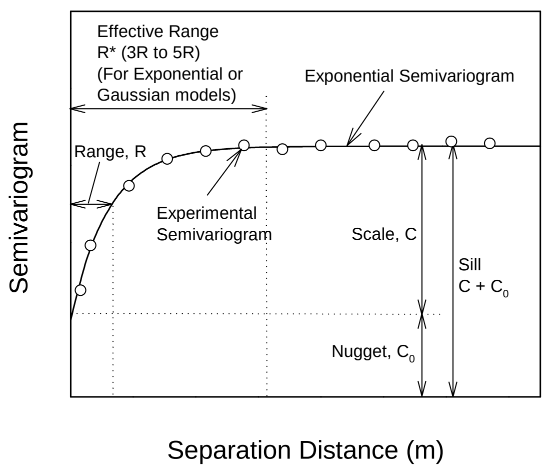

Range: As the separation distance between pairs increase, the corresponding semivariogram value will also generally increase. Eventually, however, an increase in the distance no longer causes a corresponding increase in the semivariogram, i.e., where the semivariogram reaches a plateau. The distance at which the semivariogram reaches this plateau is called as range. Longer range values suggest greater spatial continuity or relatively larger (more spatially coherent) "hot spots".

Sill: The plateau that the semivariogram reaches at the range is called the sill. A semivariogram generally has a sill that is approximately equal to the variance of the data.

Nugget: Though the value of the semivariogram at h = 0 is strictly zero, several factors, such as sampling error and very short scale variability, may cause sample values separated by extremely short distances to be quite dissimilar. This causes a discontinuity at the origin of the semivariogram and is described as nugget effect.
(Isaaks and Srivastava, 1989)

Figure 43. Description of a typical experimental and exponential semivariogram and its parameters

To evaluate the application of geostatistics, spatially referenced MDP_{80} measurement values obtained from lift 3 and CCV_{PD} measurement values obtained from lift 6 on weathered shale and lean clay subgrade fill material are analyzed. Semivariogram plots for passes 1 to 4 and comparison between change in spatial statistics (i.e., sill and range) and univariate statistics (i.e., average and coefficient of variation COV) of MDP_{80} and CCV_{PD} are presented in Figure 44 and Figure 45, respectively.

Semivariogram sill and COV of MDP_{80} (from lift 3) decreased with roller passes which represents increasing uniformity with compaction (Figure 44). The range values decreased with passes suggesting a decrease in spatial continuity in the data; however, the change was not significant (decreased from 2 m to 1.6 m). Comparatively, MDP_{80} on weathered shale fill was more uniform compared to MDP_{80} on lean clay fill with lower sill and COV values.

Semivariogram sill and COV of CCV_{PD} (from lift 6) increased with number of roller passes which represents decreasing uniformity with compaction (Figure 45). On lean clay fill, the range values increased up to pass 3 suggesting an increase in spatial continuity in the data and then decreased from passes 3 to 4 indicating a decrease in spatial continuity in the data. On weathered shale fill, change in range values with pass was not significant (increased from 1.2 to 1.3 m).

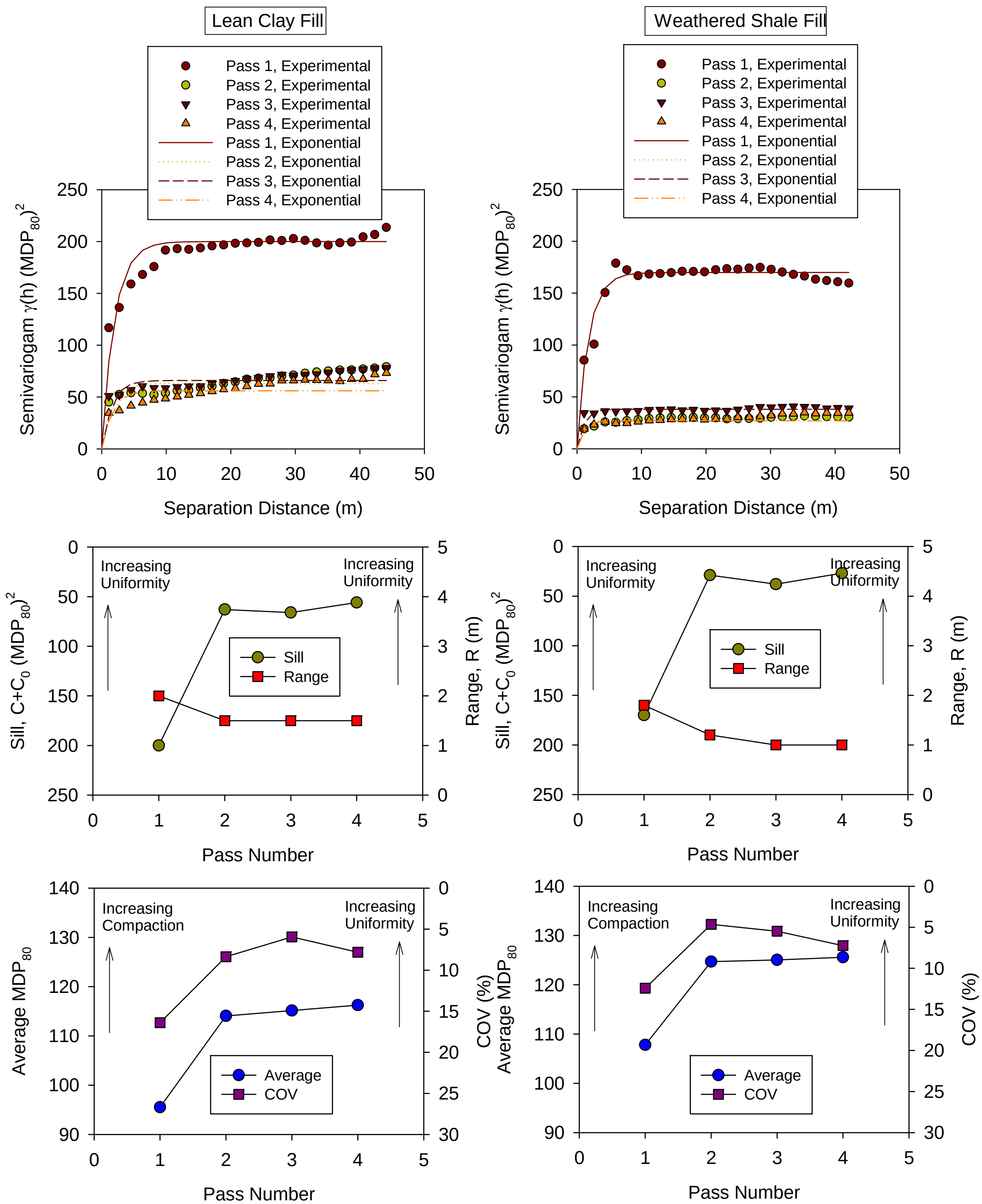

Figure 44. Change in semivariograms, spatial statistics, and univariate statistics of MDP_{80} with pass on TB3 – lift 3 lean clay and weathered shale fill materials

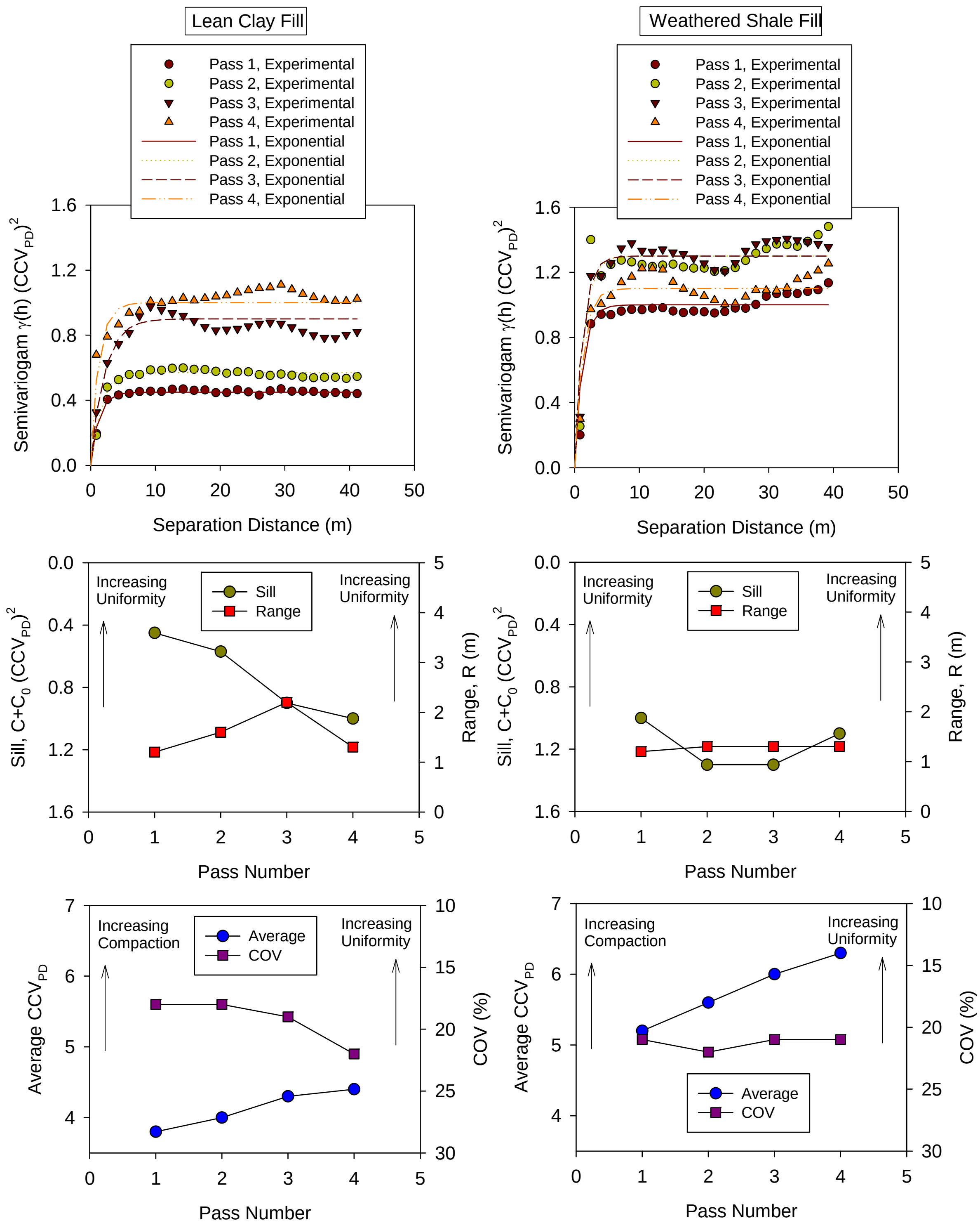

Figure 45. Change in semivariograms, spatial statistics, and univariate statistics of CCV_{PD} with pass on TB3 – lift 6 lean clay and weathered shale fill materials

Summary

Results obtained from production work during placement and construction of seven lifts of weathered shale and lean clay subgrade fill materials over wet/soft foundation subgrade layer are described above. Color-coded maps of IC measurements, pass coverage information, and elevation data are presented above from different stages of embankment construction. Analyzing and visualizing data in terms of compaction growth on average and at a given point is also demonstrated from the production data.

The color-coded maps with 100% coverage and the opportunity to visualize compaction curves as demonstrated above can be effective if utilized by the roller operator to make informed decisions on compaction process to promptly adjust process control measures. Results presented above also demonstrated that isolated soft/wet spots can be easily identified using IC maps. Application of geostatistical analysis methods to analyze IC measurement presents an opportunity to quantify non-uniformity of compacted fill materials. Implementing such analysis methods represent a paradigm shift in how compaction analysis and specifications could be implemented in the future.

Caterpillar MDP_{40} measurements on wet organic clay layer – TB5

TB5 was located in a roadway median with relatively soft and wet organic clay material. The area was mapped with 4 roller passes using static setting to obtain MDP_{40} measurements. Figure 46 shows MDP_{40}, elevation, and pass coverage maps after pass 4 on TB5. Following mapping passes, in-situ w, γ_d, $E_{LWD\text{-}Z2}$, and CBR point measurements were obtained from select test locations (see Figure 46). CBR profiles (from DCP tests) from the test bed are presented in Figure 47.

MDP_{40} values obtained from this test bed were significantly lower compared to the values obtained from other test beds. MDP_{40} at the point locations varied between 44 and 75. Range of point measurements were: $E_{LWD\text{-}Z2}$ = 0.2 to 3.1 MPa, γ_d = 14.28 to 15.54 kN/m^3, w = 26.2 to 28.4%, and CBR (upper 300 mm) = 0.2 to 1.5. Results of correlation analysis from this test bed are presented later in this report.

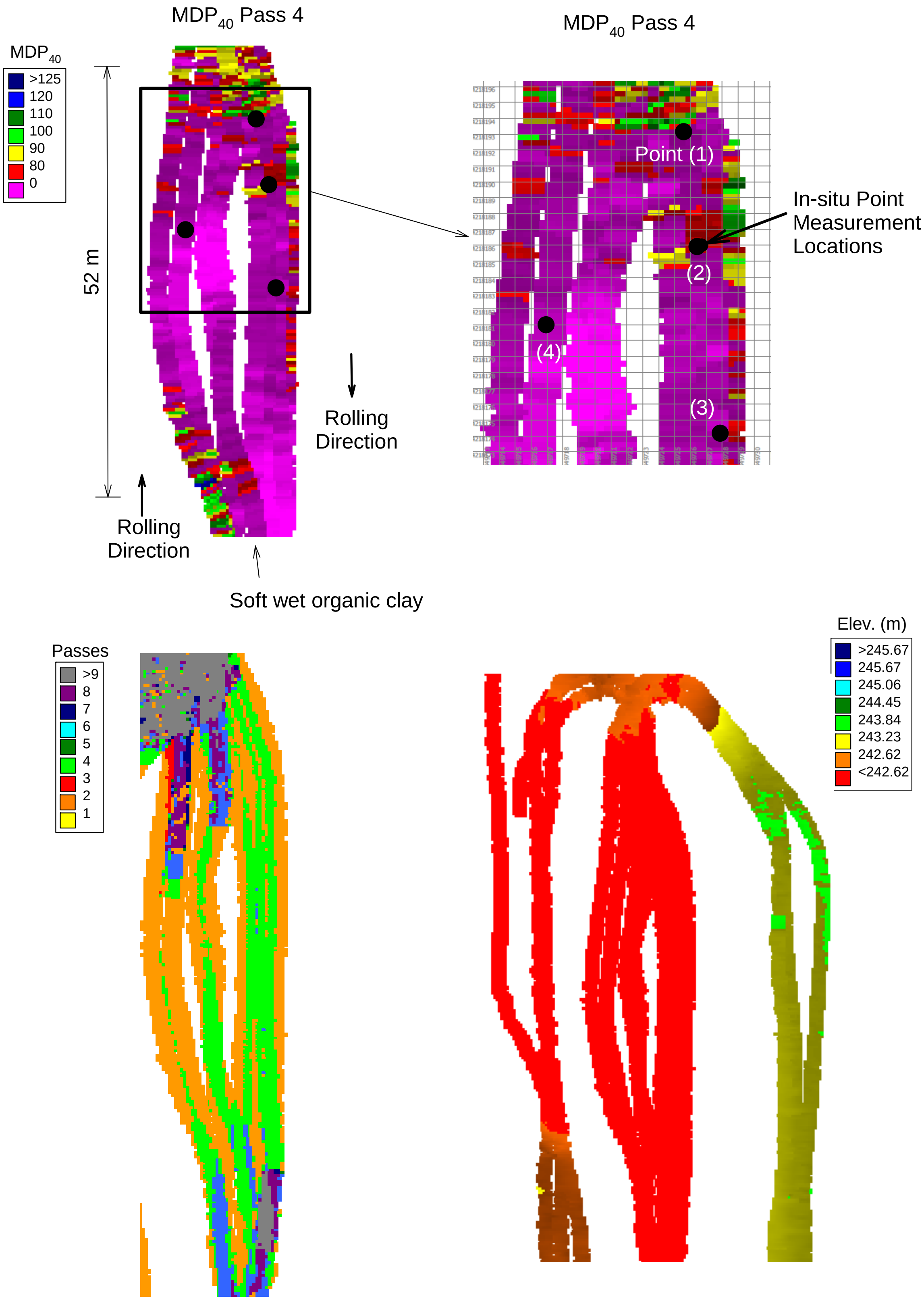

Figure 46. MDP_{40} (static mode, v = 4 km/h) measurements on pass 4, elevation, and pass coverage information – TB5 wet organic clay

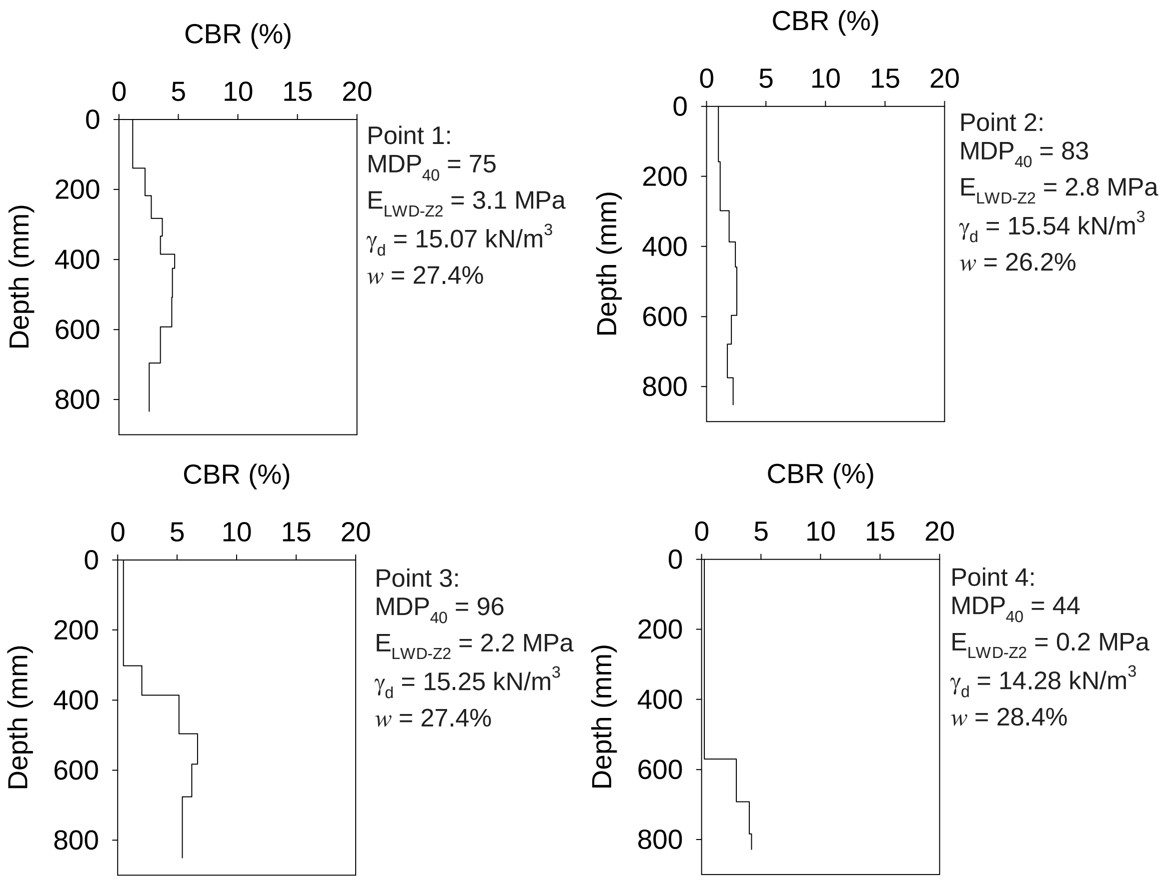

Figure 47. CBR profiles (from DCP tests) at point measurement locations – TB5 wet organic clay

Comparison between Smooth Drum and Padfoot CCV Measurements – TBs 6 and 7

Test beds 6 and 7 consisted of compacted lean clay subgrade and weathered shale subgrade materials, respectively (Figure 48). TB7 was stiffer compared to TB6. The two TBs were mapped using the Sakai roller with the padfoot configuration and with the smooth drum shell kit installed over the padfoot drum. Mapping passes were performed using low and high amplitude settings with each drum setup. The mapping passes on this TB were intended to obtain comparison CCV data from padfoot (CCV_{PD}) and smooth drum (CCV_{SD}) setups. A screen shot from the Aithon-MT software showing CCV_{SD} map from high amplitude setting is shown in Figure 49. Following mapping passes, E_{LWD-Z2}, $E_{FWD-D4.5}$, E_{V1}, and E_{V2} point measurements were obtained from select locations across each TB for correlation analysis.

CCV_{PD} and CCV_{SD} maps from TBs 6 and 7 at low and high amplitude settings are presented in Figure 50 to Figure 53. The drum configurations, nominal amplitude, frequency, and speed settings for each map are also shown on the figures. Also shown on Figure 50 to Figure 53 are histogram plots of CCV measurements separately for TBs 6 and 7. Univariate statistics (mean μ, standard deviation σ, and coefficient of variation COV) of CCV and in-situ point measurements are summarized in Table 6. On average, CCV_{PD} and CCV_{SD} measurements obtained using both high and low amplitude settings were higher on TB7 compared to TB 6. Similarly, in-situ point measurements were higher on TB7 compared to TB6. However, CCV_{PD} values at a = 2.19 mm and 0.93 mm, and CCV_{SD} values at a = 1.48 mm showed relatively better differentiation between TBs 6 and 7 than compared to CCV_{SD} values at a = 0.63 mm. The average CCV_{PD} and CCV_{SD} values on TB6 lean clay subgrade material were higher with low amplitude setting than with high amplitude setting. In contrast, the CCV_{PD} and CCV_{SD} values on TB7 weatherd shale material with low amplitude setting were lower than with high amplitude setting. This difference could be because of differences in the stress dependency of the materials; however, additional information would be required to clarify the behavior.

One objective of mapping operations on TBs 6 and 7 was to obtain a relationship between CCV_{SD} and CCV_{PD} measurement values. A regression relationship between the two measurements cannot be developed using the actual reported data since the values are not reported to exactly the same spatial location for each pass. To overcome this problem, the output data was processed in such a way that averaged data is assigned to a preset grid point along the roller path. Each grid point was spaced at approximately 0.3 m along the roller path which represents an average of measurements that fall within a window of size 0.15 m in forward and backward directions. Figure 54 shows linear regression relationships between CCV_{PD} and CCV_{SD} measurement values using the averaging procedure for low and high amplitude settings. The relationships indicate that CCV_{SD} values at a = 0.63 mm show poor correlations with CCV_{PD} measurements. But CCV_{SD} values at a = 1.48 mm show good correlations (R^2 > 0.6) with CCV_{PD} measurements. On average, CCV_{SD} values were about 1.2 times CCV_{PD} values at a = 0.93 mm and 0.7 times CCV_{PD} values at a = 2.19 mm.

Technology wise, application of CCV measurements from smooth drum are much more mature than from padfoot drum. To the author's knowledge, this is the first documented project with CCV_{PD} measurements. Although the regression relationships between CCV_{PD} and CCV_{SD} measurements shows scatter, the trends are quite encouraging. The padfoot roller measurements demonstrate similar advantages as the smooth drum roller measurements.

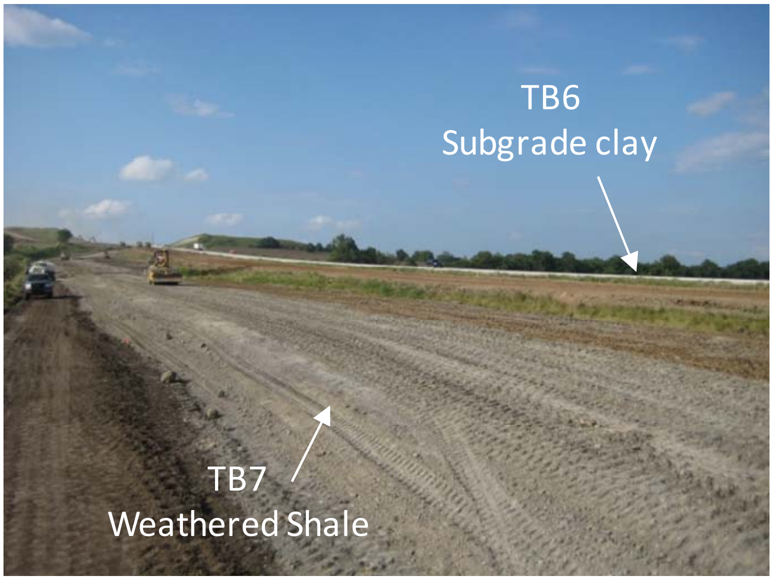

Figure 48. Picture showing TBs 6 and 7

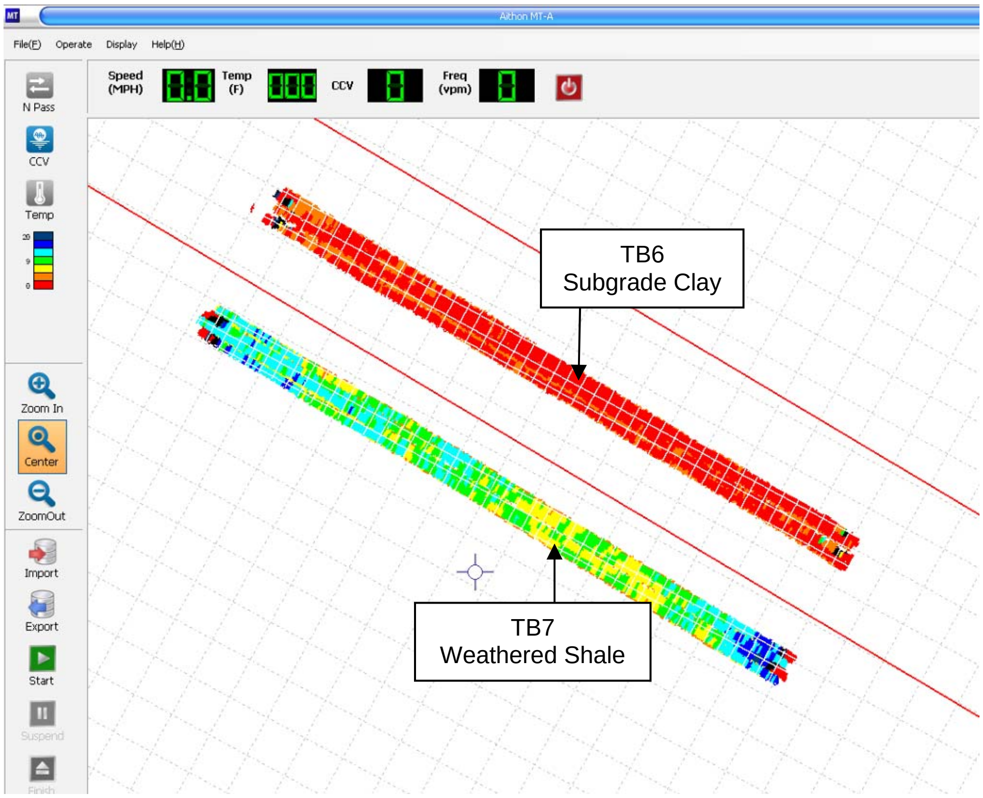

Figure 49. AithonMT display of CCV_{SD} map (*a* = 1.48 mm, *f* = 26 Hz)

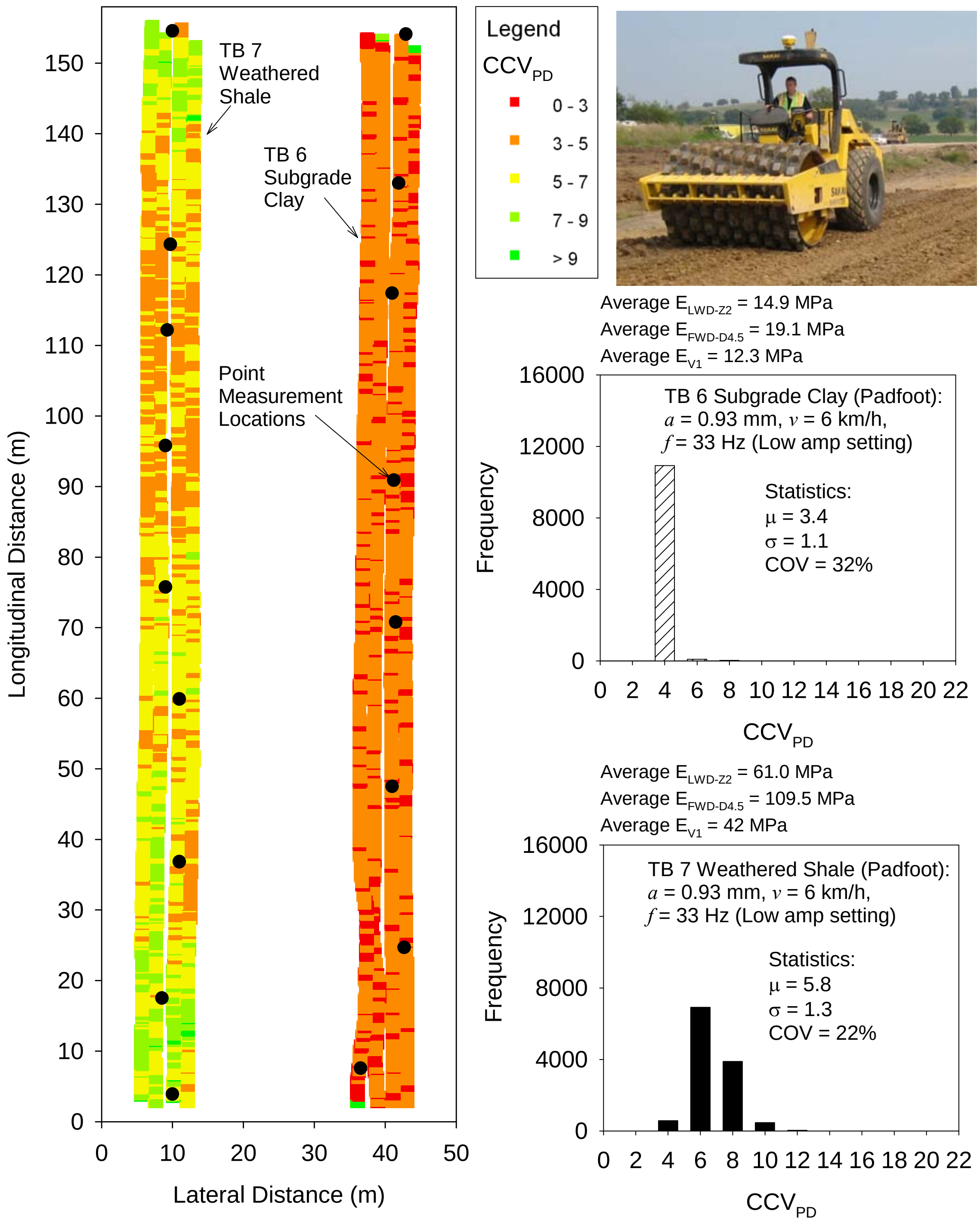

Figure 50. CCV$_{PD}$ map and histogram plots for TBs 6 and 7 (low amplitude setting)

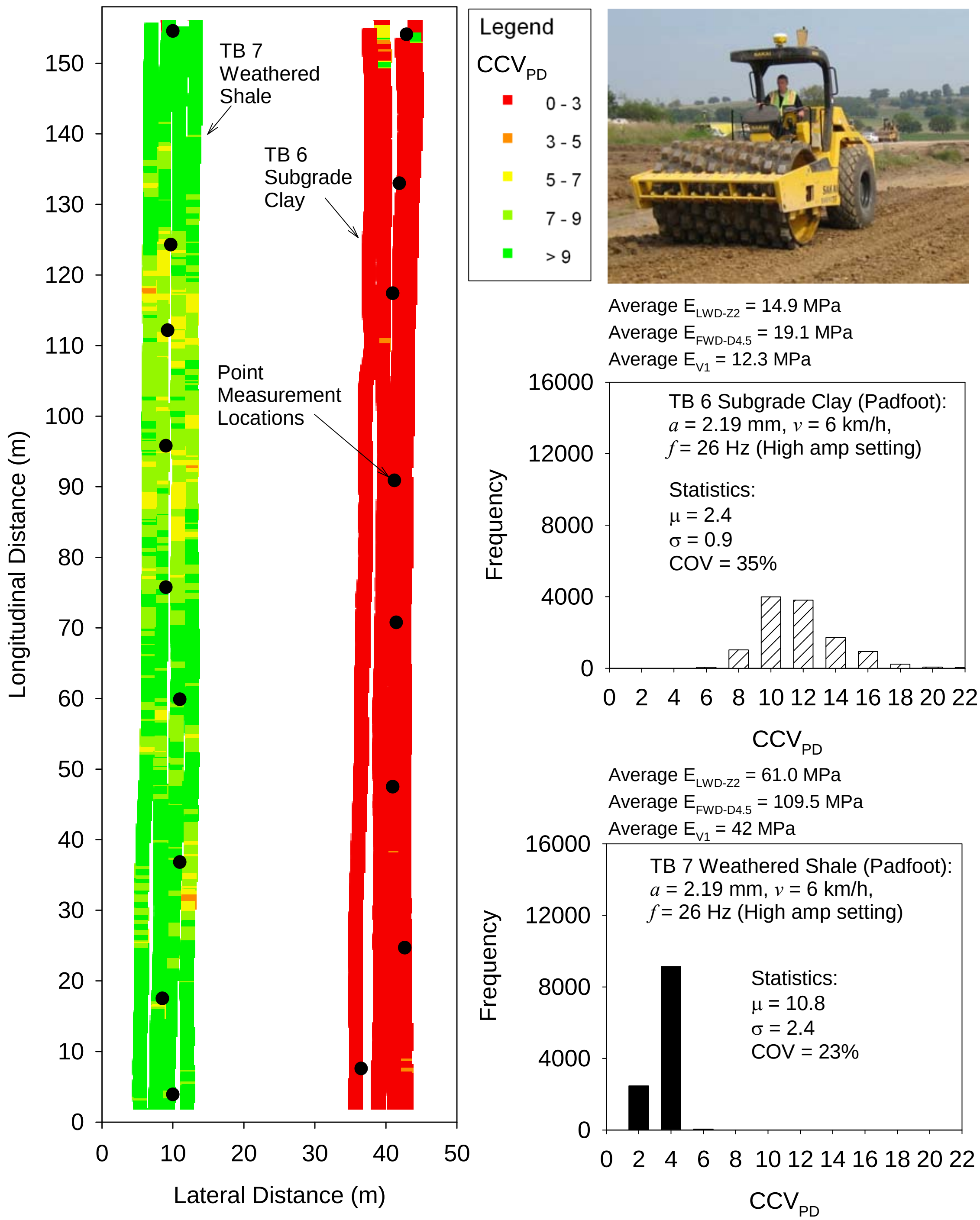

Figure 51. CCV_{PD} map and histogram plots for TBs 6 and 7 (high amplitude setting)

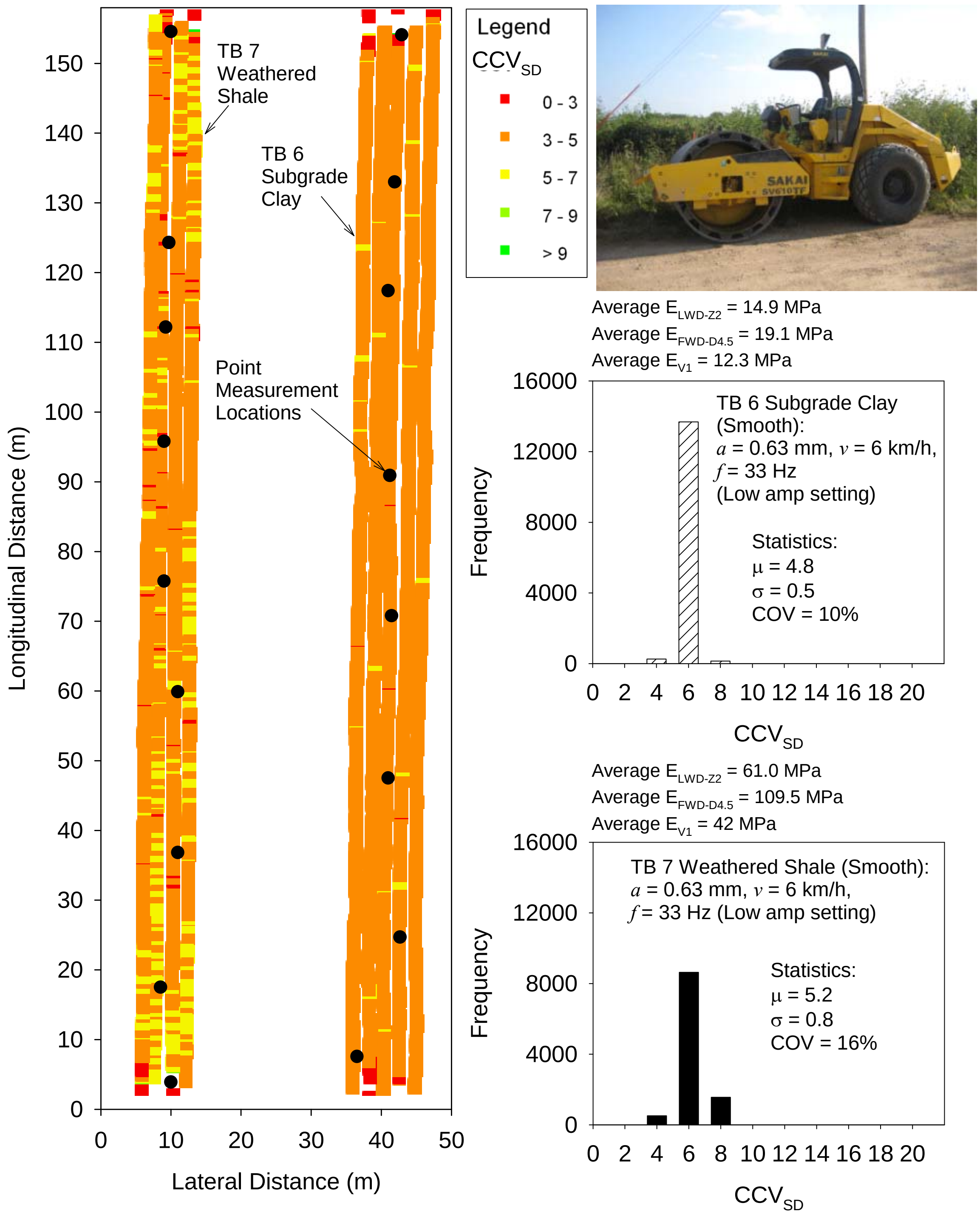

Figure 52. CCV$_{SD}$ map and histogram plots for TBs 6 and 7 (low amplitude setting)

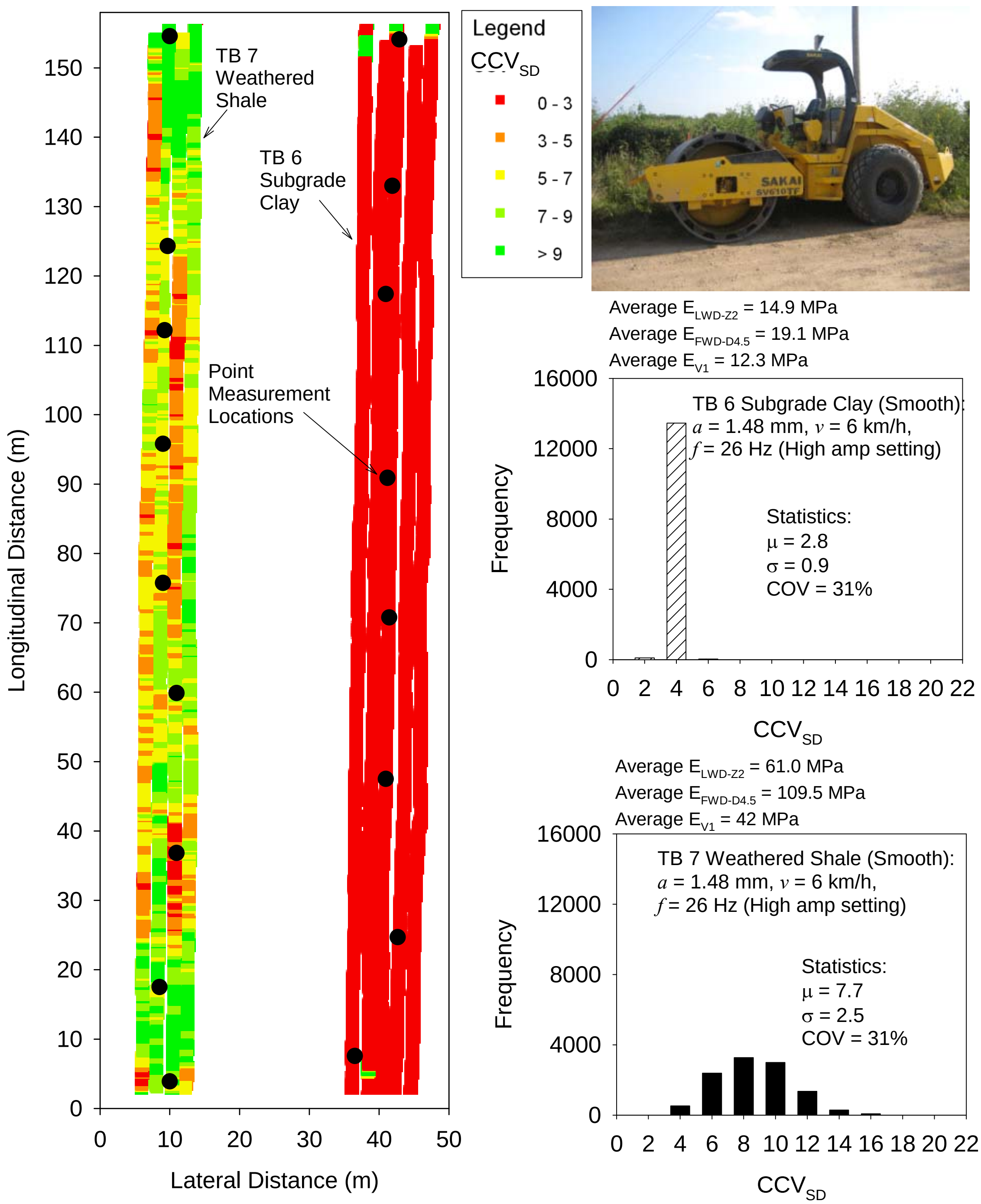

Figure 53. CCV_{SD} map and histogram plots for TBs 6 and 7 (high amplitude setting)

Table 6. Summary statistics of CCV and in-situ point measurement values on TBs 6 and 7

Measurement	TB6 (Clay)				TB7 (Weathered Shale)			
	μ	n*	σ	COV(%)	μ	n*	σ	COV(%)
CCV_{PD} (a = 0.93 mm)	3.4	11088	1.1	32	5.8	11079	1.3	22
CCV_{PD} (a = 2.19 mm)	2.4	12298	0.9	35	10.8	12111	2.4	23
CCV_{SD} (a = 0.63 mm)	4.8	11165	0.5	10	5.2	14678	0.8	16
CCV_{SD} (a = 1.48 mm)	2.8	11377	0.9	31	7.7	14132	2.5	31
E_{LWD-Z2} (MPa)	14.9	8	8.2	55	61.0	9	12.2	20
E_{V1} (MPa)	12.3	8	4.2	34	42.0	9	6.7	16
E_{V2} (MPa)	24.6	8	9.4	38	78.9	9	21.4	27
$E_{FWD-D4.5}$ (MPa)	19.1	8	1.8	10	109.5	9	45.8	42

*Number of measurements

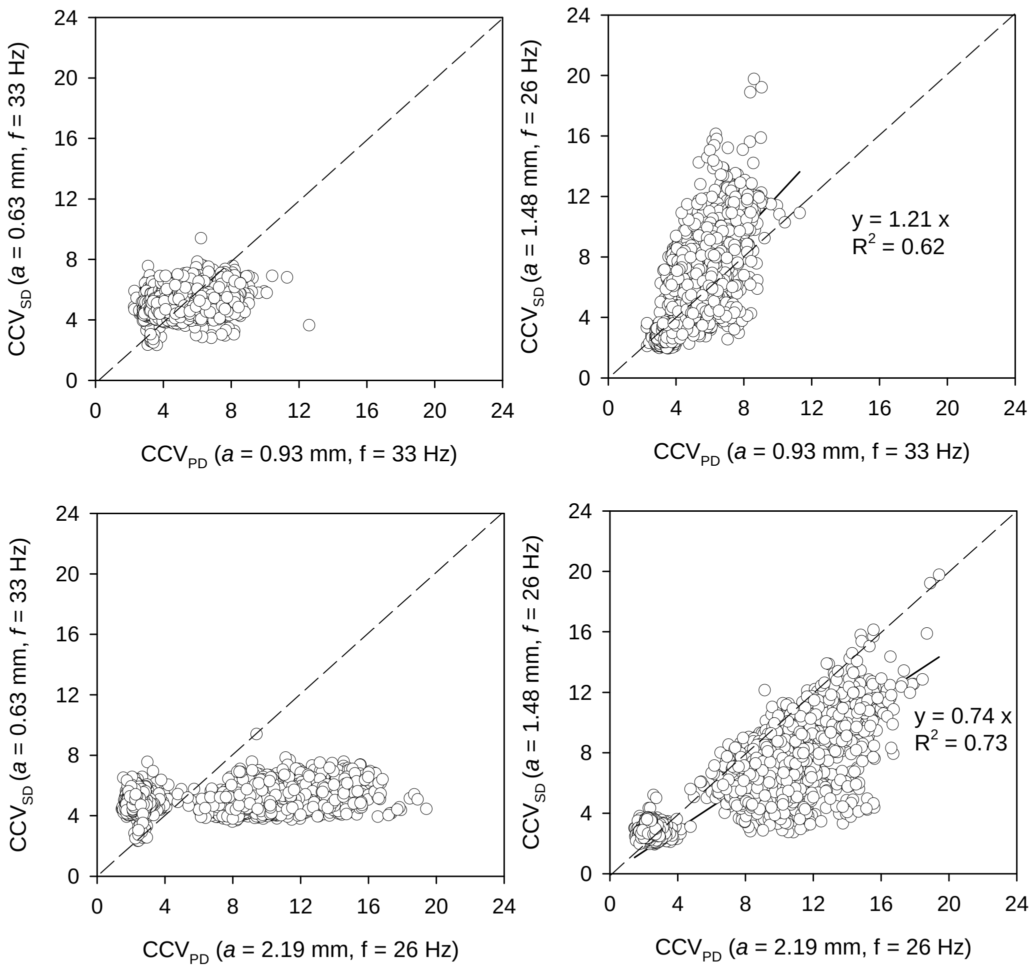

Figure 54. Regression relationships between CCV_{SD} and CCV_{PD} measurement values from TBs 6 and 7

REGRESSION ANALYSIS AND DISCUSSION

Simple Linear Regression

Simple linear regression relationships were developed between IC measurement values (IC-MV) and in-situ point measurement values (Point MV) by spatially pairing the data obtained from the test beds. The analysis was performed by considering in-situ point measurements as "true" independent variables and IC measurement values as dependent variables using the model shown in Eq. 5, where b_0 = intercept and b_1 = slope.

$$IC-MV = b_0 + b_1 \cdot Point\,MV \tag{5}$$

Statistical significance of the independent variable was assessed based on *p*- and *t*-values. The selected criteria for identifying the significance of a parameter included: *p*-value < 0.05 = significant, < 0.10 = possibly significant, > 0.10 = not significant, and *t*-value < -2 or > +2 = significant. The strength of the regression relationships are assessed by the coefficient of determination (i.e., R^2) values. In the following discussion, an R^2 value ≥ 0.5 is considered acceptable following the guidelines from European specifications. A statistical prediction interval approach for determining "target" values from the regression relationships would account for R^2 values in the relationship (see NCHRP 21-09). A regression relationship with lower R^2 values would result in higher target value and a regression relationship with higher R^2 value will result in lower target values.

Regression relationships for CCV_{PD}, CCV_{SD}, MDP_{80}, and MDP_{40} are presented in Figure 55 to Figure 57, Figure 58 and Figure 59, Figure 60 to Figure 63, and Figure 64, respectively.

Relationships presented in Figure 55 for CCV_{PD} at high amplitude setting and in Figure 58 for CCV_{SD} at high amplitude setting showed good correlations with R^2 values > 0.6. Relationships for CCV_{PD} at low amplitude setting presented in Figure 56 showed relatively low R^2 values (R^2 = 0.1 to 0.4) with γ_d and CBR measurements compared to modulus measurements (i.e., E_{LWD-Z2}, $E_{FWD-D4.5}$, E_{V1}, and E_{V2}). The reason is likely attributed to the narrow range of CCV_{PD} measurement values (ranged between 2 and 5 at point measurement locations). Regressions presented in Figure 57 from TB3 production area showed two separate trends for weatherd shale fill and lean clay fill/foundation layer materials. These separate trends could be a result of differences in the underlying support, material, and moisture conditions. CCV_{SD} at the low amplitude setting showed poor correlations with R^2 values ranging from 0 to 0.2 due to relatively narrow range of CCV_{SD} values (ranged between 4 and 5 at point measurement locations).

Figure 60 presents regression relationships between MDP_{80} obtained driving uphill (static mode) on TBs 1 and 2 and in-situ point measurements. Measurements obtained from driving uphill on TBs 1 and 2 are only considered in the regression analysis to avoid influence of driving grade slope on the relationships as demonstrated earlier. MDP_{80} showed good correlations with modulus measurements (i.e., E_{LWD-Z2} and $E_{FWD-D4.5}$) with R^2 > 0.6 and relatively poor correlations with γ_d and CBR measurements (R^2 = 0 to 0.3). Relationships presented in Figure 61 showed relatively low R^2 values (R^2 = 0 to 0.3) due to narrow range of measurements (MDP_{80} ranging between 125 and 131 at point measurement locations). Figure 62 presents regression relationships between MDP_{80} with low amplitude setting on TBs 1 and 2 and in-situ point measurements. These relationships produced good correlations with $R^2 > 0.6$. Comparison between MDP_{80} and in-situ point measurements obtained from TB3 production area are presented in Figure 63 which shows significant scatter in the relationships. These values are likely influenced by different material type's encountered and narrow range of MDP_{80} values on each material type.

Relationships between MDP_{40} and in-situ point measurements from TB3 lift 3 and TB 5 wet organic material produced good correlations ($R^2 > 0.7$). It should be noted that MDP_{40} values on TB3 were obtained at low amplitude setting and on TB5 were obtained in a static mode. However, change in amplitude is not expected to significantly affect the values obtained on TB5 with wet organic clay material.

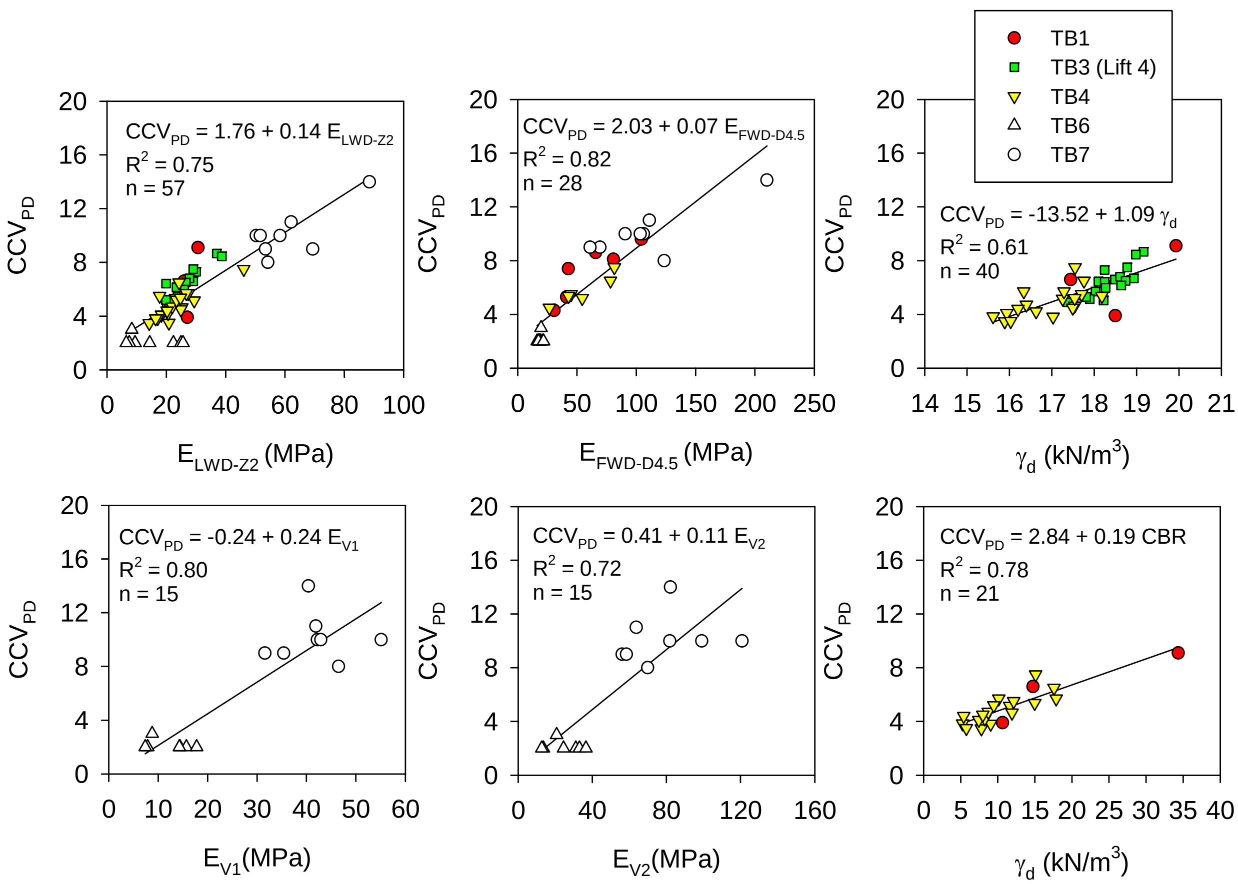

Figure 55. Regression relationships between CCV_{PD} and in-situ point measurement values from TBs 1, 2, 3, and 4 calibration test strips, and TBs 6 and 7 (*a* = 2.19 mm, *f* = 26 Hz)

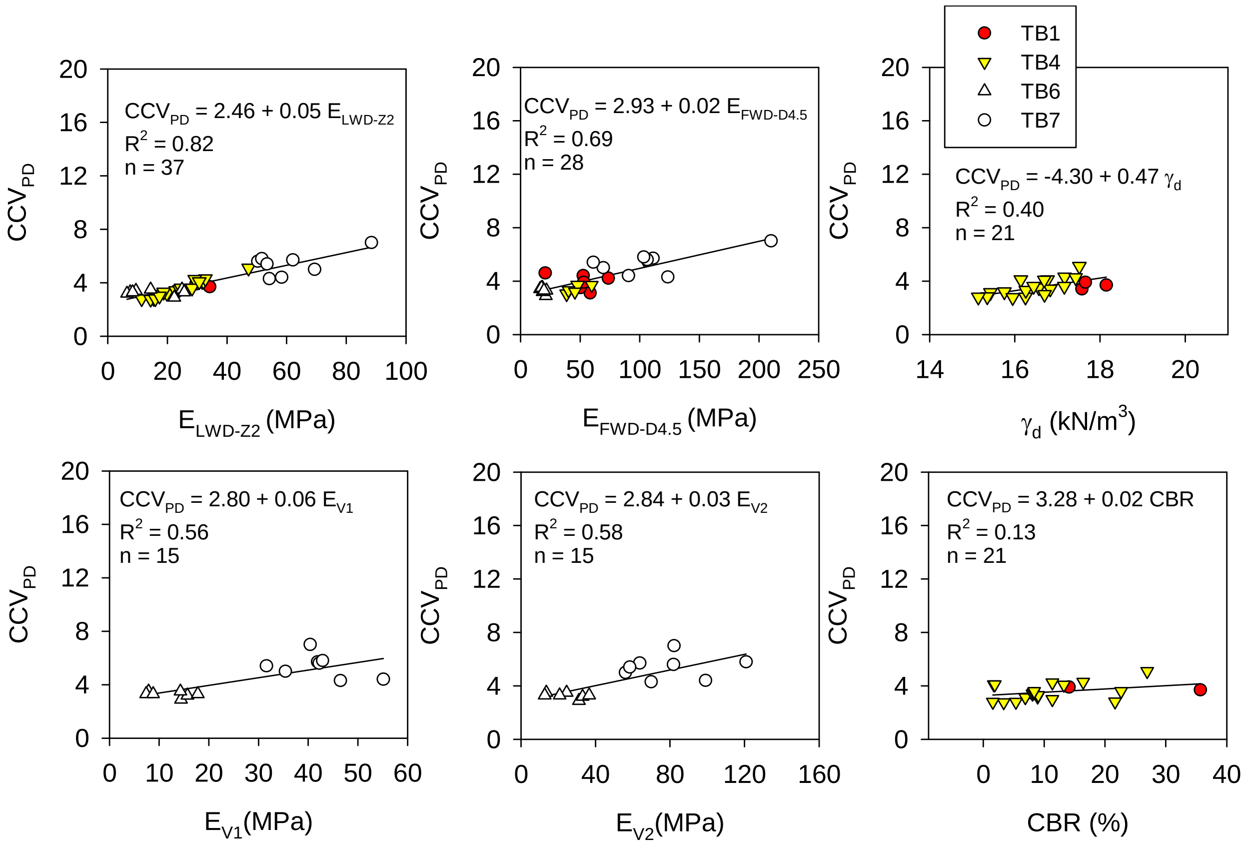

Figure 56. Regression relationships between CCV_{PD} and in-situ point measurement values from TBs 1, 2, and 4 calibration test strips, and TBs 6 and 7 (*a* = 0.93 mm, *f* = 33 Hz)

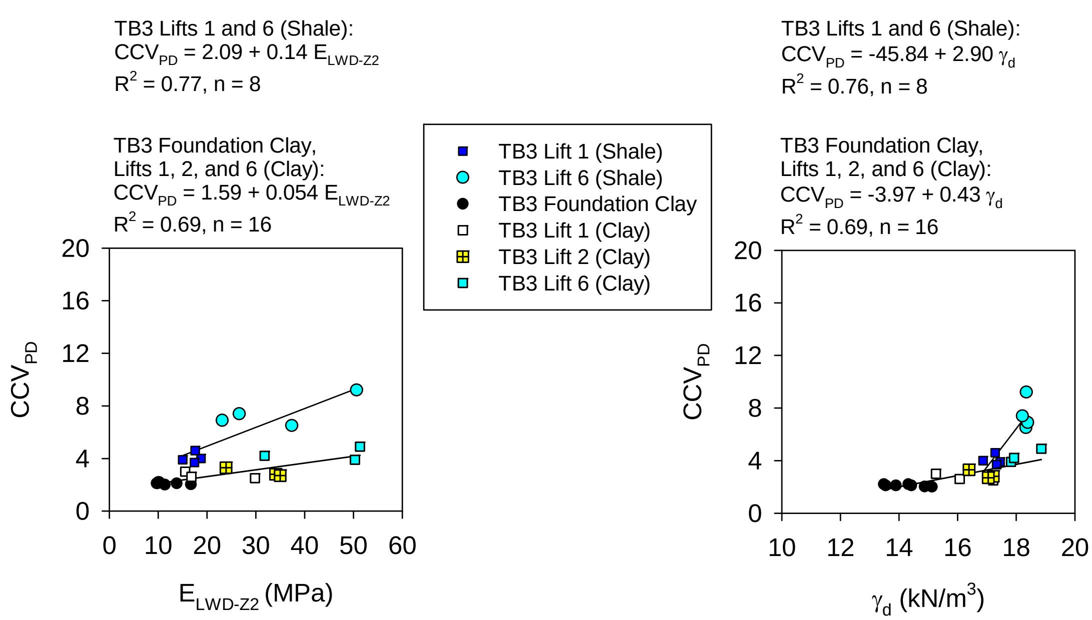

Figure 57. Regression relationships between CCV_{PD} and in-situ point measurement values from TB3 production area (*a* = 2.19 mm, *f* = 26 Hz)

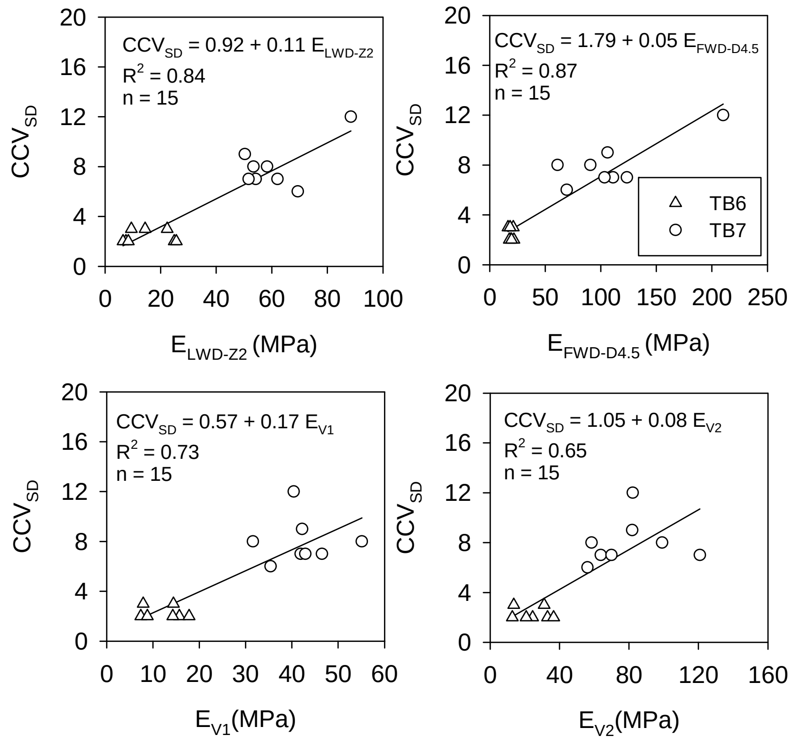

Figure 58. Regression relationships between CCV_{SD} and in-situ point measurement values from TBs 6 and 7 (a = 1.48 mm, f = 26 Hz)

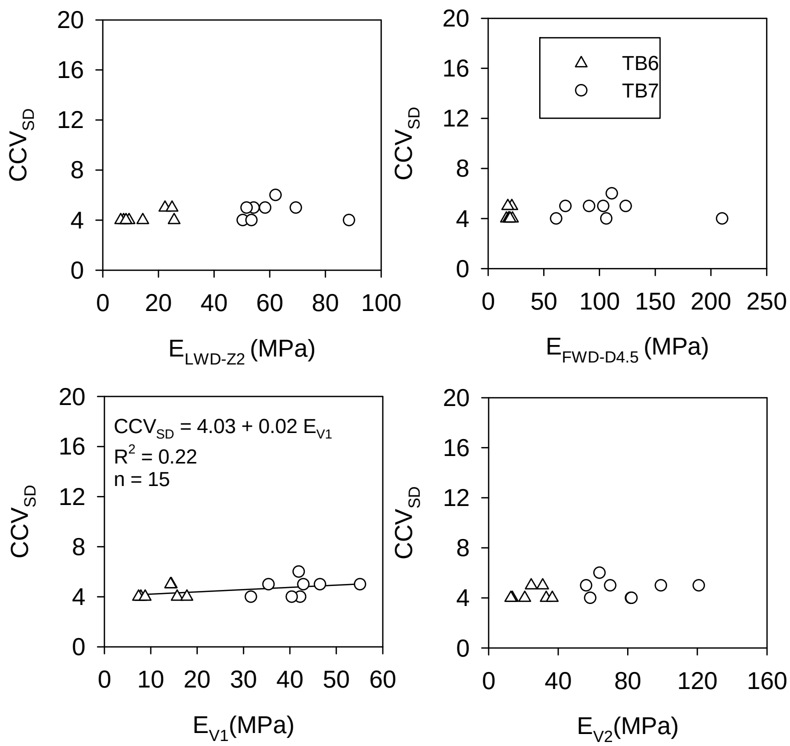

Figure 59. Regression relationships between CCV_{SD} and in-situ point measurement values from TBs 6 and 7 (a = 0.63 mm, f = 33 Hz)

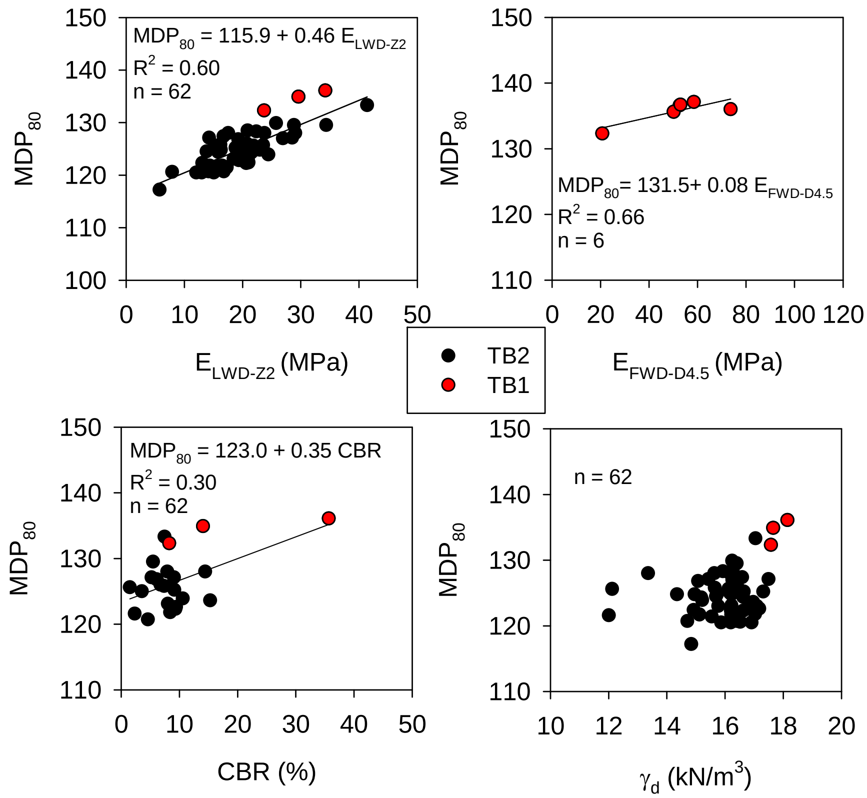

Figure 60. Regression relationships between MDP_{80} (static – driving uphill) and in-situ point measurement values – TBs 1 and 2 subgrade clay

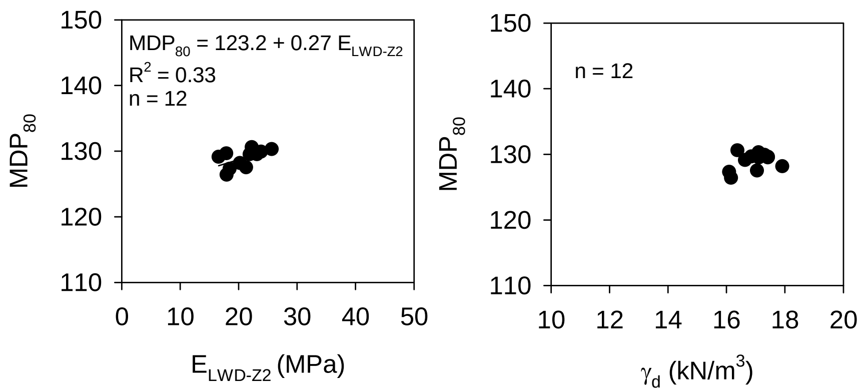

Figure 61. Regression relationships between MDP_{80} (*a* = 1.80 mm, *f* = 33 Hz, driving uphill) and in-situ point measurement values – TB2 subgrade clay

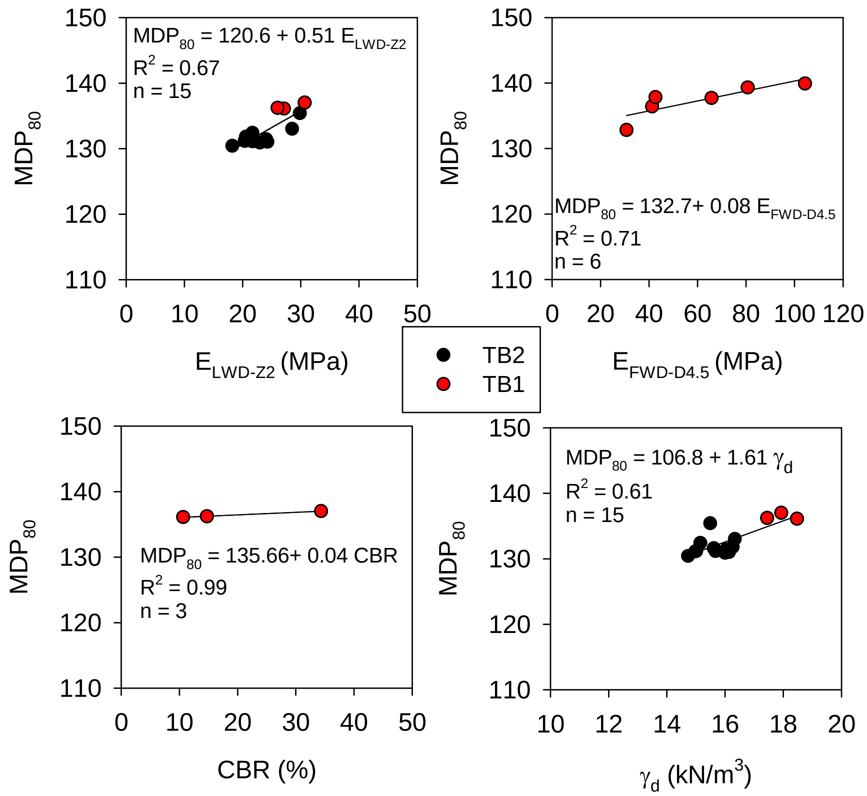

Figure 62. Regression relationships between MDP_{80} (a = 0.90 mm, f = 33 Hz, driving uphill)and in-situ point measurement values – TBs 1 and 2 subgrade clay

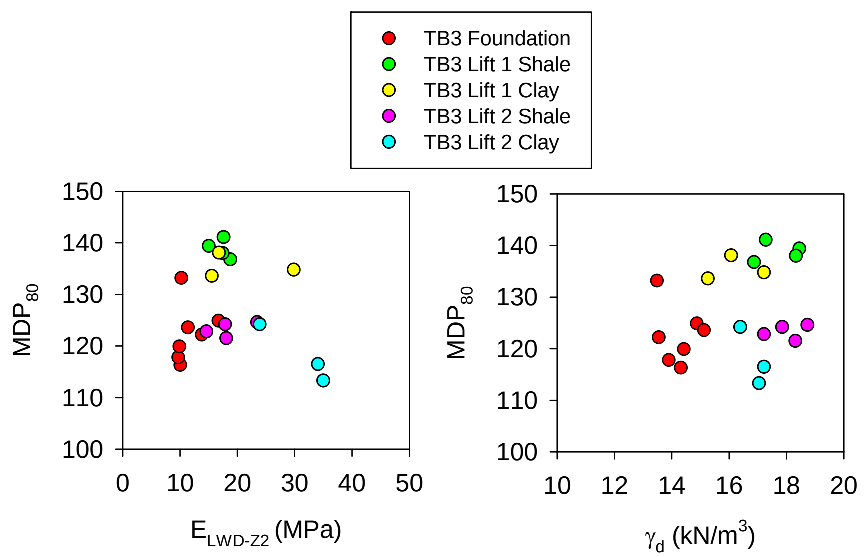

Figure 63. Regression relationships between MDP_{80} (a = 0.90 mm, f = 33 Hz) and in-situ point measurement values – TB3 foundation layer and lifts 1 to 2

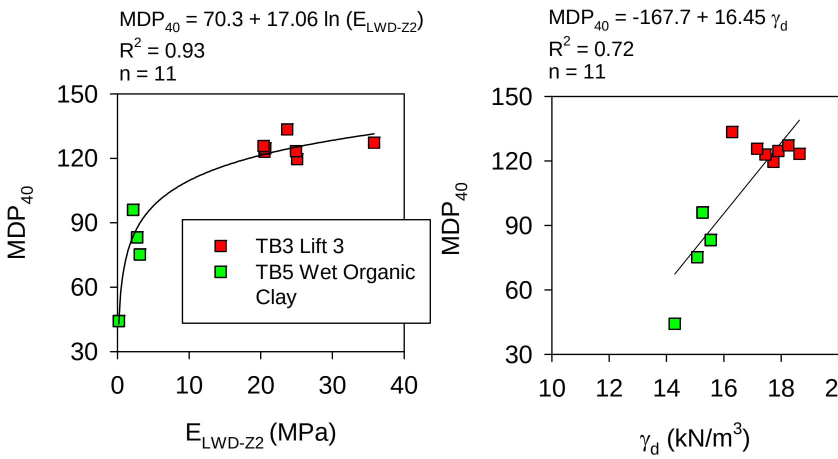

Figure 64. Regression relationships between MDP_{40} and in-situ point measurement values – TB3 lift 3 (*a* = 0.90 mm, *f* = 33 Hz) and TB5 (static)

Multiple Linear Regression

Use of multiple regression analysis to statistically assess the influence soil moisture content and vibration amplitude is presented in this section. Multiple regression analysis was performed by incorporating amplitude and moisture content as independent variables into a general multiple linear regression model as shown in Eq. 6 where b_0 = intercept, b_1, b_2, and b_3 = regression coefficients, a = amplitude (mm), and w = moisture content (%).

$$IC-MV = b_0 + b_1 \cdot Point\,MV + b_2 \cdot a + b_3 \cdot w \tag{6}$$

The analysis was performed by combining data from all test beds except TB3 production area. The statistical significance of a regression parameter was assessed based on *p*- and *t*- statistics. The selected criteria for identifying the significance of a parameter included: p-value < 0.05 = significant, < 0.10 = possibly significant, > 0.10 = not significant, and t-value < -2 or > +2 = significant. The *p*-value indicates the significance of a parameter and the *t*-ratio value indicates the relative importance (i.e., higher the absolute value greater the significance).

Results from multiple regression analysis are summarized in Table 7 and Table 8 for CCV_{PD} and MDP_{80}, respectively. Analysis on CCV_{PD} measurements showed that amplitude is statistically significant in relating all in-situ point measurement values ($E_{LWD\text{-}Z2}$, $E_{FWD\text{-}D4.5}$, γ_d, CBR, E_{V1}, and E_{V2}) while moisture content is statistically significant for $E_{LWD\text{-}Z2}$, γ_d, and CBR (note that limited *w* measurements were available at other point measurement locations). Similar to CCV_{PD}, analysis on MDP_{80} measurements showed that amplitude is statistically significant for all point measurement values ($E_{LWD\text{-}Z2}$, γ_d, and CBR) while *w* is statistically significant for γ_d.

For multiple regression models to predict CCV_{PD}, the intercept was not always statistically significant. Considering $E_{FWD\text{-}D4.5}$ for example, the R^2 value with amplitude incorporated in the model showed an R^2 = 0.68 which is lower than R^2 values obtained from simple linear regression analysis separating results from different amplitudes (R^2 = 0.69 and 0.82 see Figure 55 and Figure 56). This is important to note and in such cases, it is appropriate to interpret the relationships separately for different amplitude settings, instead of combining the results. The Nevertheless, it is recommended that all measurements obtained from calibration areas and production areas during QA should be obtained at a constant amplitude setting to avoid complication in data analysis and interpretation.

Table 7. Results of multiple regression analysis for influence of amplitude and moisture content on CCV_{PD} – TBs 1, 3(lift4), 4, 6, and 7

Model	Term	Estimate	Std Error	*t* Ratio	Prob>t	R^2
$CCV_{PD} = b_0 + b_1 E_{LWD\text{-}Z2} + b_2 a + b_3 w$	b_0	2.27	1.13	1.99	0.05	0.75
	b_1	0.10	0.02	5.97	<0.0001	
	b_2	1.36	0.20	6.89	<0.0001	
	b_3	-0.16	0.05	-3.09	0.0031	
$CCV_{PD}^{\dagger} = b_0 + b_1 E_{FWD\text{-}D4.5} + b_2 a$	b_0	-0.07	0.62	-0.11	0.92	0.68
	b_1	0.04	0.01	9.38	<0.0001	
	b_2	1.64	0.33	4.94	<0.0001	
$CCV_{PD} = b_0 + b_1 \gamma_d + b_2 a + b_3 w$	b_0	-10.47	3.16	-3.32	0.0016	0.75
	b_1	0.85	0.15	5.74	<0.0001	
	b_2	0.86	0.20	4.31	<0.0001	
	b_3	-0.06	0.06	-2.0	0.098	
$CCV_{PD} = b_0 + b_1 CBR + b_2 a + b_3 w$	b_0	3.60	1.36	2.64	0.012	0.60
	b_1	0.07	0.02	3.94	<0.0001	
	b_2	1.15	0.22	5.27	<0.0001	
	b_3	-0.13	0.08	-2.1	0.099	
$CCV_{PD}^{\dagger} = b_0 + b_1 E_{V1} + b_2 a$	b_0	-1.18	1.25	-0.95	0.35	0.61
	b_1	1.57	0.62	2.55	0.017	
	b_2	0.15	0.02	5.95	<0.0001	
$CCV_{PD}^{\dagger} = b_0 + b_1 E_{V1} + b_2 a$	b_0	-0.84	1.29	-0.65	0.52	0.57
	b_1	1.58	0.65	2.44	0.0217	
	b_2	0.07	0.01	5.47	<0.0001	

† limited *w* measurements; statistical significance based on $p < 0.10$ and $t < -2$ or $> +2$

Table 8. Results of multiple regression analysis for influence of amplitude and moisture content on MDP_{80} – TBs 1 and 2

Model	Term	Estimate	Std Error	*t* Ratio	Prob>t	R^2
$MDP_{80}^{*} = b_0 + b_1 E_{LWD\text{-}Z2} + b_2 a$	b_0	115.32	1.07	107.5	<0.0001	0.67
	b_1	0.51	0.05	9.99	<0.0001	
	b_2	2.50	0.43	5.81	<0.0001	
$MDP_{80} = b_0 + b_1 \gamma_d + b_2 a + b_3 w$	b_0	89.00	9.21	9.67	<0.0001	0.38
	b_1	1.54	0.43	3.60	0.0006	
	b_2	2.45	0.62	3.96	0.0002	
	b_3	0.84	0.25	3.37	0.0011	
$MDP_{80}^{*} = b_0 + b_1 CBR + b_2 a$	b_0	123.21	1.22	101.0	<0.0001	0.50
	b_1	0.34	0.10	3.57	0.0016	
	b_2	4.45	1.75	2.55	0.0178	

* *w* not statistically significant; statistical significance based on $p < 0.10$ and $t < -2$ or $> +2$

FIELD DEMONSTRATION – OPEN HOUSE

An open house was conducted on 08/21/2008 as part of this field investigation and included dissemination of results from previous IC field studies and results from the current field study as part of a presentation (Figure 65 and Figure 66). Demonstration of the two IC rollers, a tour of the Iowa State University geotechnical mobile lab with several laboratory and in-situ testing methods were conducted at the project location. About 40+ people attended the open house including Kansas DOT, contractor, roller manufacturer, and University of Kansas personnel. The attendees operated the IC rollers and received hands-on-experience.

Figure 65. Demonstration of in-situ testing equipment during open house

Figure 66. Iowa State University mobile lab tour during open house

Figure 67. Demonstration of real-time wireless data transfer from roller to mobile lab

SUMMARY AND CONCLUSIONS

Results obtained from a field investigation conducted on the US69 project located in Kansas from August 17–25, 2008 using Caterpillar and Sakai intelligent compaction (IC) rollers are presented in this report. The project involved constructing calibration and production test areas with fine grained cohesive subgrade materials. IC measurement values were obtained in conjunction with point measurement values at multiple roller passes with different machine amplitude settings for correlation analysis. IC measurements were obtained from production compaction operations involving construction of seven lifts to assess the advantages of the technology on cohesive subgrade materials. IC measurements were analyzed using geostatistical anlaysis methods to demonstrate its application in quantifying non-uniformity of compaction fill materials. Some key conclusions from the test bed studies are as follows:

- MDP_{80} values are repeatable provided the direction of travel along the test bed is constant. The values are not reproducible with change in direction of travel along the test bed. MDP_{80} values were influenced by the sloping grade in the direction of travel. Regression relationship between slope angle (α) and MDP_{80} values indicated a decrease in MDP_{80} values with increasing slope angle.
- The CCV_{PD} values are repeatable.
- MDP_{80} and CCV_{PD} measurement values obtained on calibration test beds generally increased with increasing pass similar to in-situ point measurements.
- The variations in MDP_{80} and CCV_{PD} measurements along the calibration test beds generally tracked well with changes observed in in-situ point measurements.
- Side-by-side lanes compacted using static, low, and high amplitude settings on TB2 showed comparatively higher relative compaction on the lane compacted using high amplitude setting. Results on TB4 showed similar relative compaction values on side-by-side lanes compacted using high and low amplitude settings.
- Color-coded maps of IC data, number of passes, and elevation data with 100% coverage provide the opportunity to visualize compaction curves (at a given point as well as

average over a given area). This can be effective if utilized by the roller operator to make informed decisions on compaction process to promptly adjust process control measures.

- Isolated soft/wet spots are easily identified using IC maps.
- Application of geostatistical parameters (i.e., range and sill) to analyze IC measurement presents a unique way of quantifying spatial continuity and non-uniformity of compacted fill materials. Implementing such analysis methods represent a paradigm shift in how compaction analysis and specifications could be implemented in the future.
- CCV_{SD} obtained using low amplitude setting (a = 0.63 m) produced poor correlations with CCV_{PD} measurements. CCV_{SD} obtained using high amplitude setting (a = 1.48 mm) produced good correlations with CCV_{PD} measurements. Although there is scatter in the relationships, the trends are quite encouraging. The padfoot roller measurements demonstrate similar advantages as the smooth drum roller measurements.
- Simple linear regression analysis between IC measurement values and point measurements produced R^2 ranging from 0 to 0.9. Reasons for cases with poor correlations are attributed to influence of underlying support conditions, variations in moisture content, and narrow range of IC measurements at the point locations. Point measurements obtained over a wide range of IC measurement values from calibration test strips will generally help producing better correlations.
- Multiple regression analysis demonstrated that IC measurement values are influenced by change in amplitude in correlation with in-situ point measurement values. Moisture content was also statistically significant for some cases.
- For some multiple regression models assessing the influence of amplitude, the intercept was not always statistically significant. This resulted in a lower R^2 value than obtained from separate simple linear regression analysis on different amplitudes. In such cases, it is appropriate to interpret the relationships separately for different amplitude settings, instead of combining the results through multiple regression anlaysis.
- Although influence of amplitude can be accounted for through multiple regression analysis, it is recommended that all measurements obtained from calibration areas and production areas during QA be obtained at a constant amplitude setting to avoid complication in data analysis and interpretation.

REFERENCES

ASTM D6951. (2003). "Standard test method for use of the dynamic cone penetrometer in shallow pavement application." American Standards for Testing Methods (ASTM), West Conshohocken, PA.

Clark, I., and Harper, W. (2002). *Practical geostatistics 2000*. 3rd reprint, Ecosse North America Llc, Columbus, Oh.

Isaaks, E. H., and Srivastava, R. M. (1989). *An introduction to applied geostatistics*. Oxford University Press, New York.

NCHRP. (2009). *Intelligent soil compaction systems – NCHRP 21-09*, National Cooperative Highway Research Program, Transportation Research Board, Washington, D.C. (in review).

Nohse, Y., and Kitano, M. (2002). “Development of a new type of single drum vibratory roller,” *Proc. 14th Intl. Conf. of the Intl. Soc. For Terrain-Vehicle Systems,* Vicksburg, MS, October 20-24.

Scherocman, J., Rakowski, S., and Uchiyama, K. (2007). “Intelligent compaction, does it exist?” 2007 *Canadian Technical Asphalt Association (CTAA) Conference,* Victoria, BC, July.

Thompson, M., and White, D. (2008). “Estimating compaction of cohesive soils from machine drive power.” J *Journal of Geotechnical and Geoenvironmental Engineering*, ASCE, 134(12): 1771-1777.

Vennapusa, P., White, D.J., Gieselman, H. (2009). “Influence of support conditions on roller-integrated machine drive power measurements for granular base.”, *Intl. Foundation Congress and Equipment Expo (IFCEE) 2009*, 15-19 March, Orlando, Florida.

Vennapusa, P., and White, D. J. (2009a). “Comparison of light weight deflectometer measurements for pavement foundation materials.” *Geotechnical Testing Journal*, 32(3), ASTM.

Vennapusa, P., White, D.J. (2009b). “Geostatistical analysis for spatially referenced roller-integrated compaction measurements, *Journal of Geotechnical and Geoenvironmental Engineering,* ASCE (in review, submitted July 2008).

White, D. J., Jaselskis, E., Schaefer, V., Cackler, T. (2005). “Real-time compaction monitoring in cohesive soils from machine response.” *Transp. Res. Rec., 1936*, Transportation Research Board, Washington D.C., 173–180.

White, D.J., and Thompson, M. (2008). Relationships between in situ and roller-integrated compaction measurements for granular soils. *Journal of Geotechnical and Geoenvironmental Engineering*, ASCE, 134(2): 1763-1770.

White, D.J, Thompson, M., Vennapusa, P. (2007a). *Field Validation of Intelligent Compaction Monitoring Technology for Unbound Materials*, Mn/DOT Report No. MN/RC 2007-10, Iowa State University, Ames, IA.

White, D. J., Thompson, M., Vennapusa, P. (2007b). *Field study of compaction monitoring systems – Tamping foot 825 and vibratory smooth drum CS-533E rollers*. Final Report, Center of Transportation Research and Education, Iowa State University, Ames, Ia.

Zorn, G. (2003). *Operating manual: Light drop-weight tester ZFG2000*, Zorn Stendal, Germany.

APPENDIX

Accelerated Implementation of IC Technology for Embankment Subgrade Soils, Aggregate Base, and Asphalt Pavement Materials

Iowa State University Research Team Field Testing, US 69, Kansas

Test Bed # 1 (08/18/2008 and 08/19/2008)

Description: The test bed consisted of compacted subgrade clay material with plan dimensions of approximately 5 m x 55 m. The area was mapped in two roller lanes for eight passes(for repeatability study) using Caterpillar padfoot roller and two mapping passes using Sakai roller. In-situ test measurements ($E_{FWD\text{-}D4.5}$, $E_{LWD\text{-}Z2}$, γ_d, w, DPI) were obtained after the mapping passes. The objectives of testing on this test bed are to evaluate the repeatability of the roller measurements and obtain correlations between roller MVs and point measurements.

Machine Nominal settings:

Caterpillar (eight passes in each lane):
- Lane 1 (static) – v = 4 km/h
- Lane 2 (low amp) – f = 30 Hz, a = 0.90 mm, v = 4 km/h

Sakai (two passes in each lane):
- Lane 1 (low amp) – f = 33 Hz, a = 0.93 mm, v = 4 km/h
- Lane 2 (high amp) – f = 26 Hz, a = 2.19 mm, v = 4 km/h

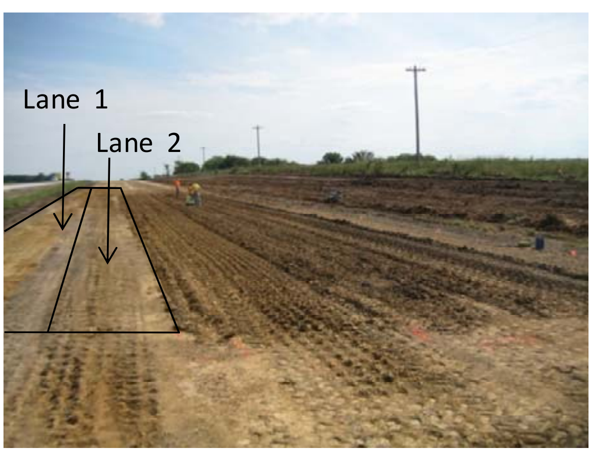

Picture of the test area

Construction/Testing Photos

Caterpillar (top) and Sakai (bottom) padfoot rollers used on the test bed

FWD Testing

Accelerated Implementation of IC Technology for Embankment Subgrade Soils, Aggregate Base, and Asphalt Pavement Materials

Iowa State University Research Team Field Testing, US 69, Kansas

Test Bed # 2 (08/18/2008)

<u>Description</u>: The test bed was constructed by scarifying the existing subgrade material to a depth of about 250 mm (10 inches) and compacted in three roller lanes. The Caterpillar CS56 padfoot roller was used for compacting the test bed for 12 roller passes. Lanes 1, 2, and 3 were compacted using nominal low amplitude, static and high amplitude settings, respectively. The objectives of this test bed were to obtain correlations between padfoot roller MVs and in-situ soil properties.

<u>Machine Nominal settings:</u>
Lane 1 (low amp) – f = 30 Hz, a = 0.9 mm, v = 4 km/h
Lane 2 (static) – v = 4 km/h
Lane 3 (high amp) – f = 30 Hz, a = 1.8 mm, v = 4 km/h

Summary of point measurements

Lane	Measurements	Pass No.	No. of Tests
1	w and γ_d	0	1
2	w and γ_d	0	3
3	w and γ_d	0	1
1, 3	w, γ_d, and E_{LWD}	12	12
2	w, γ_d, and E_{LWD}	1, 2, 4, 8, and 12	12
2	CBR	1 and 12	12

Caterpillar CS56 padfoot roller used for compaction

Construction/Testing Photos

Subgrade scarification using grader (top), disking (middle), and moisture conditioning (bottom)

In-situ test measurements

Accelerated Implementation of IC Technology for Embankment Subgrade Soils, Aggregate Base, and Asphalt Pavement Materials
Iowa State University Research Team Field Testing, US 69, Kansas

Test Bed # 3 (08/18 to 08/21/2008)

Construction Photos

Description: The test bed consisted of seven lifts of embankment subgrade clay materials (weathered shale fill and lean clay fill) placed over compacted foundation subgrade material (the foundation subgrade layer was wet and relatively soft). The foundation subgrade layer was compacted and mapped using Caterpillar and Sakai padfoot rollers. Subgrade fill materials were placed in approximately 150 to 300 mm in thickness and compacted using Caterpillar padfoot roller for 3 to 8 roller passes. Following compaction Sakai padfoot roller was used to map the production area. In-situ point measurements were obtained at seven locations on each lift. One lane calibration test strip was constructed on lift 4 and compacted using Sakai padfoot roller at high amplitude setting.

The objectives of this test bed were to demonstrate production compaction operations using IC measurements, document coverage information, and obtain data for correlations.

Accelerated Implementation of IC Technology for Embankment Subgrade Soils, Aggregate Base, and Asphalt Pavement Materials

Iowa State University Research Team Field Testing, US 69, Kansas

Test Bed # 3 continued

Construction Summary /Testing

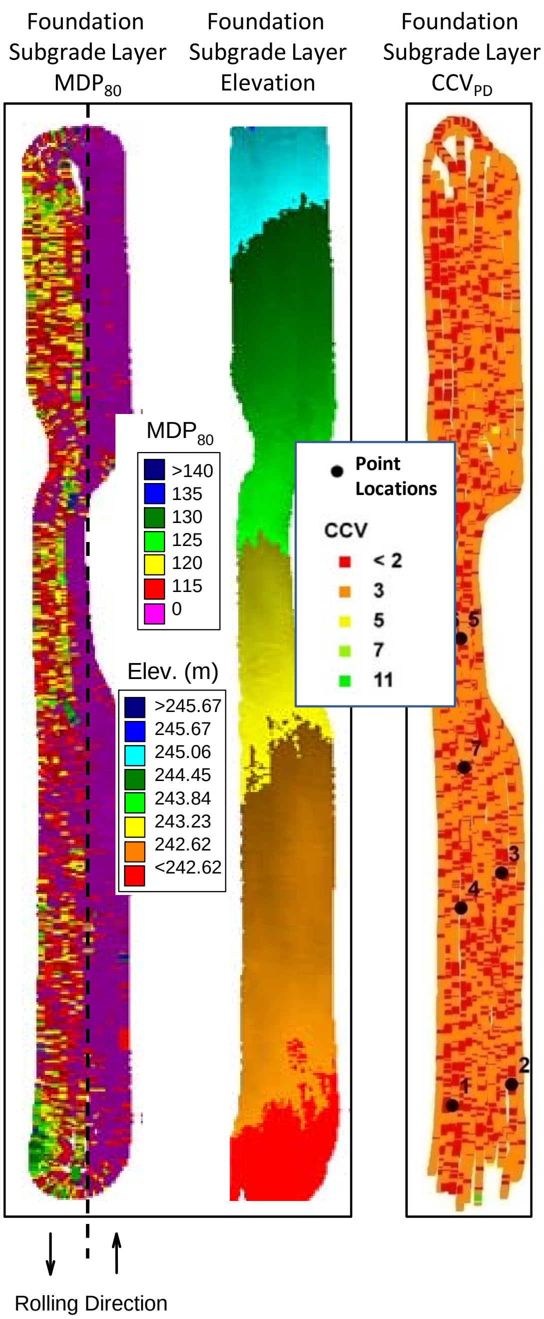

Lift	Point Measurements	Passes
Foundation Layer	w,γ_d, $E_{LWD\text{-}Z2}$, and 1m CBR	3
1	w,γ_d, and $E_{LWD\text{-}Z2}$	3 to 8
2	w,γ_d, and $E_{LWD\text{-}Z2}$	3 to 8
3	w,γ_d, and $E_{LWD\text{-}Z2}$	3 to 8
4	w,γ_d, and $E_{LWD\text{-}Z2}$	3 to 8
5	w,γ_d, $E_{LWD\text{-}Z2}$, and 1m CBR	4
6	w,γ_d, and $E_{LWD\text{-}Z2}$	4
7	w,γ_d, $E_{LWD\text{-}Z2}$, and 2m CBR	4

Lift 4 – Sakai (High Amplitude) Calibration Lane
Weathered Shale Clay Material
Summary of Point Measurements

Measurements	Pass No.	No. of Tests
w,γ_d, and $E_{LWD\text{-}Z2}$	0, 1, 2, 4, 8, and 12	4

Accelerated Implementation of IC Technology for Embankment Subgrade Soils, Aggregate Base, and Asphalt Pavement Materials

Iowa State University Research Team Field Testing, US 69, Kansas

Test Bed # 4 (08/19/2008)

Description: The test bed was constructed by scarifying the compacted TB2 to a depth of about 250 mm (10 inches). The area was then compacted in three roller lanes using Sakai SV610 padfoot roller for 13 roller passes. Lanes 1, 2, and 3 were compacted using nominal high, low, and high amplitude settings, respectively. In-situ point measurements were obtained on lanes 2 and 3. The objectives of this test bed were to obtain correlations between padfoot roller MVs and in-situ soil properties.

Machine Nominal settings:
Lane 1 (high amp) – f = 26 Hz, a = 2.19 mm, v = 6 km/h
Lane 2 (low amp) – f = 33 Hz, a = 0.93 mm, v = 6 km/h
Lane 1 (high amp) – f = 26 Hz, a = 2.19 mm, v = 6 km/h

Summary of point measurements			
Lane	Measurements	Pass No.	No. of Tests
2, 3	w, γ_d, and E_{LWD}	0	6
2, 3	CBR	1, 2, 4, and 13	6
2, 3	E_{FWD}	13	6

Dynatest 450 mm plate diameter FWD

Construction/Testing Photos

Subgrade compaction and testing in three lanes

Sakai SV610 padfoot roller used for compaction

Accelerated Implementation of IC Technology for Embankment Subgrade Soils, Aggregate Base, and Asphalt Pavement Materials
Iowa State University Research Team Field Testing, US 69, Kansas

Test Beds # 6/7 (08/20/2008 & 08/22/2008)

Construction/Testing Photos

Description: TB6 consisted of compacted subgrade clay material (relatively soft) and TB7 consisted of compacted weathered shale material (relatively stiff). Plan dimensions of the two test beds were approximately 10 m x 150 m. The two TBs were parallel to each other and were separated by a roadway median. The TBs were mapped using two amplitude and frequency settings using Sakai padfoot roller. A smooth drum shell kit was installed over the padfoot drum and used for mapping the TBs using two amplitude and frequency settings. In-situ point measurements were obtained after the padfoot roller mapping passes. The objectives of this test bed were to compare padfoot and smooth drum measurements and obtain correlations with in-situ measurements.

Machine Nominal settings:
Pass 1: Padfoot low amp
f = 33 Hz, a = 0.93 mm, v = 6 km/h
Pass 2: Padfoot high amp
f = 26 Hz, a = 2.19 mm, v = 6 km/h
Pass 3: Smooth Drum low amp
f = 33 Hz, a = 0.63 mm, v = 6 km/h
Pass 4: Smooth Drum high amp
f = 26 Hz, a = 1.48 mm, v = 6 km/h

Summary of point measurements		
TB	Measurements	No. of Tests
6	E_{LWD}, E_{V1}, E_{V2}, E_{FWD}	8
7	E_{LWD}, E_{V1}, E_{V2}, E_{FWD}	9

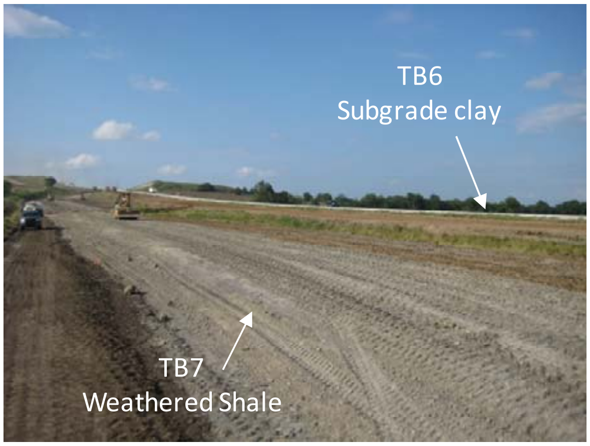

Dynatest 450 mm plate diameter FWD

Sakai SV 610 padfoot roller

Smooth drum shell kit installed on a padfoot drum

Accelerated Implementation of IC Technology for Embankment Subgrade Soils, Aggregate Base, and Asphalt Pavement Materials

Iowa State University Research Team Experimental Plan

US 69, KS

Subgrade Materials

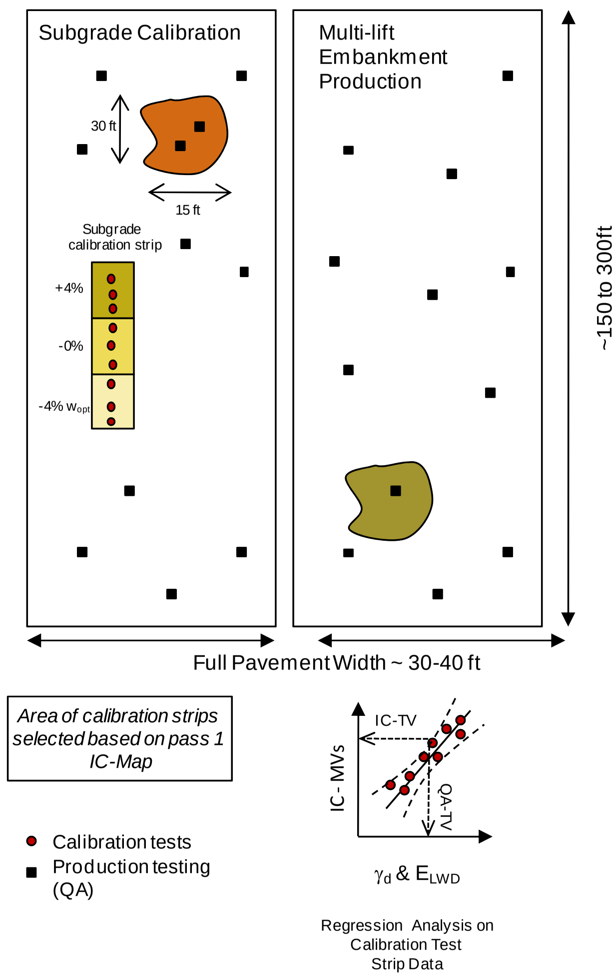

Date	TB	Strip	Machine	Amp (mm)	Spot Tests	Notes/Comments
08/17	Meet at 6:30pm. ISU mobile move to project site.					
08/18	1	Calibration/ Mapping	Sakai (pad)	0.85, 1.9	DCP, LWD, NG, ST, PLT	30' X 150' test strip (see Note A and B).12 passes. Mapping with changes in machine operations.
08/19	2	Calibration/ Mapping	Cat (pad)	Static, 0.85, 1.85	DCP, LWD, NG, ST, PLT	30' X 150' test strip (see Note A and B).12 passes. Mapping with changes in machine operations.
08/20 – 08/22	3/4	Production/ Mapping	Sakai (pad)	0.85, 1.9	DCP, LWD, NG, ST, PLT	30 ft x up to 300 ft with multi-lift compaction (~ 3 to 6 lifts). ~ 8 passes per lift. Acceptance according to KDOT criteria. Mapping at different roller operations.
			Cat (pad)	Static, 0.85, 1.85	DCP, LWD, NG, ST, PLT	30 ft x up to 300 ft with multi-lift compaction (~ 3 to 6 lifts). ~ 8 passes per lift. Acceptance according to KDOT criteria. Mapping at different roller operations.
07/25	AM: Open House, PM: ISU research team departs.					

Notes:

A. Moisture condition calibration test strip with 50' sections of -4%, 0%, and +4% of optimum moisture content. Moisture condition the production area per project QC requirements. Need water truck and mixer/reclaimer for moisture conditioning and soil mixing.

B. Perform roller repeatability passes.

ISU Research Team Contacts:
David J. White, Associate Professor, djwhite@iastate.edu, (515) 290-1080 (cell)
Heath Gieselman, Assistant Scientist, giese@iastate.edu, (515) 450-1383 (cell)